UNIVERSITÀ
DEGLI STUDI
DI BRESCIA

DOTTORATO DI RICERCA IN PRECISION MEDICINE

settore scientifico disciplinare: CHIM/03

CICLO: XXXVII

TITOLO TESI:

PAN-SPECIFIC PROBING AND SORTING OF EXTRACELLULAR NANOPARTICLES

DOTTORANDO:
Roberto Frigerio

RELATORE:
Prof. Paolo Bergese

CO-RELATORE:
Dr.ssa Marina Cretich

I dedicate this thesis to Marina Cretich, who left us during the final stages of my PhD. The time we spent discussing science, your passion for research, and your daily dedication were truly inspiring to me. Your kindness, the care you took in building relationships, and your generosity will be deeply missed and irreplaceable.

Disclosure Statement and Publications

The results presented in this thesis have been obtained during my Ph.D. studies (November 2021 – October 2024) at the University of Brescia (Brescia, Italy), CTBio Laboratory, SCITEC-CNR, Milano, and during a six-month research visit in Professor Arosio's Biochemical Engineering Laboratory at ETH Zurich. Some of the experimental chapters, hereafter described, contain several unpublished data. No intellectual property rights are granted by the delivery of this document or the disclosure of its content. The reproduction of this document or its circulation to any third party is prohibited without the author(s)'s consent.

Index

Riassunto

Nanoparticelle extracellulari (eNP), comprendono le vescicole extracellulari (EV) e le lipoproteine (LP), entrambe svolgono un ruolo cruciale nella comunicazione cellula-cellula, influenzando numerosi processi fisiologici e patologici. In particolare, le EV rivestono un grande interesse nella nanomedicina, sia per la diagnostica che per la terapia, rappresentando un vasto spazio biomarcatore per le biopsie liquide. Tuttavia, le proprietà chimico-fisiche sovrapposte rendono difficile l'isolamento specifico e l'analisi accurata delle EV. Questa tesi di dottorato mira a sviluppare un metodo altamente sensibile per analizzare singole EV in biofluidi reali, con applicazioni potenziali in ambito clinico. La ricerca affronta due sfide principali nell'analisi delle eNP: il rilevamento della single EV in biofluidi complessi e la variabilità dei marcatori superficiali delle EV. Inoltre, le interazioni tra diverse eNP potrebbero portare alla formazione di complessi biologicamente rilevanti. Come parte di questo lavoro, è stata condotta un'indagine preliminare sulle interazioni tra EV e LP utilizzando tecnologie avanzate e sensibili.

Il *Capitolo 2* presenta un confronto tra due piattaforme digitali altamente sensibili per l'immuno-phenotyping, fondamentali per affrontare la complessità dei fluidi bniologici. Le piattaforme basate sulle tecnologie SiMoA e SP-IRIS sono state utilizzate per sviluppare un protocollo per la valutazione delle EV, confrontandone le prestazioni in termini di sensibilità e specificità.

Il *Capitolo 3* introduce il Membrane Sensing Peptide, (MSP), una sonda pan-specifica progettata per affrontare l'eterogeneità dei marcatori superficiali delle EV e consentire un'analisi imparziale delle EV. Integrato nella piattaforma SiMoA, MSP facilita l'analisi di singole EV direttamente in campioni reali, dimostrando una bassa affinità per le LP e un'elevata specificità per le EV. Questo metodo rileva le EV indipendentemente dall'espressione dei marcatori superficiali, come dimostrato con le EV derivate da globuli rossi (RBC-EVs). Dal punto di vista clinico, questo approccio ha permesso di distinguere i pazienti con infarto miocardico da quelli con angina stabile, basandosi su marcatori specifici associati alle EV presenti in siero e plasma, evidenziandone il potenziale diagnostico.

Il *Capitolo 4* esplora le applicazioni di MSP, evidenziandone la versatilità sia per scopi analitici che di isolamento, senza introdurre delle variabili legati all'arricchimento di sottopopolazioni. Durante un periodo di ricerca di sei mesi presso l'ETH di Zurigo, nel gruppo del professor Arosio, MSP è stato coniugato con un polimero zwitterionico coacervato per consentire l'isolamento collettivo delle EV e fungere da "one-pot assay" per l'analisi di biomarcatori EV in fluidi complessi.

Il *Capitolo 5* descrive un "approccio bottom-up" che utilizza sistemi modello (LDL, VLDL ed RBC-EVs) per studiare le interazioni EV-LP in condizioni fisiologiche. Tecnologie avanzate di immuno-affinità, tra cui Microscopie a Super-Risoluzione (SRM), Citometria a Flusso (FACS) e saggio a singola molecola (SiMoA), sono state impiegate per analizzare in dettaglio questi complessi.

In conclusione, questa tesi introduce MSP come una nuova sonda pan-specifica per le EV, offrendo un potenziale cambio di paradigma nel campo delle EV. I risultati dimostrano i vantaggi di MSP nell'analisi e nell'isolamento delle EV, così come il suo potenziale in applicazioni cliniche, aprendo la strada a test diagnostici basati sulle EV. Inoltre, è stata condotta un'indagine preliminare sulle interazioni EV-LP utilizzando tecnologie ad alta sensibilità.

Summary

Extracellular nanoparticles (eNPs), including extracellular vesicles (EVs) and lipoproteins (LPs), play a crucial role in cell-to-cell communication and influence various physiological and pathological processes. Focusing on EVs, they hold particular promise in nanomedicine for diagnostics and therapeutics, representing a large biomarker space for liquid biopsies. However, overlapping of chemical-physical properties make it challenging a specific isolation, and accurate analysis of EVs. This PhD thesis aims to develop a highly sensitive method for analyzing single EV in real biofluids, with potential applications in clinical settings. The research addresses two major challenges in eNP analysis: detecting individual EV in complex biofluids and addressing EV surface marker variability. Additionally, interactions between different eNPs may lead to the formation of biologically relevant complexes. As part of this work, a preliminary investigation of EV-LP interactions was conducted using advanced, sensitive technologies.

Chapter 2 presents a comparison between two highly sensitive digital platforms for immunophenotyping, which are crucial for addressing the complexity of real biofluids. Platforms based on SiMoA and SP-IRIS technologies were used to develop a protocol for evaluating EVs, and their performance was compared in terms of sensitivity and specificity.

Chapter 3 introduces the Membrane Sensing Peptide (MSP), a pan-specific probe designed to address the heterogeneity of EV surface markers and enable unbiased EV analysis. Integrated into the SiMoA platform, MSP facilitates single EV analysis directly in real samples, demonstrating low affinity for LPs and high specificity for EVs. This method detects EVs independently of surface marker expression, as shown with Red Blood Cell-derived EVs (RBC-EVs). Clinically, this approach distinguished myocardial infarction patients from those with stable angina based on distinct EV-associated epitope signatures in serum and plasma, highlighting its diagnostic potential.

Chapter 4 explores the applications of MSP, highlighting its versatility for both analytical and isolation purposes without introducing biases related to sub-population enrichment. During a six-month research period at ETH Zurich in Professor Arosio's group, MSP was conjugated with a zwitterionic polymer coacervate to enable collective EV isolation and serve as a "one-pot assay" for EV biomarker analysis in complex fluids.

Chapter 5 describes a "bottom-up approach" using model systems (LDL, VLDL, and RBC-EVs) to investigate EV-LP interactions under physiological conditions. Advance immune-affinity technologies, including Super-Resolution Microscopy (SRM), Flow Cytometry (FACS), and Single Molecule Array (SiMoA), were employed to study these complexes in detail.

In conclusion, this thesis introduces MSP as a novel pan-specific EV probe, offering a potential paradigm shift in the EV field. The results demonstrate MSP's advantages in EV analysis and isolation, as well as its potential in clinical applications, paving the way for EV-based diagnostic assays. Additionally, a preliminary investigation into EV-LP interactions was conducted using high-sensitivity technologies.

Chapter 1

Challenges in separation and analysis of the nanostructured secretome

1.1 Introduction

Intercellular communication is a complex yet essential process for maintaining cellular function and tissue homeostasis. One classical strategy cells use for communication is paracrine signaling. In this process, cells release soluble molecules, known as paracrine factors, into the extracellular space, where they act on nearby cells within a limited range [1] [2]. However, paracrine signaling is not the only method cells use to share information. In the past decade, a new class of nanostructures produced by cells has gained increasing prominence in cell-to-cell communication, adding to the traditional secretome. Previously defined as the collection of soluble factors, the secretome now includes various extracellular nanoparticles (eNPs) that participate in cell communication [3] [4]. These nanoparticles play a crucial role in transferring macromolecules such as proteins, lipids, and genetic material (e.g., RNA and DNA) between cells [5], forming complementary lines of communication alongside traditional paracrine signaling. Under both physiological and pathological conditions, cells secrete a diverse array of eNPs with varied composition, structure, and function. This diversity reflects their distinct cellular origins and biogenesis pathways. Key classes of eNPs include membranous particles like extracellular vesicles (EVs), micellar structures such as lipoproteins (LPs), and protein aggregates. These nanoparticles range in size from a few to several hundred nanometers and are present in all biological fluids, including blood, urine, cerebrospinal fluid, and saliva [3]. In real biological contexts, the complexity is high because multiple eNP classes coexist in the same body fluids, with their relative abundances varying across biofluids, for example, in blood, LPs are approximately five orders of magnitude more abundant than EVs. Additionally, EVs and LPs share similar physical properties such as size and density [6] [3], and this overlap makes the separation and precise analysis of individual eNP classes particularly challenging.

However, given their unique properties, eNPs hold significant promise for nanomedicine, particularly in diagnostics and therapeutics, offering novel approaches for disease detection, monitoring, and treatment. In therapeutic applications, eNPs serve as delivery vehicles, transporting drugs or genetic material and can be engineered to target specific cells, ensuring precise delivery [7]. In diagnostics, eNPs are used as circulating biomarkers in non-invasive liquid biopsies. EVs, specifically, are valuable biomarkers because they carry extensive information from their cells of origin and are

present in all biological fluids, eliminating the need for invasive procedures [8]. This makes EVs especially useful for monitoring disease and assessing cellular health with minimal discomfort to patients.

Among the main circulating extracellular nanoparticles, EVs have attracted the most interest for liquid biopsy applications, additionally, EVs can interact with lipoproteins (LPs), and these interactions have gained increasing relevance. The central focus of this thesis is to develop methods for analyzing and isolating EVs using pan-specific probes, as well as to investigate EV-LP interactions. The sections below introduce EVs and LPs, detailing their key characteristics and proprieties.

1.2 Secretome NPs

1.2.1 Extracellular vesicles

EVs are nanosized membrane vesicles released from various cell types, displaying heterogeneity in cellular origin and biogenesis, which results in differences in molecular composition (cargo and surface proteins), structure (size), and function. Typically, EVs are categorized into three main subtypes based on size and biogenesis pathways: small EVs (30–250 nm), large EVs (250–800 nm), and apoptotic bodies. EV formation involves multiple mechanisms, as illustrated in *Figure 1*. Two primary biogenesis pathways can be distinguished: intracellular formation and membrane budding.

The first pathway, responsible for small EV biogenesis, begins with the formation of early endosomes via invagination of the plasma membrane. During the following maturation process, early endosomes fuse to form late endosomes, leading to invagination of the endosomal membrane into the lumen and form intraluminal vesicles (ILVs). This process produces multivesicular bodies (MVBs) with a characteristic multivesicular appearance. MVBs ultimately fuse with the plasma membrane, releasing ILVs into the extracellular space as EVs. Conversely, large EVs are formed by direct outward budding and fission from the plasma membrane, resembling a reverse process of endocytosis [9]. In addition to traditional biogenesis pathways, other factors also influence EV production. The cell type of origin plays a significant role, for example, mesenchymal stem cells secrete more EVs than immature dendritic cells [10]. Cholesterol metabolism may increase EV output, while cell-to-cell contact, which typically occurs when cells cease dividing, can reduce EV production. External stimuli, such as Ca2+ ionophores [11] [12] [13], and cell detachment [14], can further enhance EV secretion.

Overall, EV secretion is affected by biogenesis pathways, cell origin, and external factors, impacting both the yield and composition of the EV population. These influences lead to variations in protein biomarker expression, membrane lipids, and cargo content. Additionally, the size of EVs can vary

widely, resulting in either a narrow or broad size distribution depending on the conditions of their formation.

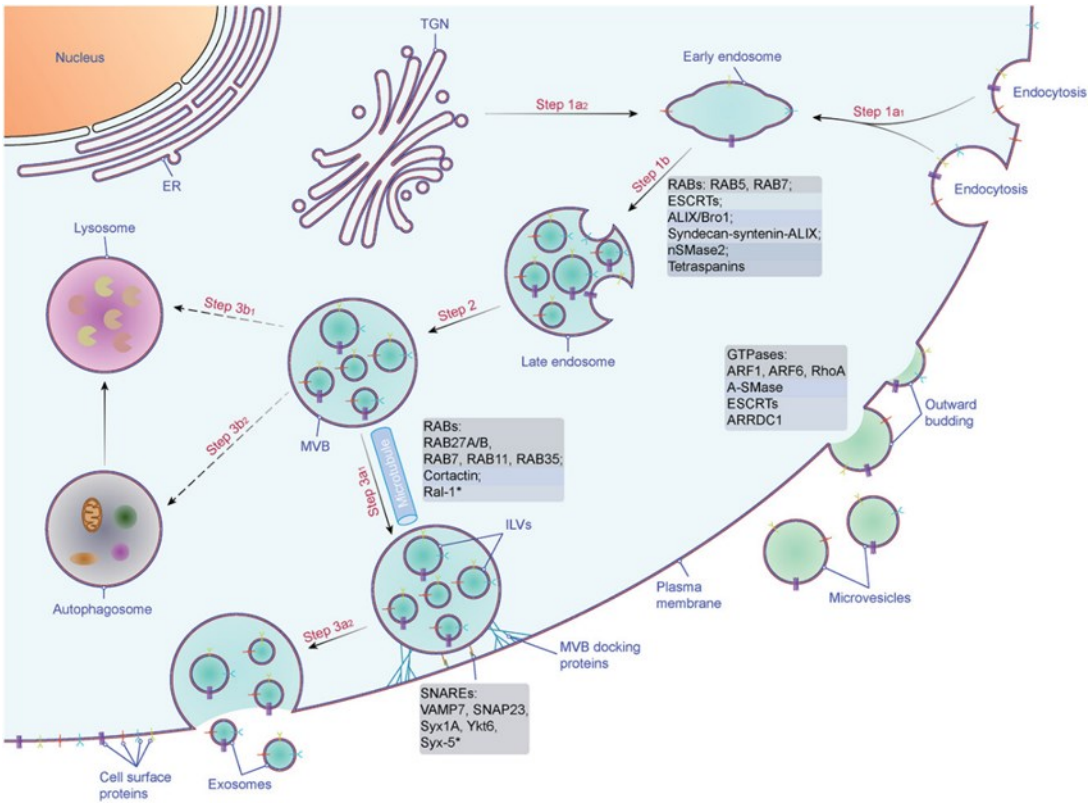

Figure 1: Two ways of EVs biogenesis and secretion are illustrated, adapted from ref [9].

1.2.2 Lipoproteins

LPs have distinct biogenesis pathways, structures, and functions compared to EVs. They are micellar structures produced by the liver and intestine, facilitating the transport of hydrophobic molecules within aqueous environments like blood plasma. Unlike EVs, LPs consist of a phospholipid monolayer surrounding a hydrophobic core of cholesteryl esters, triglycerides, and fat-soluble vitamins (A, D, E, and K), with cholesterol and apolipoproteins (Apo) embedded in the monolayer [15]. LPs are essential for lipid metabolism and homeostasis, making them clinically relevant for monitoring cardiovascular and metabolic health [16]. Additionally, LPs are valued for their colloidal properties, which have applications in drug delivery and vaccine development [16].

Lipoproteins are classified into five main types—HDL, LDL, IDL, VLDL, and chylomicrons—based on size, density, and composition, with each class reflecting specific biogenesis processes. Generally, the total lipid content inversely correlates with LP density. The main subclasses include:

***Chylomicrons**:* These are the largest lipoproteins (over 100 nm) and are produced by the intestinal epithelium to transport dietary lipids. With a density of about 0.93 g/ml,

chylomicrons undergo triglyceride breakdown by lipoprotein lipase in the bloodstream, supplying energy to various cell types. The cholesterol-rich remnants are later taken up by the liver [17].

Very low-density LPs (VLDLs): With diameters between 30 and 90 nm and a density range of 0.90–1.006 g/ml, VLDLs are secreted by the liver to transport triglycerides and cholesterol to tissues. Lipoprotein lipase hydrolyzes VLDL triglycerides for storage or energy, resulting in the formation of intermediate-density lipoproteins (IDLs) [17] [18].

Intermediate density LPs (IDLs): These 25–30 nm lipoproteins arise from VLDL metabolism, carrying a mix of triglycerides and cholesterol esters, with increased cholesterol content compared to VLDLs. IDLs are either absorbed by the liver or undergo further metabolism [19].

Low-density LPs (LDLs): Derived from IDLs, LDLs (18–30 nm, 1.019–1.063 g/ml) are the primary cholesterol carriers in the plasma. Due to their small size, LDLs can cross the endothelium, contributing to atherosclerosis [17] [20].

High-density LPs (HDLs): The smallest lipoproteins (8–15 nm, 1.063–1.210 g/ml), HDLs are synthesized by the liver and intestine, beginning with apoA-1. HDLs are critical for reverse cholesterol transport, capturing cholesterol from peripheral tissues for return to the liver or transfer to other lipoproteins. They also carry genetic material, such as miRNAs, and enzymes like metalloproteinases [17] [21].

With their diverse properties, eNPs have substantial potential as circulating biomarkers and in therapeutic applications. However, the complexity and heterogeneity of biofluids where they are present make eNP separation and analysis challenging. Notably, EVs and LPs share several physical-chemical properties. As shown in *Figure 2*, HDL overlaps in density with EVs despite being smaller, while VLDL and chylomicrons share a similar size range with EVs but differ in density. This similarity complicates achieving high-purity NPs separation and accurate analysis.

Focusing on EVs, the MISEV 2023 guidelines suggest that obtaining a sufficiently pure EV preparation typically requires a combination of at least two separation techniques, alongside highly sensitive methods when using EVs as clinical biomarkers [22]. The following section provides an

overview of traditional isolation and characterization methods, discussing their limitations and challenges.

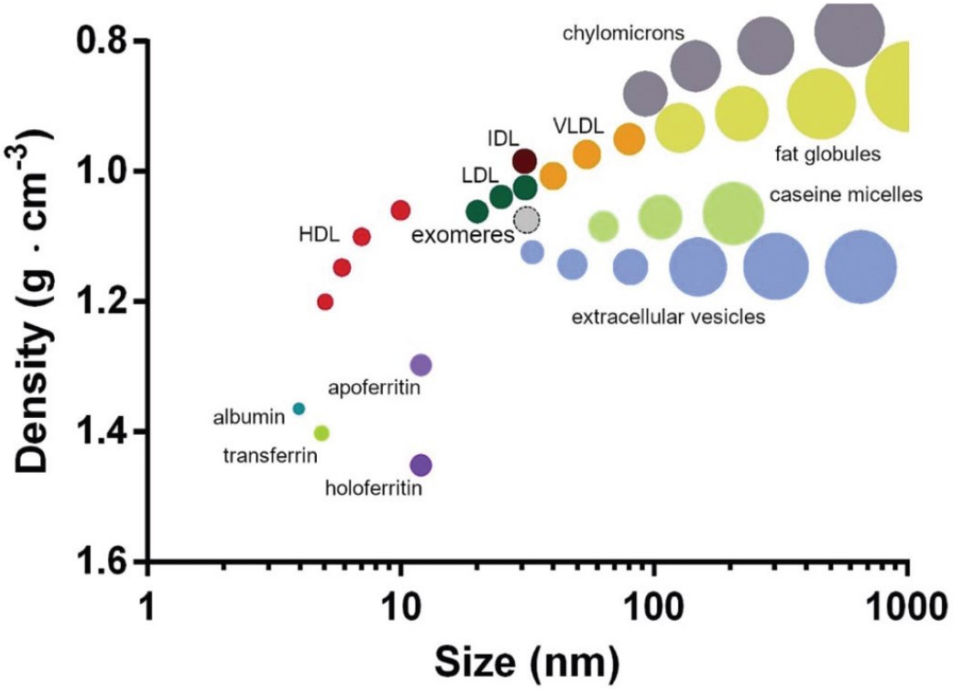

Figure 2: eNPs are plotted for density versus size. On X axis is indicated the size in nm, whereas in Y axis the density (g/cm^3). Graph shows the overlapping of EVs (blue dots) with VLDL (orange dots), chylomicrons (grey dots) and fat globules (yellow dots) , in term of size. While, HDL (red dots) shar the similar density range with EVs, adapted from ref [3].

1.3 EV isolation and analysis

1.3.1 EV isolation methods

EVs are typically characterized and analyzed after undergoing separation and concentration processes to remove other extracellular nanoparticles (eNPs) present in biological fluids. These steps are essential for obtaining pure EV samples, allowing for accurate analysis. Various techniques are employed to isolate EVs from interfering eNPs, focusing on their distinct physicochemical properties, such as size, density, charge, and surface composition (e.g., specific protein markers). The choice of method depends on the known properties of the EV source and the desired yield and purity. Common separation techniques include differential ultracentrifugation (dUC), density gradient ultracentrifugation (DG), ultrafiltration, size exclusion chromatography (SEC), polymer-based precipitation, and antibody-coupled magnetic bead affinity capture. Density-based methods, such as ultracentrifugation, separate eNPs based on their density. However, a key limitation is the potential co-isolation of particles with similar density ranges, such as certain classes of lipoproteins (e.g., HDL)

or protein aggregates. The two main types of preparative ultracentrifugation used for EV isolation are differential ultracentrifugation (dUC) and density gradient ultracentrifugation (DG). DG utilizes layers of varying sucrose concentrations to separate particles, offering higher purity in EV preparations but with trade-offs like lower yield, time-intensive processing, and limited sample volume.

Size-based approaches, including ultrafiltration (UF) and size exclusion chromatography (SEC), separate eNPs based on size or molecular weight. These methods effectively isolate EVs from protein aggregates, soluble macromolecules, and smaller lipoprotein classes (e.g., HDL and LDL), as well as from larger particles like cell debris. However, similarly sized particles such as very-low-density lipoproteins (VLDL) or chylomicrons may also be co-isolated. Polymer precipitation is another size-based technique where "polymer nets" capture eNPs within a specific size range. Although this method provides a good EV yield, it has drawbacks, including difficulties in removing residual polymers and the inability to distinguish EVs from non-EV particles of similar size.

Immunoaffinity capture is a selective method that targets specific surface markers on EVs, particularly common proteins like tetraspanins (CD9, CD63, and CD81). This approach offers high specificity but often results in low and variable yields, depending on the abundance of the target markers and the affinity of the antibodies used. Importantly, affinity-based protocols targeting a single tetraspanin are specific to certain EV subtypes, thus enriching particular EV sub-populations. However, not all EVs express tetraspanin proteins, so other surface markers can be used [23] [24].

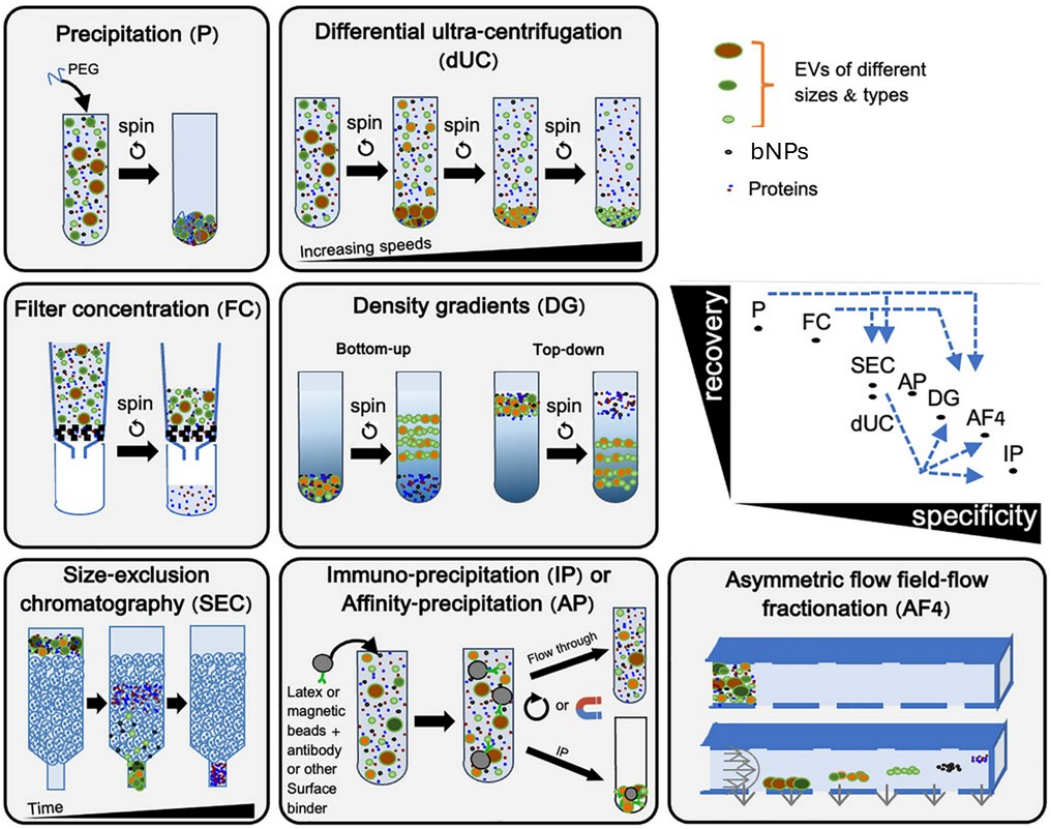

Figure 3: schemas of most common isolation methods for EVs are reported. The EVs separation by size: Size-Exclusion Chromatography (SEC), Filter Concentration (FC), Polymer Precipitation (P) and, Asymmetric flow field-flow fractions (AF4). EVs recovery based on density: Density Gradients (DG) and Differential ultra-centrifugation (dUC); method exploits specific markers, immuno-precipitation. Graph (on the right side) shows the position of some EVs isolation methods in terms of recovery (yield) versus specificity. Dashed blue arrows indicate combinations of methods resulting in increased specificity, adapted from ref [22].

All the methods discussed above and shown in *Figure 3* rely on the physical-chemical properties of EVs, which can vary across different samples. Due to the limitations of individual isolation techniques and the diverse properties of eNPs, combining techniques based on different on the physical-chemical properties of EVs is usually required to effectively separate EVs from other eNPs [22]. Although additional separation steps can enhance purity, they often result in reduced EV yield. In immune-affinity strategies, high purity is achieved through the selectivity of the capturing probes; however, this selectivity can lead to low yield due to the heterogeneous expression of surface markers. To overcome this limitation, a pan-specific EV probe capable of capturing the entire EV population while maintaining specificity could represent a significant advancement in the field. Integrating such a probe into an immunoaffinity isolation system could effectively address the challenges of both low yield and specificity.

1.3.2 EV characterization and analytical methods

Characterizing EVs is crucial not only for confirming their presence in a sample but also for assessing purity and identifying potential contributions from other eNPs. This process is challenging due to the molecular heterogeneity of EVs, the lack of universal identification methods, and the low specificity of many measurement techniques [22]. As a result, no single method can fully satisfy all the requirements for EV characterization. To address this, the MISEV 2023 guidelines strongly recommend using orthogonal methods, which involve assessing the same parameter through different approaches to reduce shared biases (e.g., measuring diameter using both optical and non-optical techniques). Using orthogonal methods is especially important to avoid misidentifying co-isolated particles as EVs [22]. The level of analysis required for EV samples can vary depending on the study's objectives. For instance, bulk analysis provides comprehensive information on the overall EV population, while some applications may require the evaluation of specific marker expression or relative abundance to monitor physiological or pathological states. In such cases, highly accurate and sensitive technologies are essential, with single-particle analyses offering the precision needed to assess biomarkers on individual EV [25].

1.3.3 Bulk analysis vs. Single vesicle

Studying the collective characteristics of an entire EV population is known as "bulk analysis." This approach provides an overall view of the molecular content of EVs, including proteins, lipids, and nucleic acids, without distinguishing the characteristics of individual vesicle. Protein content is typically measured using colorimetric assays, such as BCA or Bradford. Lipids are also assessed by colorimetric assays, with the sulfo-phospho-vanillin (SPV) assay being one of the most common for EV applications. While, PCR is frequently employed for identification, quantification, and determining localization (inside or outside the EV), of nucleic acids. These methods are valuable for obtaining broad insights into EV composition in a specific context. Other techniques that provide bulk information on specific markers include Western blotting, which identifies the presence of specific proteins after a electrophoretic separations, and ELISA, which uses immunoassay approach to quantify EV markers. Additionally, mass spectrometry enables high-throughput peptide analysis for a more comprehensive examination of EV protein composition, offering greater depth and precision in protein identification than Western blotting or ELISA [25].

In contrast, "single-vesicle analysis" focuses on studying individual EVs to characterize their specific properties and contents. Unlike bulk analysis, which provides an overview of the entire EV population, single-vesicle analysis highlights the heterogeneity within the population by examining

each vesicle individually. This approach reveals variations in size and molecular composition, including surface and cargo proteins, lipids, and nucleic acids [25]. Techniques used for single-vesicle analysis include high-resolution imaging methods such as TEM, Cryo-EM, and super-resolution microscopy. Immunophenotyping assays, like Single Molecule Arrays (SiMoA) and SP-IRIS, also enable single-particle analysis. These methods offer high accuracy and are particularly valuable for understanding and tracking fluctuations in EV biomarkers.

1.3.4 Biophysical analysis

Most characterization methods leverage EV biophysical properties to assess size distribution, particle concentration, and morphology in EV preparations. Techniques such as Nanoparticle Tracking Analysis (NTA), Dynamic Light Scattering (DLS), and Tunable Resistive Pulse Sensing (TRPS) are primarily used to determine size distribution and particle concentration. Additionally, microscopy techniques, including Atomic Force Microscopy (AFM) and various forms of Electron Microscopy (such as Transmission Electron Microscopy (TEM), Cryo-EM, and Scanning Electron Microscopy (SEM)), are commonly employed to analyze EV morphology. While the first set of techniques is suited for bulk analysis, microscopy methods can be applied to both bulk and single-vesicle analyses. For instance, AFM can assess the size distribution and nanomechanical properties of the entire EV population, while also providing detailed insights into the size and mechanical properties of individual EV [26]. TEM and Cryo-EM offer high-resolution imaging to observe the morphology and shape of individual EVs [27] [28]. Together, these methods are essential for gaining in-depth structural insights into EVs.

A recent study demonstrated fine characterization of EVs and LPs using AFM and Cryo-EM to illustrate distinct particle structures (*Figure 4*). In particular, EVs analyzed by cryo-EM appeared enclosed by a high-contrast boundary (red arrows) with disordered material at the periphery (green arrows), likely corresponding to the lipid bilayer and associated membrane proteins and glycans. Among LPs, only VLDLs and chylomicrons exhibited high-contrast boundaries (red arrows), while HDLs, IDLs, and LDLs showed no significant contrast differences between their inner and outer regions (*Figure 4*). No external decoration or internal cargo was detectable in any LP samples [29] [30].

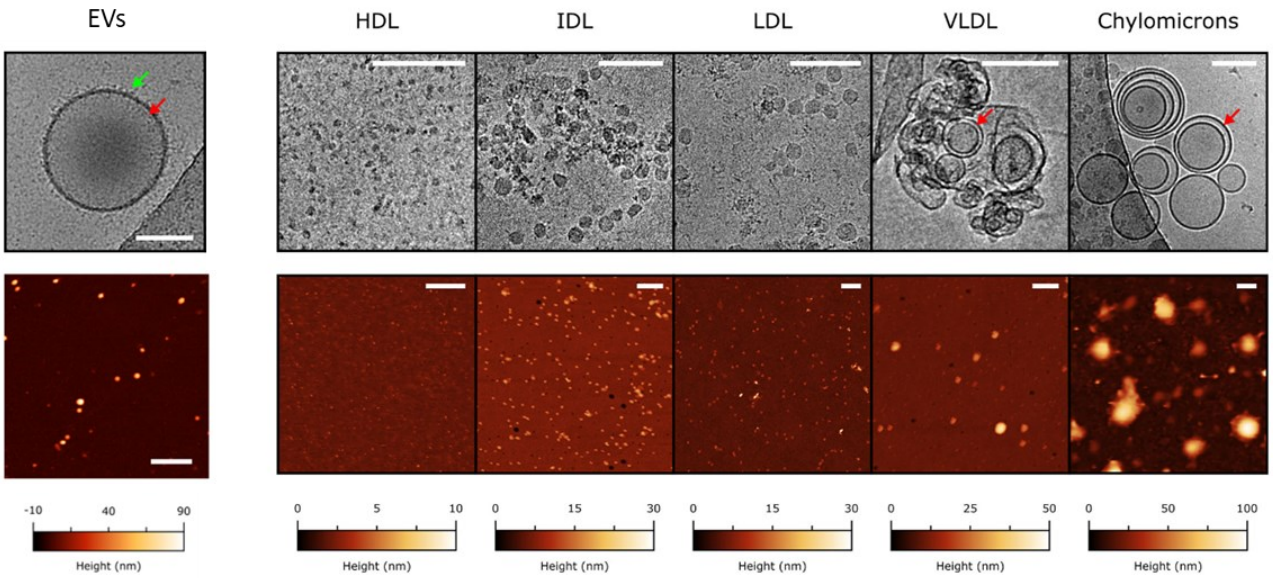

Figure 4: Typical cryo-EM and AFM images of various eNPs (EVs and LPs) are reported, adapted from ref [30] [29].

Microscopy techniques can also be used to evaluate the presence of specific EV markers through fluorescence detection, with Super-resolution Microscopy (SRM) being particularly useful for this purpose. EV membrane targets or cargo molecules are labelled with reagents, typically antibodies, containing appropriate fluorophores. Common strategies for labeling EVs include immune-affinity binding, covalent labelling, and the use of lipophilic dyes. The immune-affinity approach provide valuable information on EV phenotyping and the relative abundance of surface proteins.

1.3.5 Biomarkers analysis

The growing interest in EVs as biomarkers has driven the development of immunoassays designed to identify and quantify specific protein markers (*Figure 5*). Biomarker expression can be assessed either by analyzing the entire EV population (bulk approach) or through high-precision techniques that examine individual vesicle or molecule. Immuno-sandwich bead-based methods, such as flow cytometer bead-based assays and Single Molecule Array (SiMoA), are commonly used for EV protein profiling. Additionally, techniques like SP-IRIS, based on microarray chip methods, allow for EV phenotyping and also provide interferometric single-particle counting. These advanced methods offer high resolution in EV analysis, enhancing our understanding of EV heterogeneity and their potential as biomarkers in diagnostic applications.

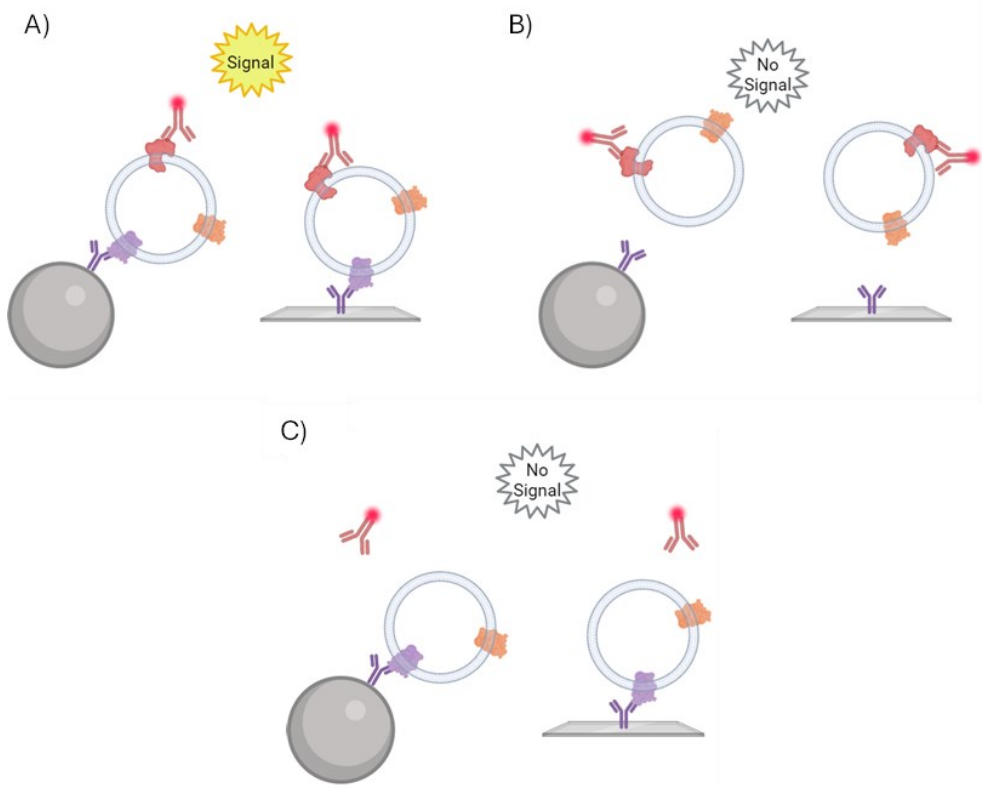

Figure 5: Generic immunophenotyping Schema: bead-based and chip-based immunoassays are illustrated. In the bead-based approach, the capture probe antibody is conjugated to a bead, while in the chip-based approach, the capture antibody is immobilized on a flat surface; for both assays detection is achieved using a labelled antibody. A) when the capture and detector protein targets are expressed on the EV surface, a positive signal is observed. In contrast, no signal is observed when the capture target is absent from the EV surface (B) or when the detector target is not present (C).

Focusing on bead-based methods, flow cytometry is widely used to investigate EV surface markers. Originally designed for microscale particles like single cells, it has been adapted for nanoscale particles like EVs through the use of microbeads. In this approach, antibody-conjugated beads capture EVs, and fluorescence-labelled antibodies used for detection. As individual particle pass through a laser beam within a sheath flow, light scattering is measured, enabling high-throughput, multiplexed analysis; the bead-based protocols allow EV bulk analysis. Staining intensity differences yield semi-quantitative results, as signal variations may reflect particle concentration, epitope density, size distribution, or the abundance of EV sub-populations.

Move on a second bead-based platform, SiMoA, was originally introduced to measure the soluble protein at single molecule level [31], but is now widely used for EV analysis. In this technique, paramagnetic beads functionalized with specific EV capture probes (such as tetraspanin antibodies or

other surface markers) are incubated with samples. Detection proceeds in two steps: incubation with a biotinylated antibody, followed by a second incubation with streptavidin-β-galactosidase (SBG), which interacts with a fluorogenic substrate. The advantages of SiMoA include its high sensitivity, enabling the detection of EV sub-populations and quantification of biomarkers expressed at low levels. Full SiMoA protocol is deeply explained in *Chapter 2*.

The SP-IRIS platform, which utilizes microarray technology, combines interferometric and fluorescence detection to evaluate particle capture by affinity agents on a microarray [32]. In the interference reflectance imaging sensor (IRIS) mode, interference patterns from scattered light are used to derive the size and number of captured particles [33]. Fluorescence detection enhances this method, allowing captured particles to be labelled with fluorescent probes across up to three simultaneous fluorescence channels; performing surface protein profiling (phenotyping). SP-IRIS technology will be discussed in detail in *Chapter 2*.

These highly sensitive platforms offer significant opportunities for in-depth profiling of EV markers. However, antibody affinity-based approaches are limited to the proteins expressed on the EV surface and the antibodies' affinity for their targets. To address the issue of EV heterogeneity, a pan-specific probe for EVs could be utilized, as proposed for isolation methods. Such a probe, targeting a consistent marker across all EVs, could have widespread applications in the EV research community. Integrating this type of probe into analytical platforms would facilitate unbiased analysis of entire EV populations, making EV-based analyses more robust and applicable in real samples and diagnostics. In the following sections, a peptide sequence from the Bradykinin protein, which has an affinity for bilayer membrane with high curvature, is proposed as a new pan-specific EV probe.

1.4 Addressing EV heterogeneity using a Pan-specific probe

In recent years, the heterogeneity of protein expression on EV surfaces has increasingly become evident in the EV field. As the vast majority of immunoaffinity methods for EV isolation is based on anti-tetraspanin (CD9, CD63, CD81) antibodies. This variability reverberates both on the isolation and downstream analysis of EVs, which should be seen as specific to tetraspanin-rich EV sub-fractions [34] [35]. Consequently, immunoaffinity-based approaches relying on single surface markers, such as individual tetraspanins, may provide incomplete data. Isolation, enrichment, and detection methods based on these limited markers can lead to missed or misleading biomarker information. Furthermore, it is well established that tetraspanin expression varies significantly in real samples, differing among patients in both pathological and physiological conditions [34] [36]. It was

demonstrated that up to 80% of diagnostically relevant EVs are missed when using a single tetraspanin for affinity isolation, and 36-47% are lost even with a tetraspanin cocktail. This variability poses additional challenges to developing robust, consistent analytical methods for EVs in diagnostic applications. A pan-specific EV probe, here defined as an affinity probe that is not biased by inconsistent surface protein expression, could therefore generate significant interest in the field. As MISEV 2023 guidelines definition, "extracellular vesicles are particles released from cells, enclosed by a lipid bilayer". In this sense, the characteristic and highly curved lipid membrane could intriguingly be identified as a pan-specific "epitope" of EVs and, as such, function as a universal target for EV affinity isolation. In the literature several protein domains or peptides are reported displaying affinity for lipids bilayers; in the following section curvature sensing proteins or peptides are introduce as a class of pan-specific affinity ligand for nano-size lipids particles, including EVs regardless of their origin of phenotyping.

1.4.1 A novel EV probe: Membrane Sensing Peptide

Many proteins play a crucial role in the dynamic regulation of membrane curvature that takes place during various cellular processes, including vesicle secretion. Notably, some proteins specifically detect and bind to highly curved membranes [37] [38] [39]. Various globular domains, such as pleckstrin homology and C2 domains, can bind to cellular membranes or particular phospholipid patterns. Structural studies of these domains have provided significant insights into membrane binding, revealing how diverse domains interact with membranes, what features they recognize, and how these interactions are regulated [37]. Furthermore, it was demonstrated that the amphipathic N-terminal helix of endophilin targets curved membranes by binding to hydrophobic packing defects in the lipid bilayer, which increase with greater membrane curvature. Additionally, the size distribution of these defects decreases exponentially with curvature. Importantly, even on highly curved membranes, defects large enough to accommodate the hydrophobic face of the helix were never observed [39]. Other examples include the Bin–Amphiphysin–Rvs (BAR) domain [40], ArfGAP1 lipid-packing sensor(ALPS) proteins [41], C2B domain of synaptotagmin-I and the effector domain of the myristoylated alanine-rich C-kinase substrate protein (MARCKS-ED) [42] and the domain of Bradykinin proteins [43].

Peptides derived from membrane-sensing proteins have emerged as effective, easily synthesized probes for targeting highly curved membranes [43] [44]. In this thesis, I will focus on molecular constructs based on a core short peptide sequence (RPPGFSPFR) derived from Bradykinin, which was reported to bind specifically to highly curved lipid nanovesicles, including EVs. Here, this sequence is referred to as Membrane Sensing Peptide (MSP). This approach potentially offers several

advantages over traditional protein-based methods and, while not displacing the need for antibody-based solutions, it could be anticipated as complementary and valuable to them. MSP shows specific affinity for highly curved lipid membranes, minimizing potential biases introduced by soluble antigens, bypassing the variability in antibody specificity and affinity that can affect EV capture efficiency, and addressing challenges associated with inconsistent or low-abundance protein markers, factors that often undermine the robustness of comparative analyses (*Figure 6*).

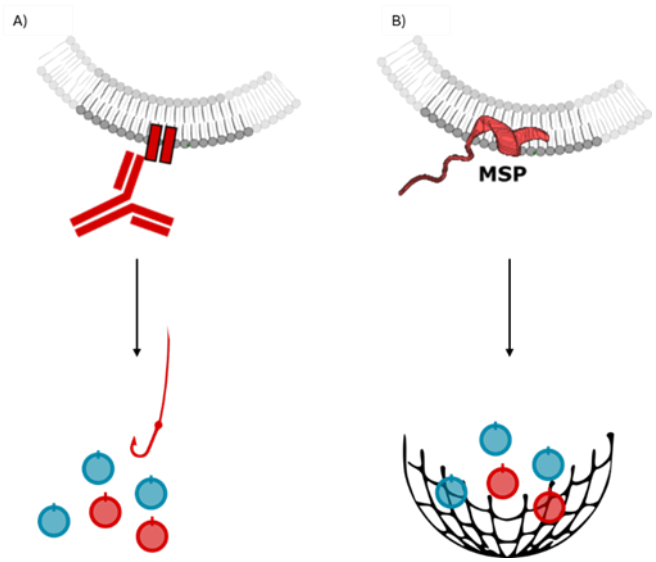

Figure 6: A schema of antibody and MSP capture are reported. On the left, the antibody approach shows how to select a sub-population of EV (A), while on the right, MSP is more comparable to a net, able to recruit all EVs.

1.4.2 Binding mechanism: MSP-membrane interaction

Targeting a specific yet "universal" EV marker like the lipid membrane could represent a significant paradigm shift, improving the consistency and robustness of analytical tools. The main difference between the MSP approach and immune-affinity protein-surface systems is that MSP-based EV recognition and capture involve multiple peptides and require a cooperative mechanism. In contrast, antibody-based systems need only a single molecule to recognize a specific surface protein and capture the EV. Small EV membranes have distinct physical and chemical properties in the extracellular space. For instance, small EVs feature highly curved membranes with outer leaflets rich in anionic, unsaturated phospholipids (such as phosphatidylserine) and characteristic lipid-packing defects [43] [44]. To explain the interaction between MSP and the lipid bilayer, a two-step binding mechanism was proposed [44]. First, initial membrane recognition and binding occur through complementary electrostatic interactions between the positively charged on the MSP chain and the

negatively charged phospholipids on the EV outer membrane. This interaction is further stabilized by hydrophobic forces; the two phenylalanine residues in the MSP chain can insert into the membrane defects typical of highly curved membranes. This two-step binding mechanism is characteristic of amphipathic peptides (*Figure 7*).

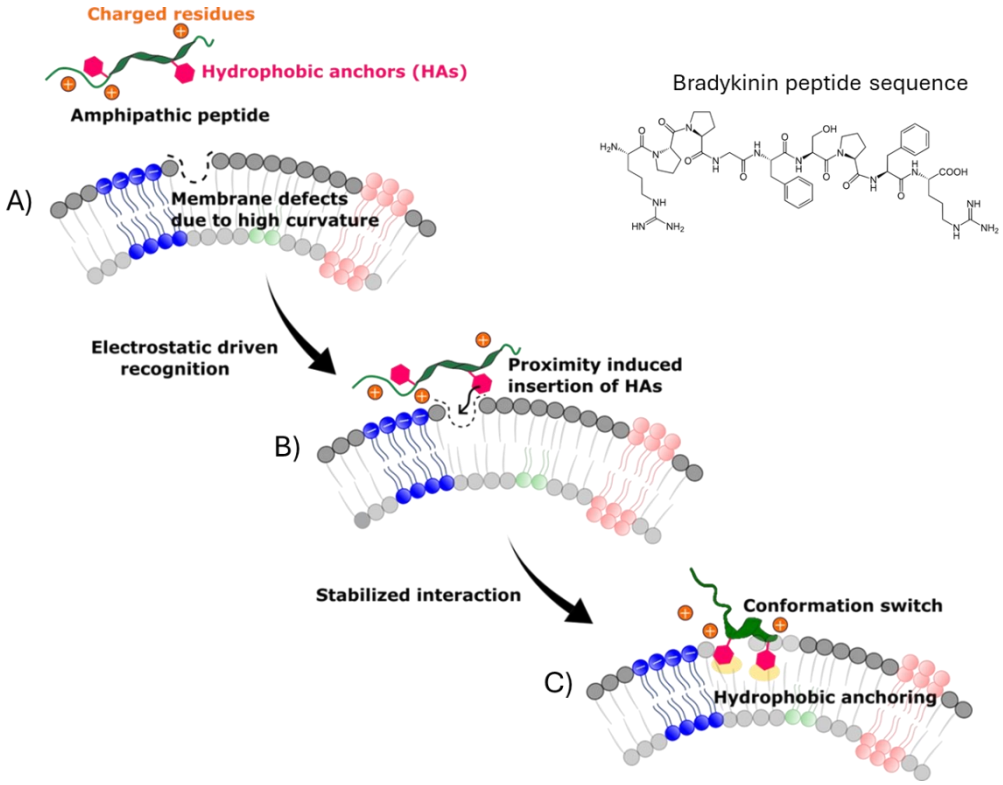

Figure 7: MSP-membrane interaction mechanism is reported. A) shows amphipathic peptide with hydrophobic residues and positive charge, and the high curvature lipid membrane. The driving force of this binding are electrostatic interactions; positive charges present on peptide sequence and negative one on the lipid membrane surface (B). Stabilization step is led by hydrophobic forces, peptide aromatic moieties anchor the lipid membrane defects (C). Furthermore, MSP Bradykinin sequence is drawn (up-right on the panel), adapted from ref [44].

1.5 Aim of the Thesis

This thesis tackles two main challenges: decoding the eNPs landscape to achieve single EV analysis in real biofluids, and addressing the heterogeneity of EV surface markers. To overcome the first challenge, digital platforms are essential for EV analysis due to their high sensitivity, which allows for the detection and analysis of single EV. In this study, immune-affinity-based protocols for EV analysis were developed for two digital platforms based on: SiMoA and SP-IRIS technologies. *Chapter 2* focuses on comparing the performance of these platforms in terms of sensitivity, specificity, and reproducibility for individual EV phenotyping.

The second challenge involves the heterogeneity of EV surface protein expression, as it is increasingly evident that no single marker consistently demonstrates robust expression across various samples, subjects, and disease stages. Therefore, a pan-specific probe offers a promising solution to overcome EV phenotype variability. In *Chapter 3*, MSP was integrated into the SiMoA platform to detect single EVs in real biofluids. While, during my visiting period at ETH Zurich, MSP was combined with a zwitterionic polymer to facilitate EV recruitment and enrichment, enabling a “one-pot assay” for comprehensive EV analysis; these results are reported in *Chapter 4.* As previously reported the secretoma landscape is crowded with eNPs, in *Chapter 5*, EV-LP interactions were studied, and single particle and immune-affinity technologies were applied to investigate these complexes. Nowadays, it is still challenging to detect these EV-LP interactions in real biofluids, so a "bottom-up approach" was applied to overcome this issue, using a model system mimicking physiological conditions.

1.6 References

[1] S. L. N. Maas, X. O. Breakefield, and A. M. Weaver, "Extracellular Vesicles: Unique Intercellular Delivery Vehicles," Mar. 01, 2017, *Elsevier Ltd*. doi: 10.1016/j.tcb.2016.11.003.

[2] R. Vescovi *et al.*, "Collapse of the plasmacytoid dendritic cell compartment in advanced cutaneous melanomas by components of the tumor cell secretome," *Cancer Immunol Res*, vol. 7, no. 1, pp. 12–28, Jan. 2019, doi: 10.1158/2326-6066.CIR-18-0141.

[3] S. Busatto *et al.*, "The nanostructured secretome," Jan. 01, 2020, *Royal Society of Chemistry*. doi: 10.1039/c9bm01007f.

[4] S. Gurunathan, M. H. Kang, M. Jeyaraj, M. Qasim, and J. H. Kim, "Review of the isolation, characterization, biological function, and multifarious therapeutic approaches of exosomes," Apr. 01, 2019, *MDPI*. doi: 10.3390/cells8040307.

[5] G. Raposo and W. Stoorvogel, "Extracellular vesicles: Exosomes, microvesicles, and friends," Feb. 2013. doi: 10.1083/jcb.201211138.

[6] R. E. Ghebosu, J. Pendiuk Goncalves, and J. Wolfram, "Extracellular Vesicle and Lipoprotein Interactions," Jan. 10, 2024, *American Chemical Society*. doi: 10.1021/acs.nanolett.3c03579.

[7] I. K. Herrmann, M. J. A. Wood, and G. Fuhrmann, "Extracellular vesicles as a next-generation drug delivery platform," Jul. 01, 2021, *Nature Research*. doi: 10.1038/s41565-021-00931-2.

[8] R. E. Veerman, G. Güçlüler Akpinar, M. Eldh, and S. Gabrielsson, "Immune Cell-Derived Extracellular Vesicles – Functions and Therapeutic Applications," May 01, 2019, *Elsevier Ltd*. doi: 10.1016/j.molmed.2019.02.003.

[9] F. Teng and M. Fussenegger, "Shedding Light on Extracellular Vesicle Biogenesis and Bioengineering," Jan. 01, 2021, *John Wiley and Sons Inc*. doi: 10.1002/advs.202003505.

[10] T. S. Chen *et al.*, "Enabling a robust scalable manufacturing process for therapeutic exosomes through oncogenic immortalization of human ESC-derived MSCs," *J Transl Med*, vol. 9, Apr. 2011, doi: 10.1186/1479-5876-9-47.

[11] A. Savina, M. Furlán, M. Vidal, and M. I. Colombo, "Exosome release is regulated by a calcium-dependent mechanism in K562 cells," *Journal of Biological Chemistry*, vol. 278, no. 22, pp. 20083–20090, May 2003, doi: 10.1074/jbc.M301642200.

[12] P. Kucharzewska *et al.*, "Exosomes reflect the hypoxic status of glioma cells and mediate hypoxia-dependent activation of vascular cells during tumor development," *Proc Natl Acad Sci U S A*, vol. 110, no. 18, pp. 7312–7317, Apr. 2013, doi: 10.1073/pnas.1220998110.

[13] H. W. King, M. Z. Michael, and J. M. Gleadle, “Hypoxic enhancement of exosome release by breast cancer cells,” *BMC Cancer*, vol. 12, Sep. 2012, doi: 10.1186/1471-2407-12-421.

[14] R. B. Koumangoye, A. M. Sakwe, J. S. Goodwin, T. Patel, and J. Ochieng, “Detachment of breast tumor cells induces rapid secretion of exosomes which subsequently mediate cellular adhesion and spreading,” *PLoS One*, vol. 6, no. 9, 2011, doi: 10.1371/journal.pone.0024234.

[15] L. Margolis and Y. Sadovsky, “The biology of extracellular vesicles: The known unknowns,” *PLoS Biol*, vol. 17, no. 7, Jul. 2019, doi: 10.1371/journal.pbio.3000363.

[16] S. Busatto *et al.*, “Lipoprotein-based drug delivery,” Jan. 01, 2020, *Elsevier B.V.* doi: 10.1016/j.addr.2020.08.003.

[17] R. W. Mahley, T. L. Innerarity, S. C. Rall, and K. H. Weisgraber, “I I revzezo Plasma lipoproteins: apolipoprotein structure and function.”

[18] J. K. Huang and H. C. Lee, “Emerging Evidence of Pathological Roles of Very-Low-Density Lipoprotein (VLDL),” Apr. 01, 2022, *MDPI*. doi: 10.3390/ijms23084300.

[19] H. N. Ginsberg, Y. L. Zhang, and A. Hernandez-Ono, “Regulation of plasma triglycerides in insulin resistance and diabetes,” May 2005. doi: 10.1016/j.arcmed.2005.01.005.

[20] M. V. Holmes and M. Ala-Korpela, “What is ‘LDL cholesterol’?,” Apr. 01, 2019, *Nature Publishing Group*. doi: 10.1038/s41569-019-0157-6.

[21] J. Heeren and L. Scheja, “Metabolic-associated fatty liver disease and lipoprotein metabolism,” Aug. 01, 2021, *Elsevier GmbH*. doi: 10.1016/j.molmet.2021.101238.

[22] J. A. Welsh *et al.*, “Minimal information for studies of extracellular vesicles (MISEV2023): From basic to advanced approaches,” *J Extracell Vesicles*, vol. 13, no. 2, Feb. 2024, doi: 10.1002/jev2.12404.

[23] J. Kowal *et al.*, “Proteomic comparison defines novel markers to characterize heterogeneous populations of extracellular vesicle subtypes,” *Proc Natl Acad Sci U S A*, vol. 113, no. 8, pp. E968–E977, Feb. 2016, doi: 10.1073/pnas.1521230113.

[24] M. Mathieu *et al.*, “Specificities of exosome versus small ectosome secretion revealed by live intracellular tracking of CD63 and CD9,” *Nat Commun*, vol. 12, no. 1, Dec. 2021, doi: 10.1038/s41467-021-24384-2.

[25] R. T. T. Morales and J. Ko, “Future of Digital Assays to Resolve Clinical Heterogeneity of Single Extracellular Vesicles,” Aug. 23, 2022, *American Chemical Society*. doi: 10.1021/acsnano.2c04337.

[26] G. Bordanaba-Florit, F. Royo, S. G. Kruglik, and J. M. Falcón-Pérez, “Using single-vesicle technologies to unravel the heterogeneity of extracellular vesicles,” Jul. 01, 2021, *Nature Research*. doi: 10.1038/s41596-021-00551-z.

[27] J. De Vrij *et al.*, "Quantification of nanosized extracellular membrane vesicles with scanning ion occlusion sensing," *Nanomedicine*, vol. 8, no. 9, pp. 1443–1458, 2013, doi: 10.2217/nnm.12.173.

[28] J. L. Höög and J. Lötvall, "Diversity of extracellular vesicles in human ejaculates revealed by cryo-electron microscopy," *J Extracell Vesicles*, vol. 4, no. 1, Jan. 2015, doi: 10.3402/jev.v4.28680.

[29] A. Ridolfi *et al.*, "AFM-Based High-Throughput Nanomechanical Screening of Single Extracellular Vesicles," *Anal Chem*, vol. 92, no. 15, pp. 10274–10282, Aug. 2020, doi: 10.1021/acs.analchem.9b05716.

[30] A. Ridolfi *et al.*, "Particle profiling of EV-lipoprotein mixtures by AFM nanomechanical imaging," *J Extracell Vesicles*, vol. 12, no. 10, Oct. 2023, doi: 10.1002/jev2.12349.

[31] D. M. Rissin *et al.*, "Single-molecule enzyme-linked immunosorbent assay detects serum proteins at subfemtomolar concentrations," *Nat Biotechnol*, vol. 28, no. 6, pp. 595–599, Jun. 2010, doi: 10.1038/nbt.1641.

[32] G. G. Daaboul *et al.*, "Digital Detection of Exosomes by Interferometric Imaging," *Sci Rep*, vol. 6, Nov. 2016, doi: 10.1038/srep37246.

[33] G. Young *et al.*, "Quantitative mass imaging of single biological macromolecules." [Online]. Available: https://www.science.org

[34] R. R. Mizenko *et al.*, "Tetraspanins are unevenly distributed across single extracellular vesicles and bias sensitivity to multiplexed cancer biomarkers," *J Nanobiotechnology*, vol. 19, no. 1, Dec. 2021, doi: 10.1186/s12951-021-00987-1.

[35] C. Han *et al.*, "Single-vesicle imaging and co-localization analysis for tetraspanin profiling of individual extracellular vesicles," *J Extracell Vesicles*, vol. 10, no. 3, Jan. 2021, doi: 10.1002/jev2.12047.

[36] N. Karimi, R. Dalirfardouei, T. Dias, J. Lötvall, and C. Lässer, "Tetraspanins distinguish separate extracellular vesicle subpopulations in human serum and plasma – Contributions of platelet extracellular vesicles in plasma samples," *J Extracell Vesicles*, vol. 11, no. 5, May 2022, doi: 10.1002/jev2.12213.

[37] M. A. Lemmon, "Membrane recognition by phospholipid-binding domains," Feb. 2008. doi: 10.1038/nrm2328.

[38] B. Antonny, "Mechanisms of membrane curvature sensing," *Annu Rev Biochem*, vol. 80, pp. 101–123, Jul. 2011, doi: 10.1146/annurev-biochem-052809-155121.

[39] H. Cui, E. Lyman, and G. A. Voth, “Mechanism of membrane curvature sensing by amphipathic helix containing proteins,” *Biophys J*, vol. 100, no. 5, pp. 1271–1279, Mar. 2011, doi: 10.1016/j.bpj.2011.01.036.

[40] V. K. Bhatia *et al.*, “Amphipathic motifs in BAR domains are essential for membrane curvature sensing,” *EMBO Journal*, vol. 28, no. 21, pp. 3303–3314, Nov. 2009, doi: 10.1038/emboj.2009.261.

[41] J. Bigay, J. F. Casella, G. Drin, B. Mesmin, and B. Antonny, “ArfGAP1 responds to membrane curvature through the folding of a lipid packing sensor motif,” *EMBO Journal*, vol. 24, no. 13, pp. 2244–2253, Jul. 2005, doi: 10.1038/sj.emboj.7600714.

[42] A. J. De Jesus, O. R. White, A. D. Flynn, and H. Yin, “Determinants of Curvature-Sensing Behavior for MARCKS-Fragment Peptides,” *Biophys J*, vol. 110, no. 9, pp. 1980–1992, May 2016, doi: 10.1016/j.bpj.2016.04.007.

[43] J. P. Saludes *et al.*, “Multivalency amplifies the selection and affinity of bradykinin-derived peptides for lipid nanovesicles,” *Mol Biosyst*, vol. 9, no. 8, pp. 2005–2009, Aug. 2013, doi: 10.1039/c3mb70109c.

[44] A. Gori *et al.*, “Membrane-binding peptides for extracellular vesicles on-chip analysis,” *J Extracell Vesicles*, vol. 9, no. 1, Jan. 2020, doi: 10.1080/20013078.2020.1751428.

Chapter 2

Advanced digital platform for EV immunophenotyping

2.1 Introduction

In a real biofluid context, where various eNPs coexist, the high sensitivity of digital platforms become critically important [1] [2]. These techniques are essential for distinguishing EVs from other nanoparticles in body fluids, allowing extraction of clinically relevant information for early disease detection and monitoring. Digital counting provides a broader linear and dynamic range of detectable target concentrations, making it more precise, quantitative, and sensitive than traditional analog measurements [1] [3]. By enabling single-particle or single-molecule detection, digital platforms allow for a comprehensive and accurate analysis that captures all EV sub-populations, including those with minor biomarker expressions. Without this sensitivity, EV sub-populations with potential clinical relevance may remain undetected, potentially altering results and limiting biomarker discovery. Thus, advanced digital platforms can fill the gap, facilitating more accurate detection and analysis, which is crucial for effective biomarker discovery and employ EVs in clinical applications. The following section details the operation of these digital platforms.

2.1.1 Digital platform for single EV analysis

Digital EV platforms not only provide low limits of detection (LOD) but also enable high-throughput processing of multiple samples, making them particularly valuable for clinical applications where sensitivity and throughput are essential. These capabilities are critical for leveraging EVs as diagnostic tools, especially in early pathological stages where EVs of interest may be in low abundance against a background of EVs shed by healthy cells. Traditional bulk EV analyses are inadequate for decoding the heterogeneity within individual EV samples, especially in clinical scenarios where rare pathological EV sub-populations may exist. High-throughput, single-EV, or 'digital' profiling methods are thus essential for dissecting the molecular content of EV subsets and addressing these analytical limitations [4].

In digital assays, individual biomolecules or particles, such as EVs, are treated as single entities, following a Poisson distribution ($\lambda = 0.1$) to minimize the likelihood of multiple entities per compartment. This enables digital counting of analytes as either positive or negative. In contrast, bulk analysis uses analog measurements, where signal strength decreases as analytes are diluted, often falling below detection thresholds. A key requirement for digital detection is achieving an optimal

ratio between target molecules and microcompartments; an excess of analyte prevents random partitioning at 0 or 1 target molecule per microcompartment, as per Poisson statistics. Signals in each compartment are amplified through chemical or enzymatic reactions and detected via fluorescence, allowing for precise counting and concentration measurement. Various partitioning methods, including droplet microfluidics, microchambers, and nanostructures, support this process. Given the heterogeneity of EVs derived from both healthy and diseased cells, digital EV assays are essential for developing accurate diagnostic methods, defining clinically relevant thresholds, and achieving sub-femtomolar detection limits [4].

In this chapter, two digital platforms based on immunophenotyping were utilized to develop a protocol for evaluating EVs, and their performance in terms of sensitivity and specificity was compared. Both platforms, the ExoView Analyzer (https://www.nanoviewbio.com) and Quanterix's SiMoA Technology (https://www.quanterix.com/simoa-technology), are prominence in the EV field. The ExoView Analyzer employs Single Particle Interferometric Reflectance Imaging Sensing (SP-IRIS) technology [5] [6], while SiMoA platform is based on Single Molecule Array (SiMoA) technology [7]. Both platforms offer digital immunoassays that enable single-particle confinement: SP-IRIS uses capture probe spots, and SiMoA uses microwells, each designed to fit a single bead [5] [6] [7]. Originally developed for different applications, label-free virus detection with SP-IRIS and soluble protein analysis in serum with SiMoA, these technologies are now commercially available and widely used for EV analysis in biomarker discovery and validation.

2.1.2 Platforms overview

The ExoView platform is a microchip-based technology that integrates two levels of detection within a single workflow: interferometric counting and fluorescence. Interferometric detection allows for precise counting of individual EV by analyzing light interference patterns, while fluorescence detection provides information about specific molecular markers on the EV surface.

The process begins with an antibody-spotted chip, which is incubated with the EV sample, followed by image acquisition to perform label-free counting of the captured EVs. Single Particle Interferometric Reflectance Imaging Sensing (SP-IRIS) is achieved when an LED source illuminates nanoparticles captured on the spot surface; light interference patterns from the sensor surface are modified by the presence of particles, producing a distinct signal [8]. In addition to counting individual particles, interferometric detection can estimate the size distribution of captured particles in the range of 50-200nm [5]. The second level of detection involves fluorescence labeling, which enables EV phenotyping through immunostaining and provides additional information on other protein markers present on individually captured vesicles for a variety of applications (*Figure 1*). A

unique aspect of this approach is its ability to quantitatively co-localize multiple protein markers on the same particle, offering valuable insights into the characteristics and functions of the particles under analysis. This method allows the fluorescence signal, which indicates the presence of specific proteins on the EV surface, to be correlated with interferometric particle counts obtained via SP-IRIS.

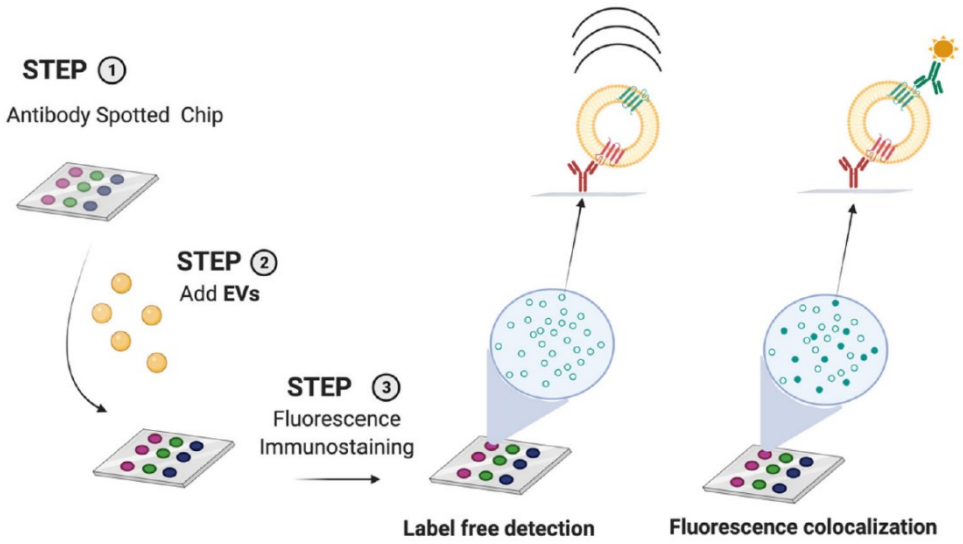

Figure 1: EVs analysis workflow on SP-IRIS platform. Anti-tetraspanin capturing antibody array chip, incubated with a EVs sample and followed by fluorescence antibodies. Two different levels of detection. Based on the Single Particle Interferometric Reflectance Imaging Sensing (SP-IRIS) principle, spots are individually imaged to count and size the captured vesicles in a label free. As a further level of characterization, staining with fluorescent antibodies provides information on the phenotyping and co-localization of EVs associated with protein markers, adapted from ref [9].

The second digital platform utilizes SiMoA Bead Technology, originally introduced as an immunoassay for measuring soluble proteins at the single-molecule level [7]. This bead-based test uses paramagnetic microbeads (2.7 µm) conjugated with a capture antibody to recognize the target. Detection is facilitated by a biotinylated antibody that binds to streptavidin-β-galactosidase (SBG), which subsequently acts on the fluorogenic substrate resorufin β-D-galactopyranoside (RGP). Following incubation with EV samples, the detection cocktail is added, and the beads are then distributed across an array of microwells, each designed to confine a single microbead (*Figure 2*). These microwells have an extremely low volume (femtoliters), creating a high local concentration of generated fluorophores, which enables a detectable signal even for a single captured target. By capturing fluorescence images of the array, 'on' signals from labeled beads (indicating EVs sandwiched between capture and detection antibodies) can be distinguished from 'off' signals from empty wells or unlabeled beads.

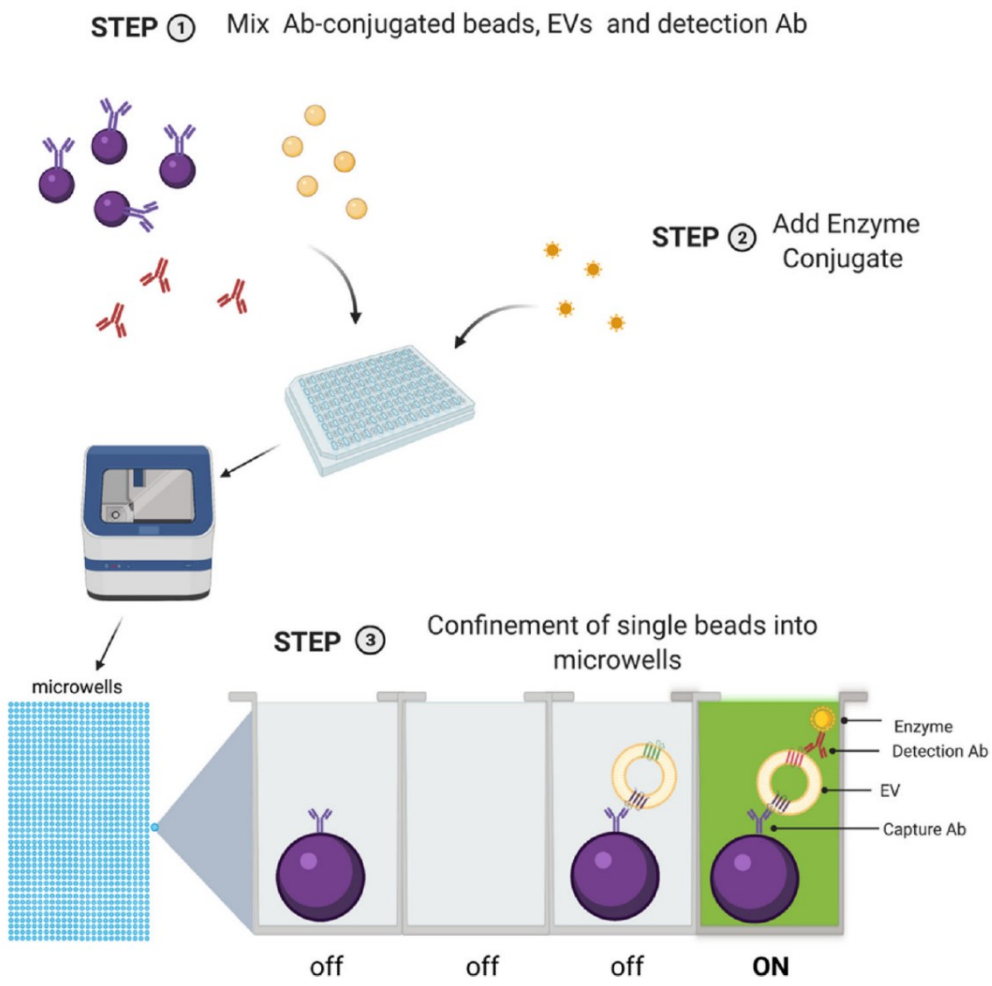

Figure 2: EVs analysis workflow on SiMoA platform. The EV sample is incubated with antibody-functionalized paramagnetic microbeads and with biotinylated antibodies. When enzymes, streptavidin-β-galactosidase (SBG) and fluorogenic substrate resorufin β-D-galactopyranoside (RGP) are added, a fluorescence signal is produced. Beads are confined in wells, one single bead each (one bead per well), where the high local concentration of generated fluorophores will ensure a detectable signal even for one captured EV. Fluorescence imaging of the microwell array will distinguish 'on' signals corresponding to labelled beads and 'off' signals corresponding to empty wells or unlabeled beads, adapted from ref [9].

This chapter presents a detailed, side-by-side multiparametric comparison of two digital platforms, focusing on key features relevant to the clinical translation of EVs. Both platforms were used to establish a protocol for evaluating EVs, comparing their sensitivity and specificity. To achieve this, three different cell lines with varying levels of tetraspanins (CD9, CD63, and CD81), the most common EV surface markers, were analyzed. Differential expression of these markers was confirmed using super-resolution microscopy (SRM), which aligned with the lower signals observed on the analytical platforms. Additionally, spiking experiments in mouse serum were performed to assess the

potential applicability of both techniques in real biofluids [9]. All results reported in this chapter have been published in Journal of Extracellular Biology [9].

2.2 Results and discussion

2.2.1 EV Characterization

EVs from human Cardiac Progenitor Cells (CPCs), produced under GMP-grade manufacturing protocol [10], were used to set up SP-IRIS and SiMoA assays. The EV sample was characterized following MISEV guidelines. Comprehensive characterization methods, including Western Blotting, Nanoparticle Tracking Analysis (NTA), Transmission Electron Microscopy (TEM), Cryo-EM, and Super-Resolution Microscopy (SRM), were employed to thoroughly analyze the EV preparation. All data are presented in *Figure 3*.

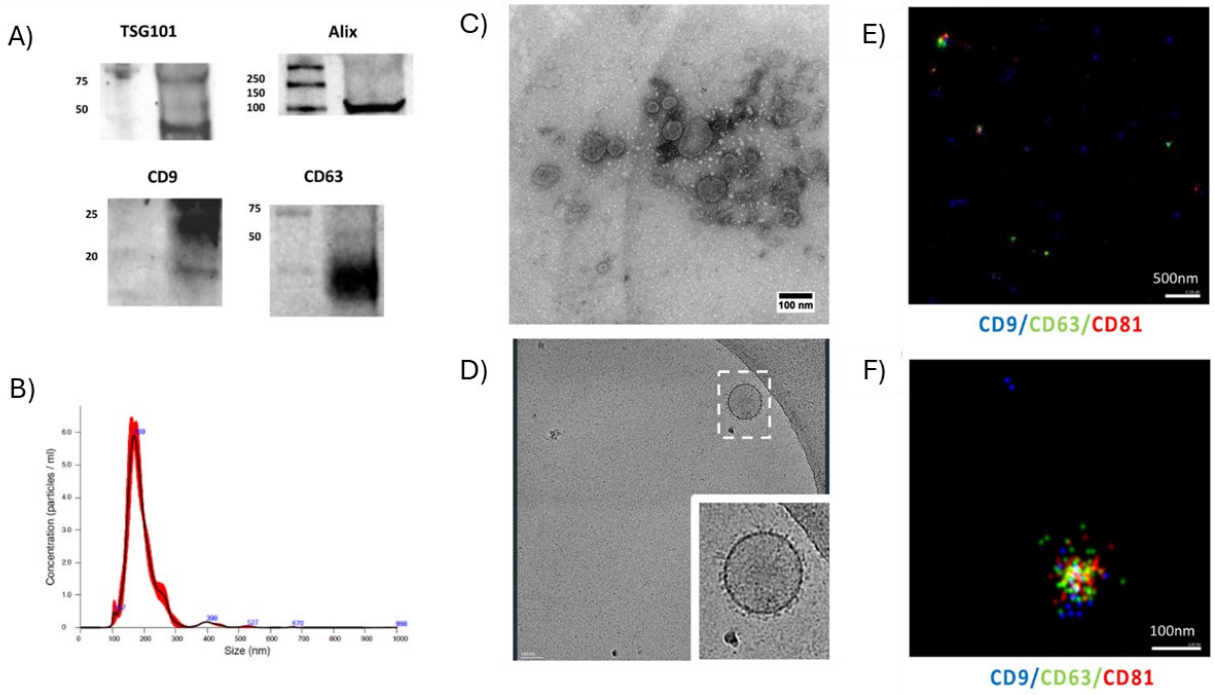

Figure 3: Characterization of EVs from human Cardiac Progenitor Cells. A) Western blot analysis confirmed the presence of internal proteins (TSG101 and Alix) and transmembrane proteins (CD9 and CD63). B) Particle concentration and size distribution, assessed via NTA, showed a mean particle size of 193 ± 2 nm and a concentration of 4.56 × 10^{10} particles/ml. C) TEM imaging revealed a heterogeneous EV preparation with particle sizes around 100 nm. D) Cryo-EM provided a typical EV image, displaying a lipid bilayer/membrane surrounding an electron-dense lumen. Representative SMR images of CPC-EVs stained with tetraspanins (CD63: green, CD81: red, and CD9: blue) were obtained, with a scale bar of 500 nm (E) and 100 nm (F), adapted from ref [9].

2.2.2 EV phenotyping assay

Both analytical platforms, SP-IRIS and SiMoA, were used to evaluate EV immunophenotyping using tetraspanin protein as the most represented and typical EV markers; widely used for relative quantification of EVs. To compare the two platforms, sandwich immunoassays were developed with monoclonal antibodies (mAbs) targeting CD9 (clone SN4), CD63 (clone AHN16.1), and CD81 (clone 1.3.3.22). These mAbs were chosen to ensure consistent data across both platforms, with custom functionalization of chips for SP-IRIS and beads for SiMoA. EVs are multi-marker analytes, often presenting multiple copies of the same protein on their surface. This enables each antibody clone to be used as both a capture and detection agent in a sandwich immunoassay. For the SP-IRIS experiments, microarray chips were printed with individual anti-CD9, CD63, and CD81 mAbs, as well as with a solution containing equal amounts of all three clones. Two detection strategies were developed:

1) Single-tetraspanin detection: EVs were captured on specific spots using an individual anti-tetraspanin mAb and then detected with the same fluorescence-labeled mAb, providing information on individual tetraspanin phenotypes (assays: StCD9, StCD63, StCD81).

2) Pan-tetraspanin detection: EVs were captured either by individual anti-tetraspanin mAbs or on a mixed-tetraspanin spot, followed by detection with a mixture of the three fluorescently-labelled mAbs (*Figure 4A*).

In SiMoA experiments, a similar approach was applied: capture beads were functionalized individually with anti-CD9, CD63, and CD81 mAbs, as well as with a mixture of all three antibodies. The two detection formats were as follows:

1) Single-tetraspanin detection: EVs were captured on each bead type, and single biotin-labelled versions of the corresponding mAb was used individually for detection (assays StCD9, StCD63, StCD81).

2) Pan-tetraspanin detection: format, a mixture of the three biotinylated mAbs was used to detect EVs captured on the different bead types (assays PtCD9, PtCD63, PtCD81, PtMix) (*Figure 4B*).

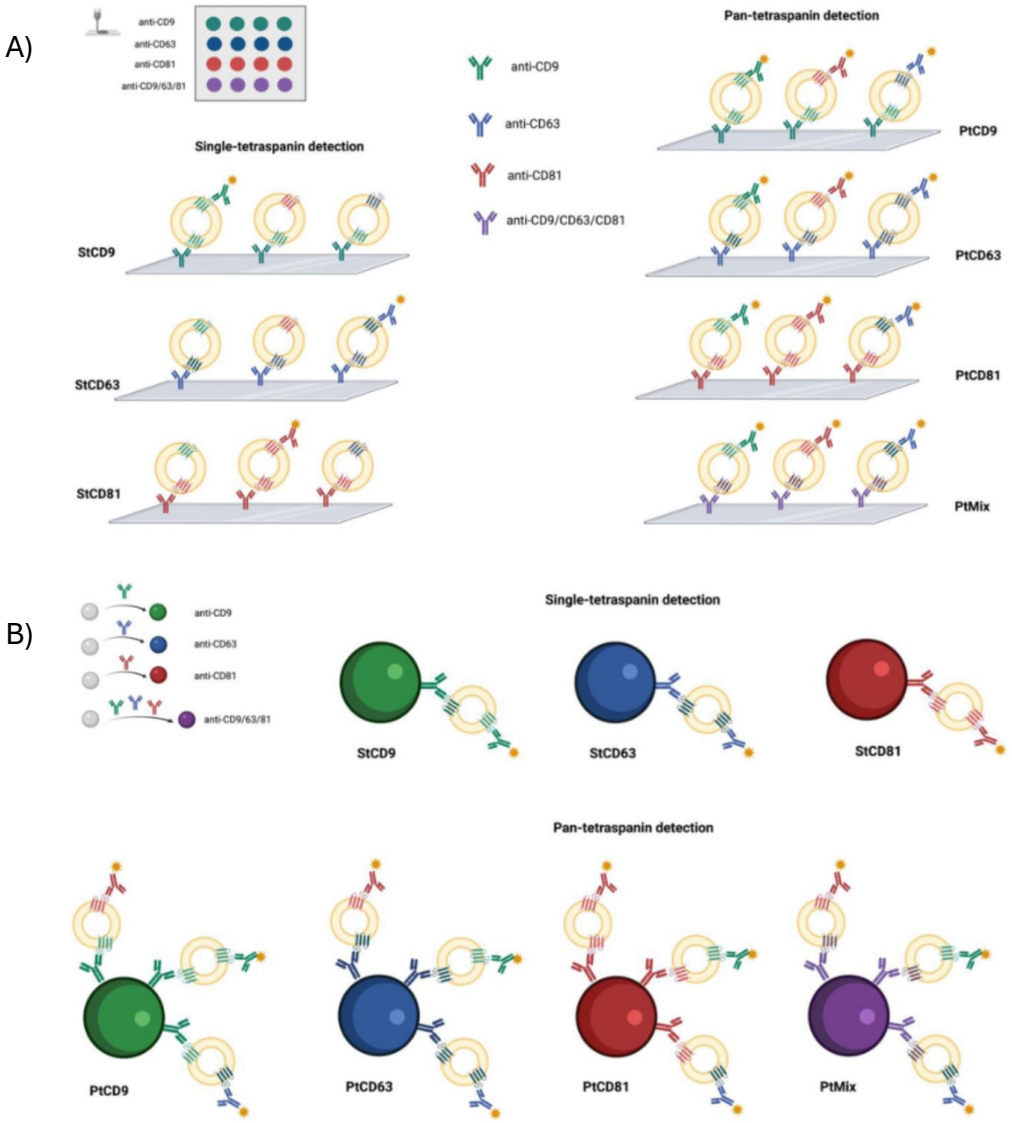

Figure 4: SP-IRIS and SiMoA strategies are reported. A) Microarrays were spotted with anti CD9, CD63, and CD81 antibodies and with a solution containing a 1:1:1 mixture of the three clones. EVs were captured on microarrays and detected by two strategies; 'Single-tetraspanin' detection (left panel), and Pan-tetraspanin detection (right panel). B) Capturing beads were functionalized with anti CD9, CD63 and CD81 antibodies and with a1:1:1 mixture of the three. In the Single-tetraspanin detection method (upper panel), individual biotin-labelled tetraspanin antibodies have been used after capturing EVs. In the Pan-tetraspanin detection method (lower panel), a mixture of detection antibodies has been used to label EVs on different bead types, adapted from ref [9].

2.2.3 SP-IRIS results

Silicon chips were coated with MCP2 polymer and spotted with tetraspanin antibodies, as described in the *2.4 Experimental section*. The chips were then incubated with varying concentrations of CPC-EVs, ranging from 0 to 10^{10} EVs/mL, as determined by NTA. After washing, both the *Single-*

Tetraspanin and *Pan-Tetraspanin* detection methods were applied. *Figure 5* shows the fluorescence particle counts detected by the ExoView R100 for both detection modes. To ensure an unbiased sensitivity comparison, all experiments were conducted on the same fluorescence channel. In both detection methods, a concentration range of 10^8 to10^{10} EVs/ml was observed. Variations among curves can be attributed to factors such as differential tetraspanin expression in the EV preparation and differences in mAb affinity. Additionally, the pan-tetraspanin approach did not show any advantage in terms of linear range or detection limits, which varied from10^6 to 10^9 EVs/ml, depending on the assay.

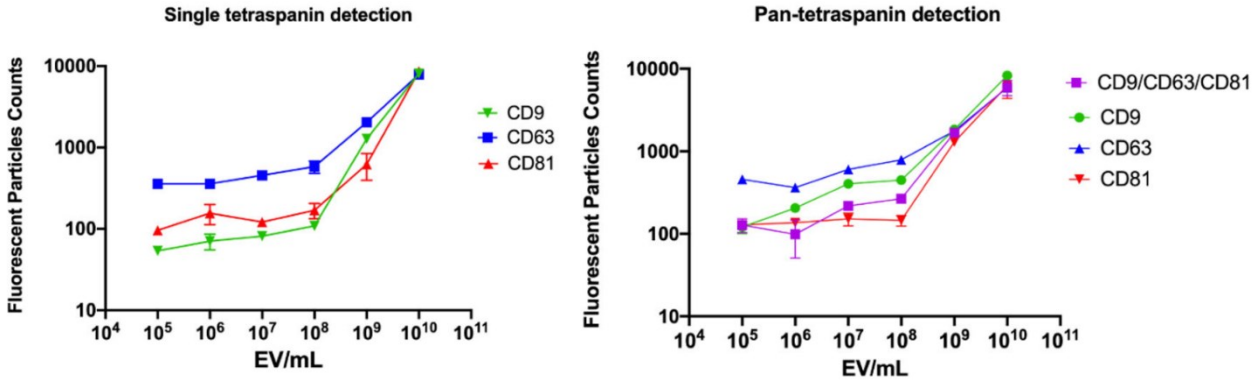

Figure 5: Fluorescent particle counts for CPC-derived EV samples, detected by SP-IRIS using the ExoView R100 platform, ranged between 10^5 and 10^10 particles/ml are reported. The left panel presents data from the 'Single tetraspanin' protocol, while the right panel shows results from the 'Pan-tetraspanin' detection method. These results were obtained from two biological replicates, adapted from ref [9].

For evaluating the Limit of Detection (LOD) across all conditions, the lowest EV concentration providing a fluorescence signal statistically different from the background ($p < 0.05$) using a Student's t-test, was considered.

The lowest LOD was obtained with CD9 assays (LOD=10^6 EVs/mL), achieved by both the single and pan-tetraspanin methods, suggesting a relatively high abundance of CD9 on the EV surface in this sample. Moreover, the highest LOD was recorded for the CD81 assays, with both detection approaches showing an LOD of 10^9 EVs/mL, indicating a lower abundance of this marker. All LODs are reported in *Table 1*.

Assay	Single tetraspanin detection	Assay	Pan-tetraspanin detection
StCD9	10^6 EV/ml	PtCD9	10^6 EV/ml
StCD63	10^8 EV/ml	PtCD63	10^7 EV/ml
StCD81	10^9 EV/ml	PtCD81	10^9 EV/ml
		PtMix	10^8 EV/ml

Table 1: Limits of Detection (LODs) for the SP-IRIS platform calculated considering the lowest EV concentration providing a fluorescence signal significantly ($p < 0.05$) different from blank control, adapted from ref [9].

2.2.4 SiMoA results

Para-magnetic beads were functionalized following Quanterix Homebrew assay instructions, as outlined in the experimental section, and a two-step assay was conducted. Similar to the SP-IRIS assay, dilution curves of CPC-EVs from 0 to 10^{10} EVs/ml were analyzed; using both single- and pan-tetraspanin detection strategies. For both methods, the detection range was broader compared to the SP-IRIS platform, with an operational range from 10^5 to10^{10} EV/ml (*Figure 6*).

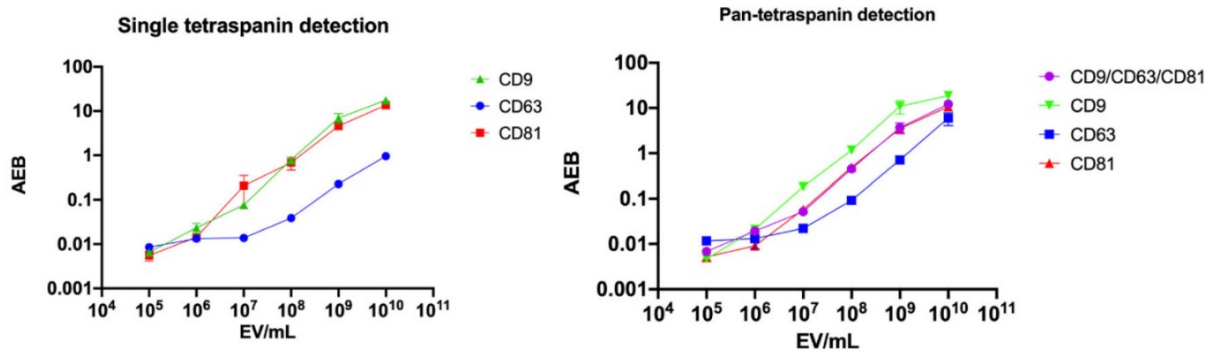

Figure 6: SiMoA results of the CPCs derived EVs sample are expressed as Average Enzyme per Bead (AEB. The curves of Single tetraspanin mode are shown in the left panel, whereas the Pan-tetraspanin mode in right panel). Data were obtained from two biological replicates, adapted from ref [9].

The LODs were calculated as previously described, based on the lowest concentration yielding a fluorescence signal statistically different ($p < 0.05$) from the blank sample. The LODs were found to range from 10^5 to10^7 EVs/ml, depending on the assay scheme. The best sensitivity (10^5 EV/ml) was achieved with the Single-Tetraspanin CD81 detection, Pan-Tetraspanin CD9 detection, and Pan-Tetraspanin CD81 detection (*Table 2*). However, determining whether these differences in LODs reflect the true differential abundance of tetraspanins or variations in antibody affinity is challenging.

Assay	Single tetraspanin detection	Assay	Pan-tetraspanin detection
StCD9	10^6 EV/ml	PtCD9	10^5 EV/ml
StCD63	10^6 EV/ml	PtCD63	10^6 EV/ml
StCD81	10^5 EV/ml	PtCD81	10^5 EV/ml
		PtMix	10^6 EV/ml

Table 2: Limits of Detection (LODs) for the SiMoA platform calculated considering the lowest EV concentration providing a fluorescence signal significantly ($p < 0.05$) different from blank sample, adapted from ref [9].

2.2.5 Relative abundance of tetraspanin Vs. LOD

To correlate the LODs obtained by SP-IRIS and SiMoA with the tetraspanin abundance (CD9, CD63, and CD81) in CPC-EV preparation, two additional EV preparations from HEK and HeLa cells were analyzed using the single-tetraspanin detection assay (*Figure 7*). Tetraspanin expression levels in all EV preparations were further assessed using SRM, where three-color staining was performed with fluorescence labelled anti-CD9, anti-CD63, and anti-CD81 antibodies. The relative abundance of each marker was calculated as a percentage of positive events on total events at the SRM, and compared with the single-tetraspanin curves from SP-IRIS and SiMoA (*Figure 7*).

In all three EV samples, SRM analysis identified CD9 as the most abundant marker, while CD63 and CD81 levels varied across samples. The high abundance of CD9 was consistently reflected in the strong intensity of the SiMoA dilution curves for all three samples. While, CD63 was less expressed in HEK-EVs, corresponding to the lower intensity of the dilution curves for both SP-IRIS and SiMoA, but it was more abundant in HeLa-EVs, as confirmed by the SiMoA. CD81 was highly expressed in CPC-EVs, which was confirmed by both platforms, although the relative differences among the EV types were only clearly reflected in the SiMoA results.

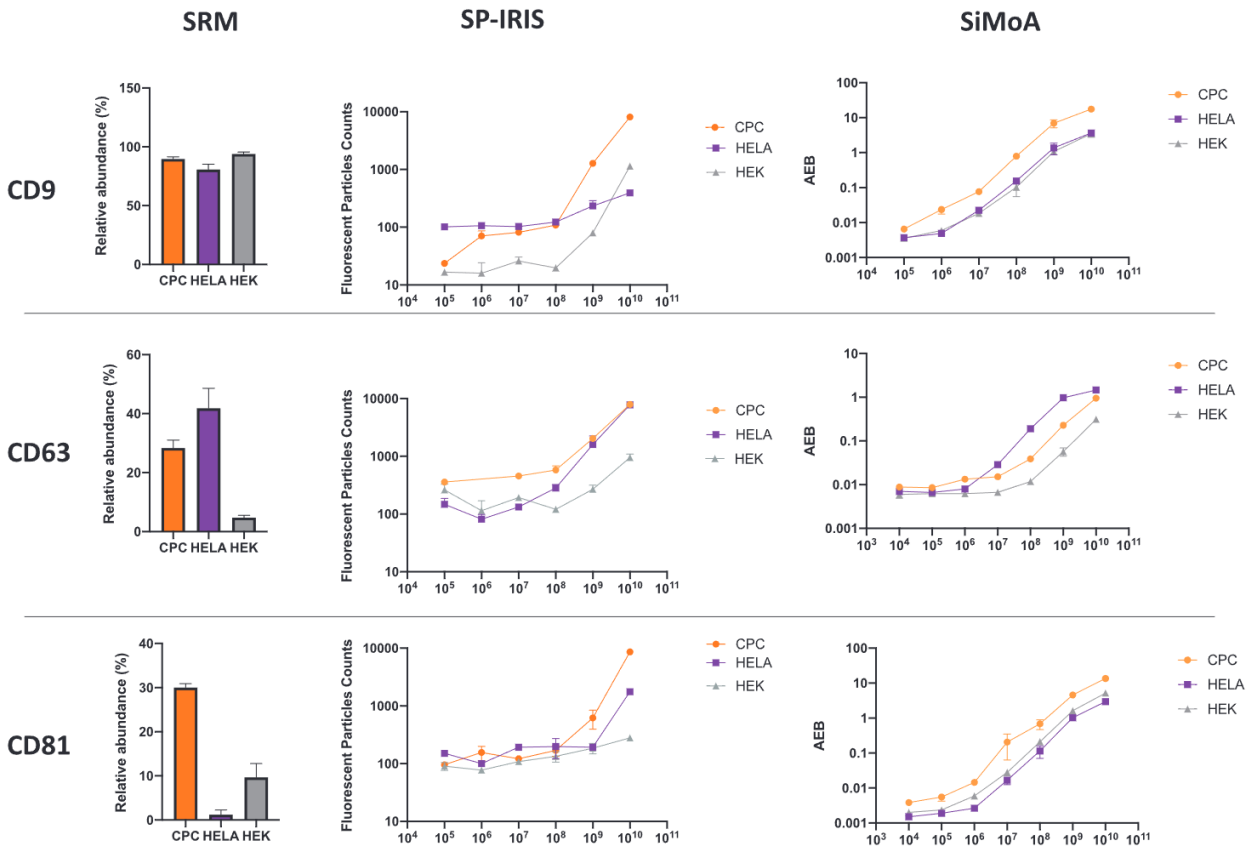

Figure 7: Comparison of EVs derived by CPC, HeLa and HEK cell line, detected by CD9/CD63/CD81 detection, as determined by SRM (left panel), SP-IRIS (central panel) and SiMoA (right panel) following single-tetraspanin assays, adapted from ref [9].

Notably, LODs depend not only on marker abundance but also on noise factors, including antibody cross-reactivity (non-specific binding between capture and detection probes) and other background sources. As shown in *Table 3*, the high CD9 signal does not correspond to lower LODs. While low CD81 expression in HeLa-EVs and low CD63 in HEK-EVs resulted in higher LODs on the SP-IRIS platform, this effect was not observed on SiMoA, where sensitivity was maintained despite low abundance. This difference in detecting low-abundance markers may be partly attributed to the suspension array format of SiMoA, which better mitigates mass-transport limitations that can interfere with biomolecular interactions at the solution- surface interface [11].

A)

SP-IRIS	CPC-EV	HeLa EV	HEK EV
LOD CD9	10^6 EV/ml	10^8 EV/ml	10^9 EV/ml
LOD CD63	10^7 EV/ml	10^8 EV/ml	10^{10} EV/ml
LOD CD81	10^9 EV/ml	10^{10} EV/ml	10^8 EV/ml

B)

SiMoA	CPC-EV	HeLa EV	HEK EV
LOD CD9	10^6 EV/ml	10^7 EV/ml	10^6 EV/ml
LOD CD63	10^6 EV/ml	10^7 EV/ml	10^7 EV/ml
LOD CD81	10^5 EV/ml	10^6 EV/ml	10^6 EV/ml

Table 3: Limits of Detection (LODs) for single-tetraspanin assay calculated considering the lowest EV concentration providing a fluorescence signal significantly ($p < 0.05$) different from blank sample. Table (A) reports the SP-IRIS data, whereas, table (B) shows SiMoA results.

2.2.6 Spiking assay in real biofluids

High-sensitivity detection of EV sub-populations in biological fluids is essential for EV-based liquid biopsy [12]; as it allows for the direct detection of EVs in real samples. Otherwise, isolation and enrichment steps, such as ultracentrifugation, size-exclusion chromatography, and polymer precipitation, are required, which may introduce pre-analytical biases, including selective enrichment of specific EV sub-populations and co-isolation of contaminants [13].

Achieving robust and sensitive immunophenotyping of EVs in actual biofluids is thus critically important for clinical applications. For this purpose, CPC-EVs were spiked into mouse serum and analyzed using both the SiMoA and SP-IRIS platforms to simulate a liquid biopsy scenario. First, it was confirmed that the tetraspanin monoclonal antibodies used did not cross-react with mouse proteins. To validate this, mouse serum without CPC-EVs was tested, results are shown in the bars labeled “0.” These signals are negligible compared to those observed in samples containing CPC-EVs. This finding supports the use of a 'Pan-tetraspanin' detection approach on both platforms.

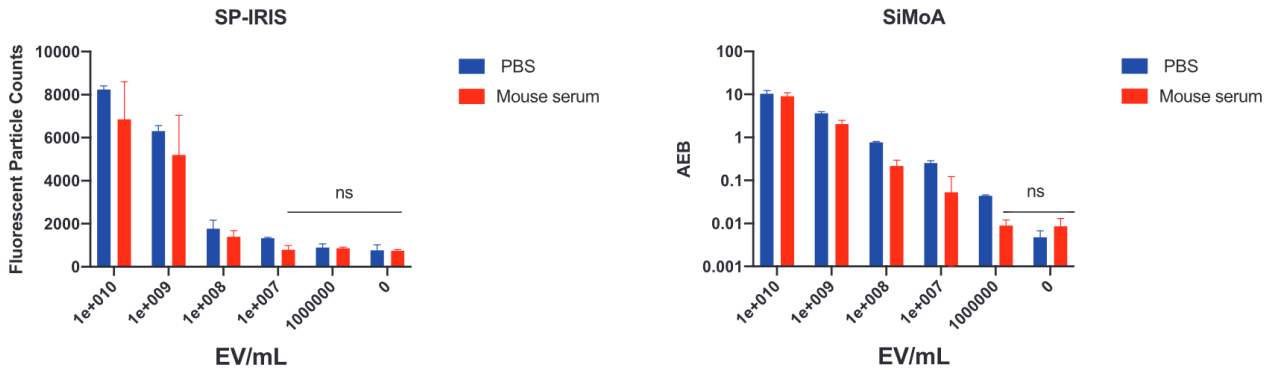

Figure 8: Results obtained from immune-phenotyping of spiking CPCs-EVs in mouse serum and in PBS using Pan-tetraspanin strategy. Left panel reports SP-IRIS data, while the right panel shows SiMoA results; in both assays t test was used to evaluate what is the lowest EV concentration providing a detection signal significantly different from the one provided by the blank sample ($p < 0.05$), adapted from ref [9].

Results shown in *Figure 8* indicate that the lowest detectable concentration of CPC-EVs in mouse serum was 10^8 EVs/ml for the SP-IRIS platform and 10^7 EVs/ml for the SiMoA platform. In both systems, the sample matrix (mouse serum vs. PBS) impacted sensitivity, resulting in higher detection limits in serum (*Table 4*), with a one-order-of-magnitude decrease in sensitivity in the more complex matrix. This finding underscores a common challenge in blood-based liquid biopsies, where disease-related EV subpopulations represent only a minor fraction of the total EV population [14].

	SP-IRIS	SiMoA
PBS	10^7 EV/ml	10^6 EV/ml
Mouse Serum	10^8 EV/ml	10^7 EV/ml

Table 4: LODs of human CPCs - EVs into mouse serum and PBS by the SP-IRIS and SiMoA platforms, adapted from ref [9].

While antibody selectivity was assumed to be optimal, factors such as serum contaminants (e.g., lipoproteins, protein aggregates) could influence sensitivity, contributing to an increase in LOD. The diagnostic accuracy of these platforms also depends on the relative abundance of EV surface biomarkers. Additionally, the heterogeneous distribution of tetraspanins (CD9, CD63, CD81) across EV complicates their use as universal capture markers, introducing bias in biomarker discovery [15] [16].

2.3 Conclusion

In light of these results, the SiMoA platform appears to be more appealing compared to SP-IRIS for clinical purposes. Specifically, SiMoA demonstrates superior performance under conditions of low EV concentration or low marker expression. Additionally, its capacity to process large number of samples simultaneously enhances its clinical applicability. In contrast, SP-IRIS provides more comprehensive data by simultaneously analyzing three fluorescence channels and interferometric counts, making it well-suited for research purposes or in-depth investigations of smaller sample cohorts.

In conclusion, utilizing a highly sensitive digital platform allows us to perform single-vesicle analysis directly in biofluids, eliminating the need for pre-isolation and enrichment steps. This direct approach facilitates the acquisition of clinically relevant data, advancing the potential translation of EV-based assays into clinical contexts.

Furthermore, digital platforms typically require minimal sample volumes, which is a crucial point for real-clinical applications. However, the use of EV-based assays for diagnostic purposes remains challenging due to the heterogeneity of surface protein markers targeted by capture probes. Surface protein expression and relative abundance significantly impact operative range, LODs, and absolute signa, affecting both SP-IRIS and SiMoA platforms, as seen in single-tetraspanin assays. This limitation is not entirely mitigated by the pan-tetraspanin approach. A major advancement would be the development of an EV capture probe targeting a 'universal EV marker,' with lipid membranes presenting a potential universal epitope for EVs.

Throughout this thesis, a pan-specific EV capture probe, MSP [17], has been introduced to address EV heterogeneity. In the following chapter, MSP will be integrated into the SiMoA platform, identified here as the most promising platform for sensitivity, high-throughput capability, and clinical translation potential.

2.4 Experimental section

2.4.1 Cell culture

Three cell lines were used in this study. Cardiac mesenchymal cells (CPCs) were derived from atrial appendage explants of patients without coronary artery disease. EVs were isolated from conditioned media (CM) through tangential flow filtration (TFF) as previously described [10].

HEK 293 and HeLa cell lines were expanded in T150 flasks. After one week of cell culture, the conditioned medium containing EVs was collected and centrifuged at 3,000 × g for 20 minutes at 10°C to remove larger debris, followed by 10,000 × g for 15 minutes at 10°C to deplete larger vesicles. The CM was then concentrated using Amicon Ultra Centrifugal Filters (Merk Millipore) with a 30 kDa cut-off filter.

2.4.2 Nanoparticle Tracking Analysis

EV preparations were analyzed using a NanoSight NS300 (Malvern Technologies, UK) with a 532 nm laser. Following the manufacturer's instructions, samples were diluted in filtered PBS to achieve an ideal range of 20-120 particles per frame. A syringe pump provided a constant flow, and three 60-second videos were captured and analyzed with NTA software (v3.2). The mean, mode, and median EV size from each video were used to calculate the concentration of nanoparticles, expressed as particles/ml.

2.4.3 Western Blot analysis

5X Laemmli buffer was added to the EV samples, which were then boiled for 5 minutes at 95°C. Proteins were separated by SDS-PAGE (4%-20% Mini-Protean TGX Precast Protein Gel, Bio-Rad) and transferred onto a nitrocellulose membrane (Bio-Rad, Trans-Blot Turbo). The membrane was blocked in TBS-T with 1% BSA for 1 hour and incubated overnight at 4°C with primary antibodies: anti-CD9 (1:1000, BD Pharmingen), anti-CD63 (1:1000, BD Pharmingen), anti-Alix (1:1000, Santa Cruz), and anti-TSG101 (1:1000, Novus Bio). After washing with TBS-T, membranes were incubated with horseradish peroxidase-conjugated secondary antibodies (1:3000 in TBS-T with 1% BSA) for 1 hour. Signals were developed using Bio-Rad Clarity Western ECL Substrate and visualized with a Chemidoc XRS+ system (Bio-Rad).

2.4.4 Super-resolution microscopy

Acquisition of EVs was performed using Nano imager S Mark II microscope from ONI (Oxford Nanoimaging, Oxford, UK) equipped with a 100x, 1.4NA oil immersion objective, an XYZ closed-loop piezo 736 stage, and triple emission channels split at 640, 488 and 555 nm. EV profiling was carried out with the EV Profiler Kit (ONI) per the manufacturer's protocol. Fluorescent antibodies (anti-CD9-488, CD63-568, CD81-647) were included in the kit. Images were acquired in dSTORM

mode using total internal reflection fluorescence (TIRF). Data were filtered using NimOS software (v1.18.3, ONI) and analyzed on the Collaborative Discovery (CODI) online platform (alto.codi.bio, ONI), utilizing the drift correction pipeline (v0.2.3) (Skovronova et al., 2021).

2.4.5 ExoView Antibody microarray

Silicon chip, with 80 nm oxide layer, was coated with MCP-2 polymer (Lucidant Polymers). The microarrays were produced using a non-contact S12 Spotter (Scienion Co., Berlin, Germany), depositing a drop for each spot (400 pL). Final concentration of antibodies spot solution is 1 mg/ml in PBS and 50 mM Trehalose. Printed chips were placed in humid chamber overnight at room temperature and subsequently were washed in a blocking solution (ethanolamine 50mM, Tris HCl 0.1 M, pH 9).EV samples were diluted in filtered PBS and incubated on chips for 2 h at room temperature in static conditions. Chips were then placed in a 24 wells plate where 1 ml of filtered PBS was added in each well. Plate was incubated on an orbital shaker at 300 rpm for 3 min, 750 µl of PBS were removed and replaced with fresh PBS. Chips were washed three times and dried. Chips were then incubated with fluorescent antibodies, (monoclonal anti-CD81, anti-CD63, anti-CD9 from Ancell) in house labelled by Cyanine5 NHS ester from Biotium. Fluorescent antibodies were diluted in filtered incubation buffer (0.05M Tris HCl, pH 7.6, 0.15M NaCl and 0.02% tween 20), 1:1000 ratio and 1 ml added in each well, the plate was placed on shaker 1 h at 300 rpm. After immuno-staining incubation chips were washed and dried. The chips were imagined with ExoView R100 reader using nScan software to acquire the data to be analyzed by ExoView Analyzer software.

2.4.6 SiMoA protocol

Beads conjugation to antibodies was performed according to Quanterix Homebrew kit instructions using the recommended buffers as follows. Conjugation of 150 µl of carboxylate paramagnetic beads (2.8×10^9 prt/ml) are washed three times with 300µl of Bead Wash Buffer (Quanterix, phosphate buffer with detergent), after every washing step the beads are pulsed spin and placed on a magnetic separator for 1 min to aspirate the supernatant. The beads are washed three more times with 300 µl of Bead Conjugation Buffer (Quanterix, 50 mM MES buffer pH6.2) and then are activated with EDC 0.3 mg/ml for 30 min at 4◦C undermixing/shaking. Eighty micrograms of antibody (CD9, CD63, CD81) are buffer exchanged with a 50 KDa Amicon filter and antibodies recovered in the Quanterix Bead Conjugation Buffer, after buffer exchange antibody concentration is measured with a Nanodrop spectrophotometer (ThermoFisher) and adjusted to 0.2 mg/ml with Bead Conjugation Buffer. Three hundred microlitres of a 0.2 mg/ml antibody solution are added to the activated paramagnetic beads and incubated for 2h at 4◦C under mixing/shanking. After the conjugation step the beads are washed two times with Bead Wash Buffer and then are blocked with Bead Block Buffer (Quanterix,

phosphate buffer with BSA) for 45 min at room temperature under mixing/shaking. After blocking, beads are washed three times with Bead Diluent and stored until use at 4◦C. SiMoA two-step assay Beads solution are prepared at the concentration of 2×10^7 beads/ml in Bead Diluent. The detector antibody (biotinylated CD9,CD63, CD81 antibodies) solutions (1 µg/ml) are diluted in Homebrew Sample Diluent (Quanterix), similarly, each sample is diluted 1:4 in Homebrew Sample Diluent (Quanterix). Twenty five microlitres of beads are transferred into a 96 microwell plate and mixed with 20 µl of detector antibody and 100 µl of sample. Sample, beads and detector are incubated for 30 min at 25◦C at 800 rpm. After incubation, beads are washed with an automatic plate-washer and then each incubated for 10 min with a 150 pM SBG solution (in SBG Diluent, Quanterix). After the SBG incubation step the plate is washed again by the automatic plate-washer and then inserted into the Quanterix SR-X instrument for analysis where RGP automatically added. Data were analyzed and processed by Reader Software SiMoA 1.1.0.

2.5 References

[1] M. Cretich, G. G. Daaboul, L. Sola, M. S. Ünlü, and M. Chiari, "Digital detection of biomarkers assisted by nanoparticles: Application to diagnostics," Jun. 01, 2015, *Elsevier Ltd*. doi: 10.1016/j.tibtech.2015.03.002.

[2] H. Liu and Y. Lei, "A critical review: Recent advances in 'digital' biomolecule detection with single copy sensitivity," *Biosens Bioelectron*, vol. 177, Apr. 2021, doi: 10.1016/j.bios.2020.112901.

[3] L. Cohen and D. R. Walt, "Highly Sensitive and Multiplexed Protein Measurements," Jan. 09, 2019, *American Chemical Society*. doi: 10.1021/acs.chemrev.8b00257.

[4] R. T. T. Morales and J. Ko, "Future of Digital Assays to Resolve Clinical Heterogeneity of Single Extracellular Vesicles," Aug. 23, 2022, *American Chemical Society*. doi: 10.1021/acsnano.2c04337.

[5] G. G. Daaboul *et al.*, "Digital Detection of Exosomes by Interferometric Imaging," *Sci Rep*, vol. 6, Nov. 2016, doi: 10.1038/srep37246.

[6] A. Yurt, G. G. Daaboul, J. H. Connor, B. B. Goldberg, and M. Selim Ünlü, "Single nanoparticle detectors for biological applications," *Nanoscale*, vol. 4, no. 3, pp. 715–726, Feb. 2012, doi: 10.1039/c2nr11562j.

[7] D. M. Rissin *et al.*, "Single-molecule enzyme-linked immunosorbent assay detects serum proteins at subfemtomolar concentrations," *Nat Biotechnol*, vol. 28, no. 6, pp. 595–599, Jun. 2010, doi: 10.1038/nbt.1641.

[8] G. G. Daaboul, C. A. Lopez, J. Chinnala, B. B. Goldberg, J. H. Connor, and M. Selim Ünlü, "Digital sensing and sizing of vesicular stomatitis virus pseudotypes in complex media: A model for ebola and marburg detection," *ACS Nano*, vol. 8, no. 6, pp. 6047–6055, Jun. 2014, doi: 10.1021/nn501312q.

[9] R. Frigerio *et al.*, "Comparing digital detection platforms in high sensitivity immune-phenotyping of extracellular vesicles," *Journal of Extracellular Biology*, vol. 1, no. 8, Aug. 2022, doi: 10.1002/jex2.53.

[10] G. Andriolo *et al.*, "Exosomes from human cardiac progenitor cells for therapeutic applications: Development of a GMP-grade manufacturing method," *Front Physiol*, vol. 9, no. AUG, Aug. 2018, doi: 10.3389/fphys.2018.01169.

[11] X. Wang, M. Zhao, D. D. Nolte, and T. L. Ratliff, "Prostate specific antigen detection in patient sera by fluorescence-free BioCD protein array," *Biosens Bioelectron*, vol. 26, no. 5, pp. 1871–1875, Jan. 2011, doi: 10.1016/j.bios.2010.02.009.

[12] L. Min *et al.*, “Advanced Nanotechnologies for Extracellular Vesicle-Based Liquid Biopsy,” Oct. 01, 2021, *John Wiley and Sons Inc*. doi: 10.1002/advs.202102789.

[13] Y. Tian *et al.*, “Quality and efficiency assessment of six extracellular vesicle isolation methods by nano-flow cytometry,” *J Extracell Vesicles*, vol. 9, no. 1, Jan. 2020, doi: 10.1080/20013078.2019.1697028.

[14] K. B. Johnsen, J. M. Gudbergsson, T. L. Andresen, and J. B. Simonsen, “What is the blood concentration of extracellular vesicles? Implications for the use of extracellular vesicles as blood-borne biomarkers of cancer,” Jan. 01, 2019, *Elsevier B.V.* doi: 10.1016/j.bbcan.2018.11.006.

[15] R. R. Mizenko *et al.*, “Tetraspanins are unevenly distributed across single extracellular vesicles and bias sensitivity to multiplexed cancer biomarkers,” *J Nanobiotechnology*, vol. 19, no. 1, Dec. 2021, doi: 10.1186/s12951-021-00987-1.

[16] R. Skovronova, C. Grange, V. Dimuccio, M. C. Deregibus, G. Camussi, and B. Bussolati, “Surface marker expression in small and medium/large mesenchymal stromal cell-derived extracellular vesicles in naive or apoptotic condition using orthogonal techniques,” *Cells*, vol. 10, no. 11, Nov. 2021, doi: 10.3390/cells10112948.

[17] A. Gori *et al.*, “Membrane-binding peptides for extracellular vesicles on-chip analysis,” *J Extracell Vesicles*, vol. 9, no. 1, Jan. 2020, doi: 10.1080/20013078.2020.1751428.

Chapter 3

Integration of MSP probe into digital platform for single vesicle analysis

3.1 Introduction

The importance of using advanced digital platforms for single EV analysis was widely demonstrated in *Chapter 2*. Due to their high sensitivity, these technologies allow for minimal sample volumes and can handle a high throughput of samples, both essential characteristics for clinical translation. Beyond sensitivity, addressing EV heterogeneity is crucial; in this regard, the pan-specific EV probe introduced in *Chapter 1* represents a potential paradigm shift in the EV field. In this chapter, MSP was integrated with SiMoA technology to capture and analyze the entire EV population, independent of specific surface protein expression.

Initially, MSP was immobilized on agarose beads to isolate EVs from biofluids such as serum and plasma, demonstrating both its specificity for EVs in untreated samples and its low binding affinity for contaminants like LPs or protein aggregates [1] [2]. Additionally, MSP was integrated on SiMoA beads for EV immunophenotyping. The presented data showcase the use of MSP-based SiMoA for EV analysis in real biofluids, confirming low affinity for lipoproteins and enabling single-step EV analysis. Moreover, MSP-based SiMoA assays facilitated the detection of an EV-associated marker not present in tetraspanin-positive EVs. This was validated using Red Blood Cell-derived EVs (RBC-EVs), which lack typical EV markers like tetraspanins, underscoring the versatility of the MSP probe. Finally, the clinical potential of this method was demonstrated by analyzing EV-associated epitope signatures in serum and plasma samples to differentiate patients with myocardial infarction from those with stable angina [2]. All results reported in this chapter have been published in Journal of Extracellular Biology [2].

3.2 Results and Discussion

3.2.1 Agarose beads: EVs isolation

Blood is a highly complex matrix that presents challenges for reproducible EV isolation and biomarker analysis, as EVs coexist with other eNPs, such as LPs, with overlapping size and density [3]. For this reason, multiple isolation steps or a combination of at least two approaches are often required to obtain EVs with minimal contaminants [4]. To evaluate the efficiency and selectivity of MSP for isolating EVs, experiments were conducted using serum and plasma. Agarose resins functionalized with MSP, leveraging His-Tag chemistry, enabled the capture and subsequent release

of EVs. This facilitated the application of techniques such as NTA and TEM to assess the presence and integrity of EVs. Additionally, Western blotting (WB) and immune-dot blot assays were used to confirm the presence of EVs and assess contamination levels, as detailed in the *3.4 Experimental section.*

Following EV capture on agarose resins, the integrity, size, and morphology of released EVs were confirmed through TEM and NTA. Western blotting was used to detect typical EV-associated surface tetraspanins (CD63 and CD81) and luminal markers (TSG101 and Alix) that confirmed the presence of intact EVs in the release fraction. TEM images of released EVs revealed membrane-enclosed vesicles consistent with the size distribution measured by NTA, with a mean size of 139 ± 1.5 nm by NTA and 122 ± 16.5 nm by TEM. It is well established that NTA tends to slightly overestimate EV size compared to TEM analysis. Crucial point is the selectivity binding for EVs, and not against the most abundant blood contaminants, such as lipoproteins and soluble proteins. To assess this, apolipoproteins (Apo-A, Apo-B, Apo-E) and albumin were evaluated using immune-dot blot analysis. As shown in *Figure 1*, signals for contaminants in the serum EV released fraction are negligible. Similar results were obtained with plasma, independently from the pre-analytical conditions.

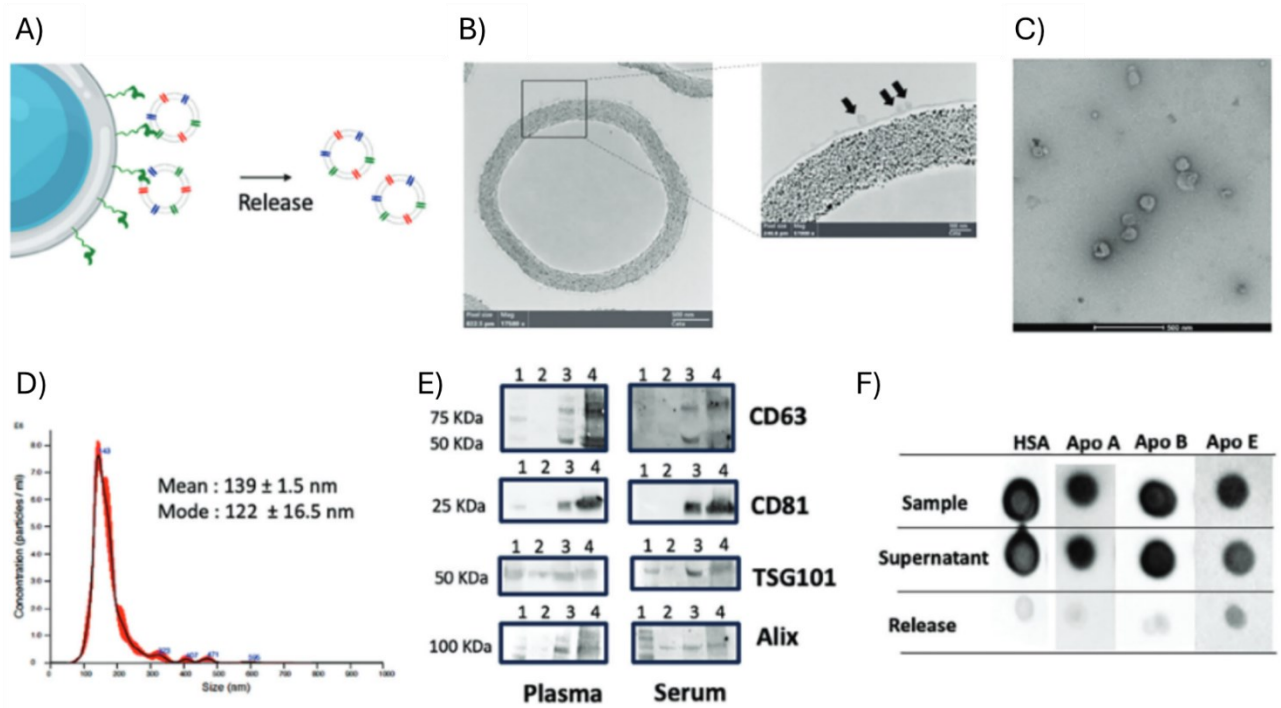

Figure 1: A) Catch and release schema of blood EVs and their release in intact conditions. B) TEM image of agarose beads and surface captured EVs (Black arrows). C) TEM image of captured EVs from serum after release with 0.5 m imidazole, showing intact vesicles. D) NTA analysis of captured EVs from serum and released after imidazole treatment. E) Typical EV-associated surface (CD63 and CD81) and luminal (TSG101 and Alix) markers are observed with Western Blot. Capturing from Plasma (left panels) and Serum (right

panels). Lane 1: Molecular Marker. Lane 2: Red Blood Cell EVs (negative control for tetraspanin). Lane 3: released EVs. Lane 4: Commercial standard of HEK cells derived EVs (positive control). F) Immune dot-blot analysis to check presence of common contaminants: Human Serum Albumin (HSA), Apo-A, Ap-B, Apo-E, adapted from ref [2].

3.2.2 Immobilization of MSP on SiMoA beads

MSP probe was conjugated to SiMoA microbeads through a customized protocol, and employed in a direct immunoassay for EVs using a combination of detector antibodies targeting CD9, CD63 andCD81 (pan-tetraspanin detection) as shown in *Figure 3*. SiMoA beads surface were functionalized with MSP via cysteine-maleimide click reaction, a bio-orthogonal reaction that enabled precise orientation of the peptide ligand. The entire process was monitored by RP-HPLC, a calibration curve of MSP-cys was used to quantify the amount of conjugated peptide on the beads surface. The reproducibility of the conjugation was monitored in four conjugation batches leading to average conjugation efficiency of 96.43% ± 2%.

To assess the efficiency of the new MSP modifying SiMoA beads, they have been compared at the reference pan-tetraspanin beads (*Figure 2*); and detection was performed using a cocktail of anti-tetraspanins. Both beads preparations, MSP and Tetra beads, were directly used with a serial dilution of a pool of plasma samples from healthy controls, and pan-tetraspanin in detection; SiMoA protocol assay was performed as explained in *Chapter 2*. Both systems demonstrated similar performance, enabling the direct detection of tetraspanin-positive EVs from plasma without the need for pre-isolation across a dilution range of 1:50 to 1:2000. Notably, the MSP beads offered a broader dynamic range. The Average Enzyme per Bead (AEB) signals at each plasma dilution for both bead types are presented in *Figure 2*.

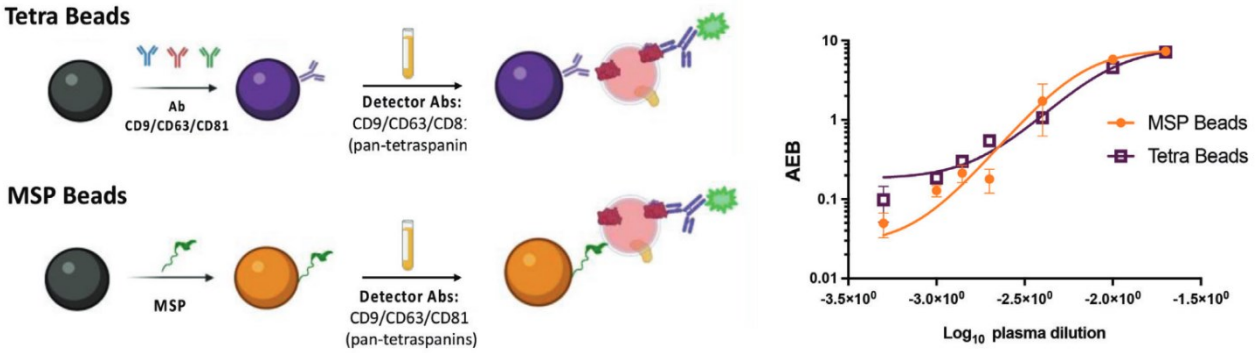

Figure 2: On the left, a diagram illustrates SiMoA beads functionalized with a combination of antibodies targeting CD9, CD63, and CD81 tetraspanins (Tetra Beads), alongside MSP-functionalized beads (MSP Beads). Both types of beads are employed for pan-tetraspanin detection of EVs from plasma samples. On the right, a graph displays the AEB signal obtained from Tetra Beads and MSP Beads during a SiMoA three-step

assay, showing the results of serial dilutions (ranging from 1:50 to 1:2000) of a plasma pool from healthy donors, adapted from ref [2].

3.2.3 Specificity of MSP on SiMoA platform

The specificity of MSP for capturing EVs was comprehensively demonstrated in *section 3.2.1*. To further validate these findings, an additional assay was designed to assess potential non-specific interactions particularly focusing on the binding of lipoproteins to MSP-functionalized beads. This was accomplished by detecting any apolipoproteins bound to the beads using antibodies specific to Apo-A and Apo-B. The experiment involved incubating the MSP beads with a 1:100 diluted plasma sample. The AEB signals for apolipoprotein markers were minimal compared to the pan-tetraspanin signal obtained from EV capture in the same plasma sample. To support these findings, unconjugated beads (Ctrl Beads) lacking MSP functionalization were also tested. This allowed a direct comparison to determine whether any observed binding was specifically mediated by MSP or resulted from non-specific interactions. The results show that AEB signals for both Apo-A and Apo-B detected on MSP beads were comparable to those of control beads without MSP functionalization *(Figure 3)*. This indicates that both conditions, the beads themselves (Ctrl beads) and, functionalized with MSP, do not significantly bind lipoproteins.

These findings highlight the high specificity of MSP for EV capture, with minimal interference from common plasma contaminants such as lipoproteins. The assay provides clear evidence that the EV binding observed is mediated by the MSP functionalization and not due to non-specific adherence of plasma components. This specificity is crucial for ensuring the purity and reliability of isolated EVs in downstream analyses.

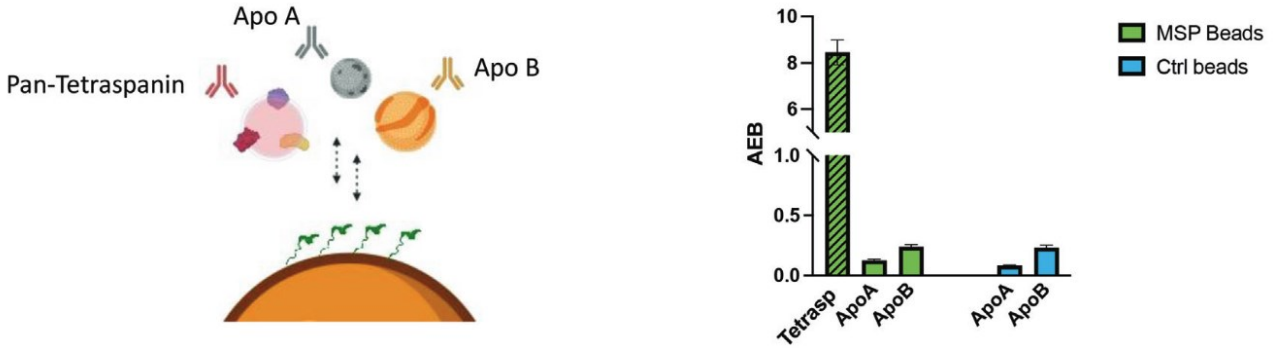

Figure 3: Assay designed to evaluate potential non-specific interactions of lipoproteins with SiMoA MSP beads (left panel). A three-step plasma EV analysis (1:100 dilution) was conducted using CD9/CD63/CD81, anti-Apolipoprotein A, or Apolipoprotein B as detection antibodies. The resulting AEB signals (right panel) indicate minimal interaction between MSP beads and lipoproteins, especially when compared to the

tetraspanin signal (displayed on a logarithmic scale). Importantly, the lipoprotein interaction signals were similar to those observed with non-functionalized control beads, adapted from ref [2].

3.2.4 Relative abundance of tetraspanin as EV markers

As previously discussed in this thesis, variability in tetraspanin expression on EV surfaces in real samples has become increasingly relevant, as it can differ based on both pathological and physiological states and vary significantly from patient to patient. This issue was investigated by analyzing plasma from six healthy donors. SiMoA microbeads functionalized with a combination of antibodies against CD9, CD63, and CD81 tetraspanins (Tetra beads) were used as a reference for unbiased capture of tetraspanin-positive EVs, irrespective of the relative abundance of each marker. Detection was performed using single antibodies against each tetraspanin. Results were directly compared to the MSP bead assay, revealing an almost identical pattern in the relative abundance of each tetraspanin across both MSP and Tetra bead methods (*Figure 4*). These results suggest that MSP binding does not lead to a biased selection or enrichment of specific EV subtypes, confirming its representativeness and reliability for use in unbiased EV-associated biomarker discovery. Furthermore, the results highlight sample heterogeneity and the uneven distribution of the three tetraspanins, underscoring that immune-based enrichment relying on individual anti-tetraspanin probes may lead to loss of information in EV analysis.

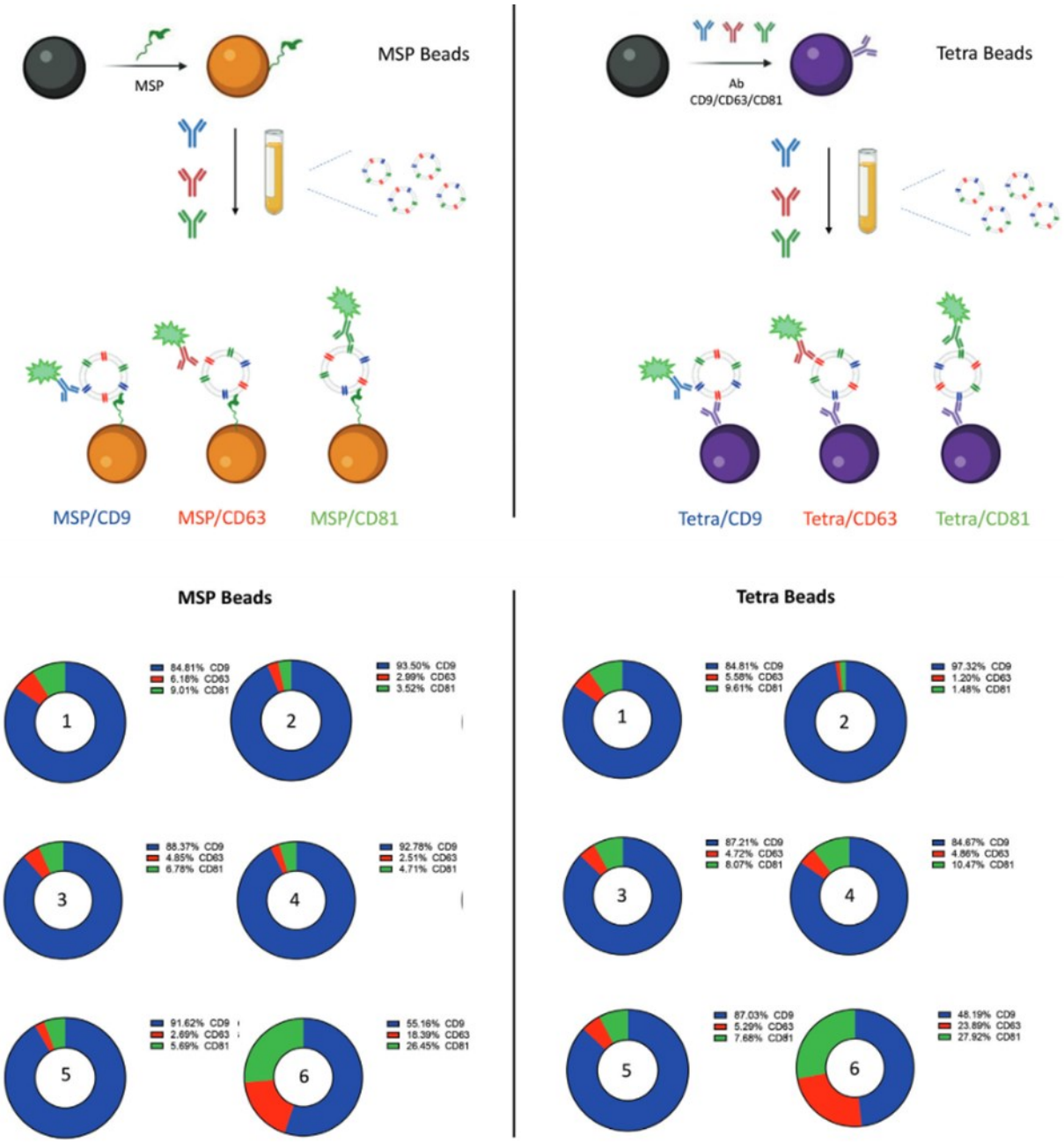

Figure 4: SiMoA Beads were modified by MSP (left panel) and by Pan-tetraspanin (right panel). Single tetraspanin immune-phenotyping of plasma EVs from 6 healthy donors was run in parallel on the two types of beads. For both strategies, total AEB was calculated, and single tetraspanin expression level is calculated as the AEB% over the total AEB. The heterogeneity of EVs samples with remarkable accordance of the two systems in terms of differential tetraspanin profiling, adapted from ref [2].

3.2.5 Lacking of tetraspanin

To emphasize one of the primary advantages of MSP technology, its ability to capture particles independently of surface protein markers; RBC-EVs were chosen as a model due to their lack of typical tetraspanin expression. The final goal was to demonstrate that standard tools targeting tetraspanins are ineffective for characterizing and analyzing such vesicles, along with other EV

mimics or any EVs that do not express canonical surface markers. Since RBCs lack an endolysosomal system, they generate EVs exclusively through plasma membrane budding. Consequently, RBC-EVs do not express common EV tetraspanins (CD81, CD63, CD9) but are enriched with the erythrocyte-specific Band 3 anion transport protein, making them ideal for this purpose [5] [6]. MSP beads and Tetra beads were compared in the analysis of RBC-EVs using SiMoA, with anti-Band 3 as the detection antibody and serial dilutions of an RBC-EV sample (*Figure 5*). The results show that MSP beads successfully captured RBC-EVs, exhibiting a clear dose-response signal, whereas Tetra beads and non-functionalized control beads demonstrated neither a dose-response relationship nor a significant signal-to-noise ratio. Notably, MSP beads also effectively captured RBC-EVs when spiked into a plasma sample *(Figure 5)*, confirming their capability to analyze RBC-EVs that lack canonical EV markers, even within complex sample matrices.

It is important to emphasize that, while RBC-EVs are well-characterized and have allowed us to select a specific protein marker for phenotyping (Band 3), other emerging EVs analogues may not be as well understood and might lack known distinctive surface protein markers. This would make it more challenging to select appropriate analytical tools and highlights the necessity for pan-specific EV ligands that facilitate downstream biomarker screening.

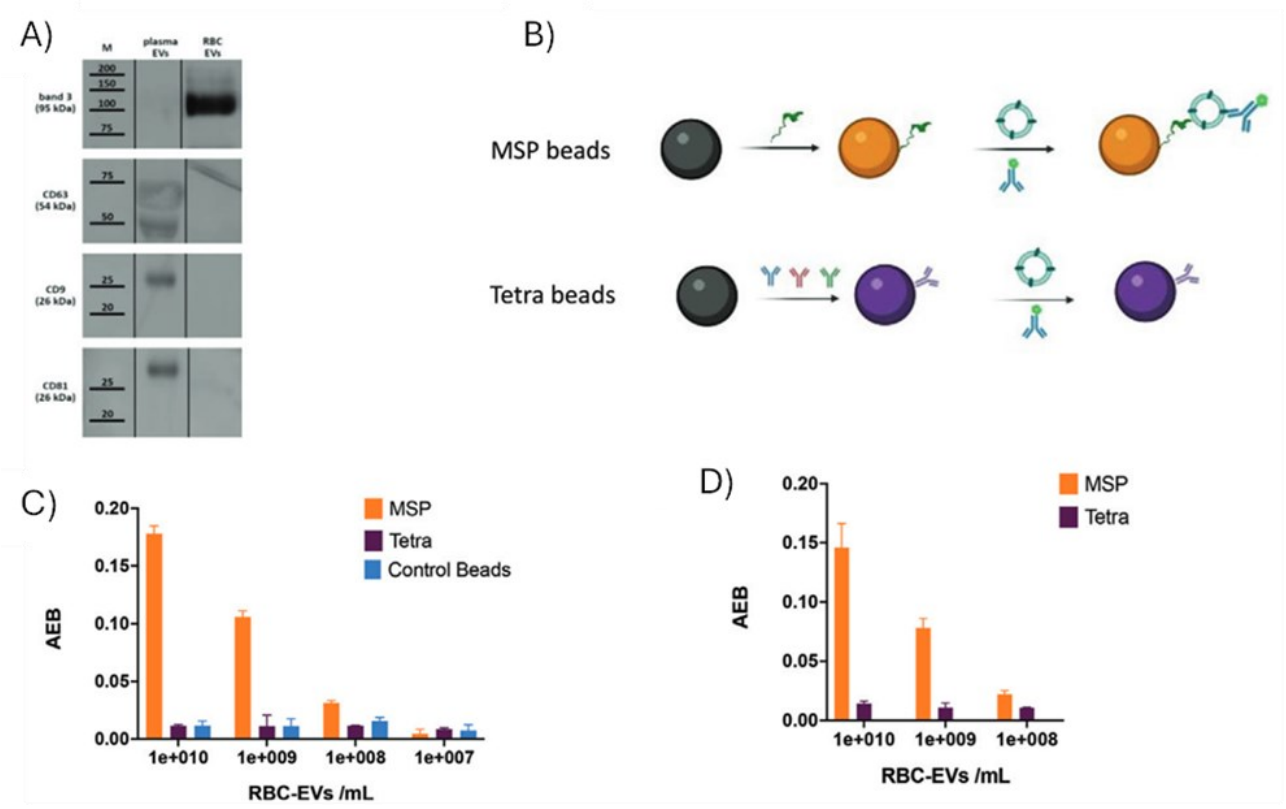

Figure 5: A) Western blot analysis of RBC-derived EVs shows low expression of the tetraspanin (CD63, CD9, and CD81), in contrast to plasma-isolated EVs, reflecting their biogenesis from the RBC plasma membrane.

Legend: M = Marker; Plasma EVs = EVs isolated from plasma using MSP-agarose-modified beads; RBC-EVs = RBC-derived ectosomes. B) SiMoA beads functionalized with MSP and mix of tetraspanin were used to capture serial dilutions of RBC-EVs, with anti-Band 3 antibodies for detection. C) The detection signals, reported as Average Enzyme per Bead (AEB) after subtracting blank signals, demonstrate MSP beads' ability to capture RBC-EVs down to 10^8 EVs/mL with a clear dose-response, which is not observed with Tetra or control (unfunctionalized) beads. D) Detection of RBC-EVs spiked into plasma samples, adapted from ref [2].

3.2.6 EV marker assessment in Clinical setting

Recent study highlighted that EV analysis can detect early signs of cell stress in cardiomyocytes, which occur before the release of troponin, a biomarker used to diagnose acute coronary syndrome (ACS). Specifically, increased levels of EV responsive to tetraspanin, along with endothelial and platelet antigens (CD42a and CD62P), were identified in patients experiencing ST-elevation myocardial infarction (STEMI), a precursor to myocardial injury [7]. Here, the MSP probe was employed for EV analysis within a clinically relevant workflow, using a direct approach with blood-derived samples. The method adopted a "one bead – multiple markers" strategy to evaluate whether MSP-based EV epitope profiling could provide diagnostic value comparable to antibody-based probes used in previous research [7]. A MSP-SiMoA assay was performed to assess EV-associated markers (CD9/CD81/CD63 tetraspanins, CD42a, and CD62P antigens) in serum and plasma samples without prior EV isolation. These markers were tested for their ability to differentiate between patients with STEMI (n=12) and those with stable angina (n=12) (*Figure 6*). The results indicated higher serum levels of all evaluated EV-associated markers in STEMI patients compared to those with stable angina (*Figure 6*).

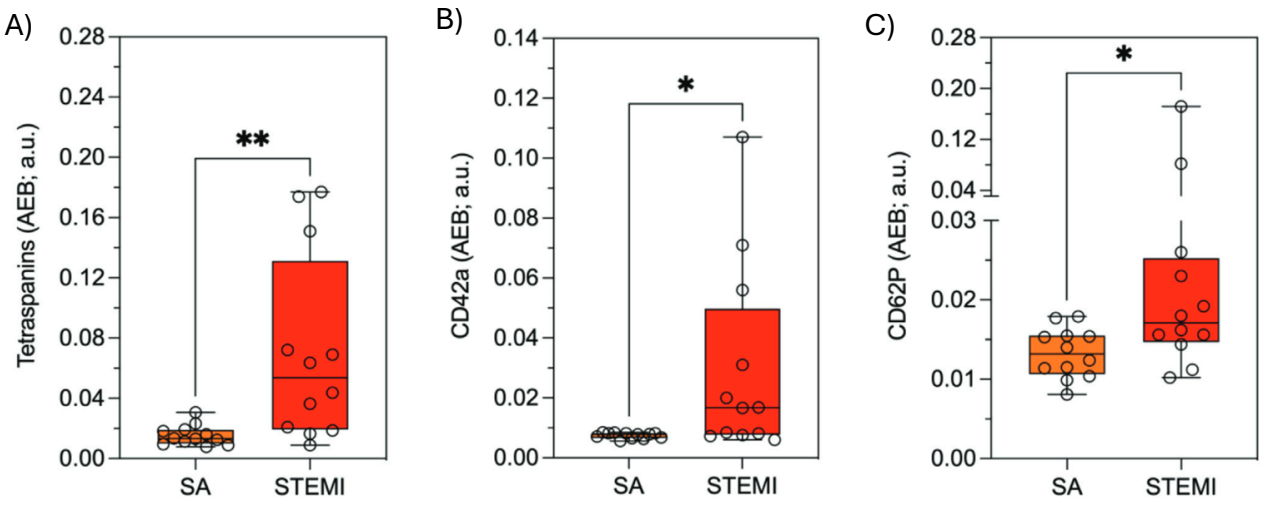

Figure 6: MSP-beads were used to conduct the experiment; A) Expression of Tetraspanins CD9/CD81/CD63, B) CD42a and C) CD62P in serum of patients with ST-segment elevation myocardial infarction(STEMI; red,

n = 12), stable angina (SA; orange, n = 12). t Test: Tetraspanins, p = 0.002; CD42a, p = 0.018; CD62P, p = 0.014, adapted from ref [2].

In a previous study, EV analysis focused primarily on tetraspanin-responsive EV populations, potentially overlooking or underestimating the value of additional vesicular markers that do not co-localize well with CD9/CD81/CD63, which could impact analytical sensitivity [7]. To demonstrate that tetraspanin-independent MSP binding can provide additional insights, the current study selected three markers: CD2, CD3, and CD326; that lacked strong diagnostic relevance in the prior study. These markers were tested on a small subset of STEMI samples (n=4) using both Tetra beads and MSP beads in comparative assays (*Figure 7*).

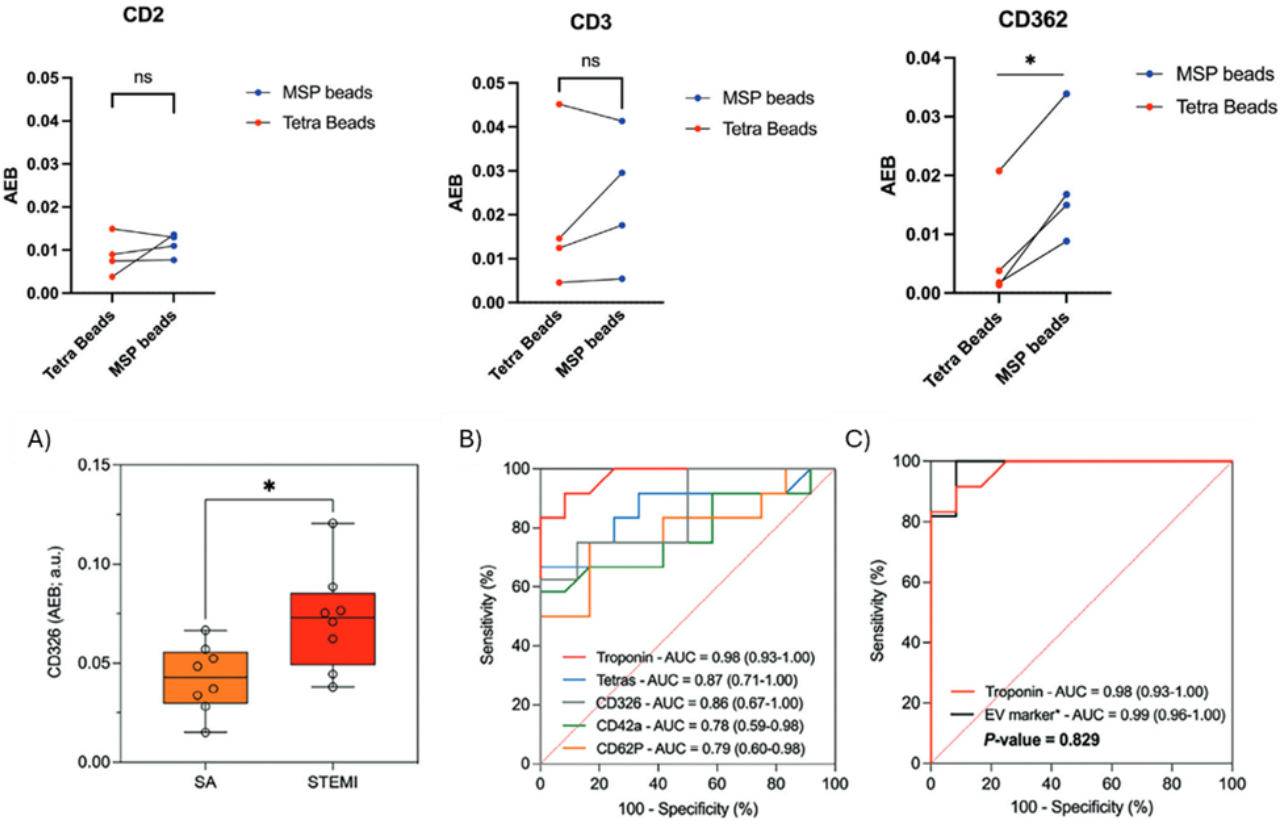

Figure 7: AEB signals for detection of CD2, CD3, CD362 in serum samples from STEMI patients (n = 4) using either MSP or Tetra beads in a SiMoA assay. While CD2 and CD3 AEB signals were not enhanced, CD362 signal resulted to be statistically different (higher) when using MSP beads. The panel below reports the CD326 expression in serum of patients with STEMI (red, n=8), and stable angina (SA; orange, n=8). t Test CD326: p = 0.015 (A). ROC curve analysis for individual EV markers: CD9/CD81/CD63 tetraspanins (blue curve), CD42a (green curve), CD62P (orange curve), CD326 (grey curve), and hs Troponin (red curve) (B). Diagnostic performance of combined EV markers (black curve) in comparison with the gold standard hs troponin(red curve) (C), adapted from ref [2].

The current work demonstrated that the CD362 marker showed significantly higher levels in the MSP-based workflow compared to Tetra beads ($p = 0.0071$), indicating poor co-localization with CD9/CD81/CD63 and explaining its ineffectiveness in previous analyses (*Figure 7*) [7]. This led to the inclusion of CD362 in the marker panel, and when tested in STEMI versus stable angina (SA) patients, it showed a statistically significant differential expression. ROC curve analyses demonstrated high sensitivity of these markers in distinguishing between STEMI and SA patients. An aggregate marker combining EV tetraspanins, CD62P, CD42a, and CD362 had excellent diagnostic performance (AUC 0.99), comparable to the high-sensitivity troponin assay (AUC 0.98). Confirming that using the proposed EV markers in a MSP-SiMoA assay showed diagnostic performances comparable with traditional hs-troponin (P-value = 0.829).

3.3 Conclusions

In this current thesis work, MSP was proposed as a novel tool for the direct analysis of blood-circulating EV. MSPs are an emerging class of affinity ligands that enrich small vesicles based on their membrane biophysical properties, rather than pre-selecting EV sub-populations base on surface markers expression through antibodies. MSP offer several advantages over antibody-based immunocapture: (I) they avoid biases in EV sub-population selection before biomarker analysis; (II) they are ideal when EV surface markers are unknown or when no abundant proteins are available for general capture; (III) they are not species-specific, making them useful for samples lacking validated antibodies (e.g., animal or bacterial samples); and (IV) MSP share typical peptide advantages over antibodies, such as lower cost, longer shelf life, and no batch-to-batch variability.

Here, it was demonstrated MSP's specificity for capturing EVs from real biofluids such as serum and plasma. MSP was integrated on agarose resin, and subsequently on SiMoA beads, to demonstrate its low binding affinity for LPs and soluble proteins. These findings indicate that MSP-based SiMoA can be employed for direct EV analysis in real biofluids. This represents the first peptide-based SiMoA assay incorporated into a streamlined workflow for direct EV analysis. After verifying its selectivity for EVs, MSP's representativeness was further confirmed by assessing single tetraspanin expression in plasma samples from six healthy donors. Results suggest that MSP binding does not lead to a biased selection or enrichment of specific EV subtypes, thus affirming its reliability for use in unbiased EV-associated biomarker discovery. This novel approach enhances the clinical applicability of EV assays for biomarker monitoring. Notably, MSP-based analysis distinguished STEMI from stable angina with diagnostic performance comparable to the gold-standard hs-troponin assay, establishing its clinical relevance. An additional advantage of MSP as an analytical probe was demonstrated using RBC-EVs, which lack the tetraspanins CD9, CD63, and CD81. This highlights

MSP's advantage over tetraspanin-based tools, confirming its utility for analyzing non-conventional EVs lacking known surface markers.

In light of these findings, MSP can be seamlessly integrated into various isolation and analytical EV platforms without introducing biases related to sub-population enrichment based on protein expression. The next chapter presents application of MSP for both analytical and isolation purposes.

3.4 Experimental Section

3.4.1 Agarose beads: EVs isolation and characterization

For EVs catch and release in blood derived samples (serum and plasma), high cobalt density agarose resin were conjugated [1]. For blood-derived specimen EVs isolation,0.1 mL of MSP-beads suspension was added to 50 µL of sample, serum or plasma EDTA, plasma heparin, or plasma citrate diluted 1:10 in PBS, to a final volume of 500µL, and incubated 1h at RT under rotation. Then, supernatant was recovered, beads were washed three times; and EVs release was performed adding 100µL of Imidazole solution 0.5 M in PBS for 15 min under shaking, at RT.

To assess contaminants evaluation, Dot and Western Blot were performed. 3 µL of pure sample was dropped off on nitrocellulose membrane. After drying at room temperature for 15 min, the membranes were blocked with 5% of BSA in TBS containing 0.05% of Tween 20 (TBS-T), for 1 hour. The membranes were incubated with using anti-ApoA1 (1:1000, Santa Cruz, CA, USA), anti-ApoE and anti-ApoB (1:500, Santa Cruz, CA, USA), and anti-human serum albumin (1:500, Santa Cruz, CA, USA). After washing with TBS-T, membranes were incubated with horseradish peroxidase-conjugated (JacksonImmunoResearch, Tucker, GA, USA) secondary antibodies diluted 1:5000in TBS-T with 1% BSA for 1 h. While, Western Blot analysis of RBC-EVs and plasma EVs, 5X Laemmli buffer was added, and samples were boiled for 5 min at 95 °C. Proteins (30 µg) were separated by SDS-PAGE (10% polyacrylamide) and transferred onto a PVDF membrane. The blocking step was carried out with a 5% fat-free milk in PBS-0.05% Tween-20 (PBS-T) for 1 h at 37 °C. Membranes were incubated overnight at 4 °C with the following antibodies diluted in 1% fat-free milk PBS-T: anti-CD9 (1:500, Santa Cruz, CA,USA), anti-CD81 (1:500, Santa Cruz, CA, USA) anti-CD63 (1:500, Merck-Millipore, MA, USA), and anti-BAND3 (1:1000, Santa Cruz, CA, USA). The membranes were washed thrice for 10 min with PBS-T and incubated for1 h with rabbit anti-mouse HRP conjugated secondary antibody diluted1:3000 in 1% fat-free milk PBS-T (Bethyl, TX, USA). Images were acquired with Chemibox Syngene.

The procedure for Transmission Electron Microscopy (TEM) involved two methods. For negative staining, 2 µL of the sample was applied to a formvar/carbon-coated grid, stained with 2% uranyl acetate, air-dried, and observed with a Talos L120C microscope at 120 kV. Images were captured

with a Ceta CCD camera. For conventional TEM, EVs absorbed on agarose magnetic beads were fixed with 2.5% glutaraldehyde in the cacodylate buffer, washed, and postfixed with reduced osmium. After additional washes, samples were stained with uranyl acetate, dehydrated, embedded in epoxy resin, and polymerized. Ultrathin sections (70–90 nm) were stained and examined using the same microscope. Whereas, for Nanoparticles Tracking Analysis (NTA), the procedure previously described in chapter 2 was used.

3.4.2 SiMoA beads conjugation

Pan-tetraspanin SiMoA beads were functionalized as explained in experimental section, chapter 2. While for the MSP conjugation on SiMoA beads, 150 µL of SiMoA carboxylate paramagnetic beads (2.8×10^9 prt/ml) were activated with EDC according to Quanterix Homebrew kit instructions as described above, then 300 µL NH 2 -Maleimide linker (from Sigma-Aldrich)solution 10 mm in PBS (adjusted to pH 8.6) was added and shacked for 2 min RotoFlex. Beads were then washed two times with PBS to remove NH 2 -Maleimide in excess and incubated with 300 µL of 100 µm solution of MSP in PBS (adjusted to pH 8.6, with two equivalents DIEA and 1 mm TCEP).Peptide reacts for 1 h under mixing. After the conjugation step the beads were washed two times with PBS and then were blocked with Bead Block Buffer (Quanterix) for 15 min at room temperature under mixing/shaking.After blocking, beads were washed with Bead Wash Buffer (Quanterix) and stored in Bead Diluent (Quanterix) at 4 °C.

3.4.3 SiMoA Assay

In pan-tetraspanin tree-step assay, beads were prepared following the Quanterix protocol, as reported in chapter 2,. Here, serum samples were diluted 1:4 in Homebrew Sample Diluent, whereas, plasma samples were diluted 1:10 in Homebrew Sample Diluent, then 25 µL of beads, 100 µL of sample were transferred into a 96 wells plate and incubated for 30 minutes at 25 °C at800 rpm. After incubation, beads were washed with an automatic plate-washer and then incubated for 10 min with 100 µl of detector antibody After incubation, beads were washed and incubated for 10 min with a 150 pm SBG solution (in SBG Diluent, Quanterix). After the SBG incubation step the plate was washed again and then inserted into the Quanterix SR-X instrument for analysis where RGP was automatically added. Data were analyzed and processed by Reader Software SiMoA 1.1.0. For the MSP SiMoA protocol, the assay was run as described above for pan-tetraspanin beads except that samples and detector antibodies were incubated in PBS. The detector antibody (biotinylated CD9, CD63,CD81 antibodies or CD42a, CD62P, CD2, CD3, and CD326 by Milteny-Biotech or anti-band 3 from Santa Cruz) was used at the concentration of 0.6 µg/ml.

3.4.4 Apolipoprotein Interaction Assay

The assay was run as described for MSP beads using biotinylated anti-ApoA1 and anti-ApoB (Santa Cruz, CA, USA) were used at the concentration of 0.6 µg/mL . Plasma was diluted 1:10. 25 µl of beads were transferred into a 96 microwell plate and mixed with 100 µl diluted sample and incubated for 30 min at 25 °C at800 rpm. After incubation, beads were washed with an automatic plate-washer using optimized Tween concentration and then incubated for 10min with 100 µl of detector antibody. After that, beads were washed with an automatic plate-washer and incubated for 10 min with a 150 pm SBG solution (in SBG Diluent, Quanterix). After the SBG incubation step the plate was washed and then inserted into the Quanterix SR-X instrument for analysis where RGP is automatically added. Data were analyzed and processed by Reader Software SiMoA 1.1.0.

3.4.5 Red Blood Cell Derived – EVs

RBCs from type O+ healthy volunteers were used to isolate EVs via calcium ionophore induction. The blood transfusion unit at Ospedali Civili di Brescia provided RBCs with written consent and ethical approval (NP5705). After ethical approval, RBCs were washed with PBS, transferred to culture flasks, and treated with calcium ionophore. After incubation, RBCs were collected and debris removed through differential centrifugation. The supernatants were filtered and EVs were isolated by ultracentrifugation at 50,000×g, followed by layering on a sucrose cushion for further purification. The EVs were washed, resuspended in PBS, and stored at −80°C. Multiple centrifugation steps were performed using different Beckman centrifuges and rotors.

3.4.6 Serum and Plasma Samples for the Clinical Validation

Peripheral venous blood samples were collected from patients at Istituto Cardiocentro Ticino (Lugano, Switzerland) following ethical approval and informed consent in line with the Declaration of Helsinki. The study included patients diagnosed with ST-elevation myocardial infarction (STEMI) and chronic coronary artery disease (CAD) with stable angina (SA), based on European Society of Cardiology guidelines. Blood from STEMI patients was collected in sodium citrate tubes for plasma and in heparin-free tubes for serum, which was centrifuged at 1600 g to remove cellular components. Serum and platelet-free plasma underwent differential centrifugation, and the supernatant was stored at −80°C until analysis.

3.5 References

[1] B. Benayas *et al.*, "Proof of concept of using a membrane-sensing peptide for sEVs affinity-based isolation," *Front Bioeng Biotechnol*, vol. 11, 2023, doi: 10.3389/fbioe.2023.1238898.

[2] A. Gori *et al.*, "Addressing Heterogeneity in Direct Analysis of Extracellular Vesicles and Their Analogs by Membrane Sensing Peptides as Pan-Vesicular Affinity Probes," *Advanced Science*, vol. 11, no. 29, Aug. 2024, doi: 10.1002/advs.202400533.

[3] S. Busatto *et al.*, "The nanostructured secretome," Jan. 01, 2020, *Royal Society of Chemistry*. doi: 10.1039/c9bm01007f.

[4] J. A. Welsh *et al.*, "Minimal information for studies of extracellular vesicles (MISEV2023): From basic to advanced approaches," *J Extracell Vesicles*, vol. 13, no. 2, Feb. 2024, doi: 10.1002/jev2.12404.

[5] A. Ridolfi *et al.*, "Particle profiling of EV-lipoprotein mixtures by AFM nanomechanical imaging," *J Extracell Vesicles*, vol. 12, no. 10, Oct. 2023, doi: 10.1002/jev2.12349.

[6] A. Musicò *et al.*, "Surface functionalization of extracellular vesicle nanoparticles with antibodies: a first study on the protein corona 'variable,'" *Nanoscale Adv*, vol. 5, no. 18, pp. 4703–4717, Jul. 2023, doi: 10.1039/d3na00280b.

[7] J. Burrello *et al.*, "An extracellular vesicle epitope profile is associated with acute myocardial infarction," *J Cell Mol Med*, vol. 24, no. 17, pp. 9945–9957, Sep. 2020, doi: 10.1111/jcmm.15594.

Chapter 4

Integration of MSP with zwitterionic polymer for EV separation and analysis

4.1 Introduction

In the previous chapter has been demonstrated MPS effectiveness in selectively sorting EVs from other biological nanoparticles, such as LPs, and its applicability in a sensitive digital platform for single-vesicle analysis, such as SiMoA. MSP showed strong ability to directly bind EVs in real biofluids, representing the entire EV sample without bias toward specific sub-populations. Additionally, MSP provided the added benefit of detecting EVs lacking tetraspanins, which are often missed by traditional methods. Based on this data, MSP may be incorporated into various substrates for both analytical assays and EV isolation processes.

During the third year of my PhD program, I spent six months in Professor Arosio's Biochemical Engineering Laboratory at ETH Zurich (https://arosiogroup.ethz.ch/), a leading group in biomolecular condensates. Leveraging the group's expertise in polymer coacervates, we developed zwitterionic polymer coacervates conjugated with the MSP to collective isolation of EVs and serves as an analytical "one-pot assay" for biomarker signature analysis of EVs in complex fluids. The conjugated coacervates use affinity interactions and the phase-separation properties of zwitterionic polymers to selectively isolate EVs from biological matrices. This programmable zwitterionic copolymer can self-assemble into polymer-rich coacervates through electrostatic interactions, responding to environmental factors such as ionic strength and temperature. These coacervates offer several advantages over traditional solid materials used in separation technologies. Their liquid-like nature provides a gentle phase that preserves analyte integrity during isolation. Additionally, zwitterionic polymers exhibit strong anti-fouling properties, minimizing non-specific interactions and selectively recruiting target molecules into functionalized coacervates [1] [2]. Moreover, the technology is scalable and adaptable to various products and instrumentation, with potential applications in bioanalysis, biosensing, and bioprocessing.

Two applications of this new coacervate-based isolation strategy were developed: first, as a preparative step for downstream analysis, and second, as part of an analytical "one-pot assay" for analyzing EV in complex fluids *(Figure 1)*. The following section illustrates the results obtained using this novel system.

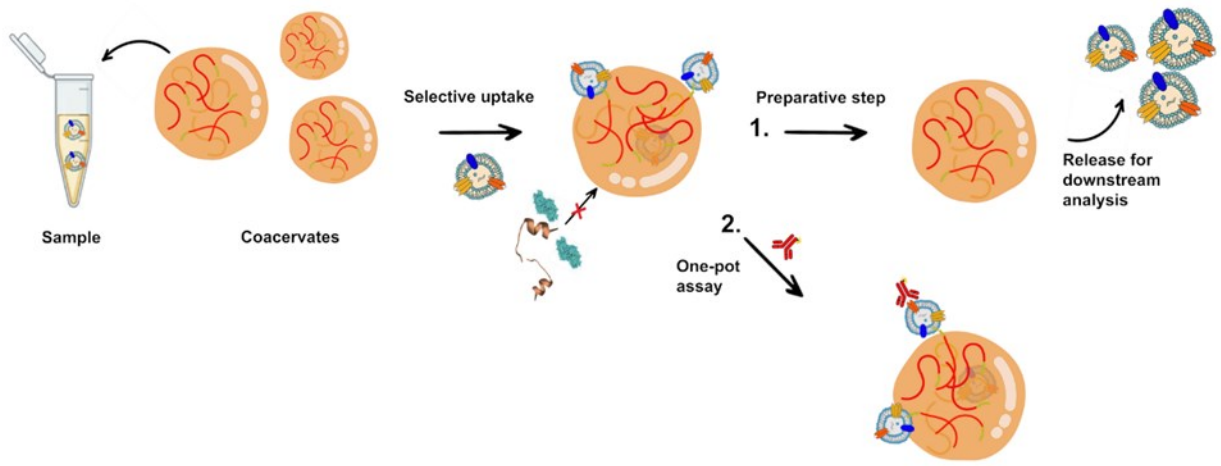

Figure 1: Schema of the two applications: 1) isolation of EVs for downstream analysis, preparative step; 2) "One-pot assay", analysis of EV surface markers into polymer coacervates.

4.2 Results and Discussion

4.2.1 Isolation with zwitterionic coacervate-MSP

Zwitterionic polymer scaffold was functionalized with MSP using the biorthogonal click chemistry reaction, (azide/DBCO), as described in the *4.5 experimental section*. When the ionic strength of the solution is reduced, the functionalized zwitterionic polymer undergoes enthalpy-driven phase separation due to electrostatic interactions, resulting in the formation of a polymer-rich coacervate phase (dense phase) surrounded by a polymer-depleted phase (liquid phase) [1] [2]. The binding and isolation capacity of the functionalized zwitterionic polymer were tested with HEK-EVs spiked into artificial urine at a final concentration of 9×10^8 EVs/mL, using a final polymer concentration of 3.3 g/L. After EV recruitment, release was achieved by increasing the ionic strength of the solution (600 mM NaCl and 500 mM $MgCl_2$). Several techniques evaluated the uptake and subsequent release of intact EVs into the coacervates. Confocal microscopy confirmed the binding of labelled DiO-EVs at the coacervate interface *(Figure 2A),* while, TEM analysis confirmed that the isolated EVs maintained their integrity and typical round ("cup-shaped") morphology with diameters of approximately 40–200 nm, showing no morphological changes upon isolation (*Figure 2B*) [3]. Moreover, the TEM image of the starting sample revealed a significant presence of protein contaminants, which were substantially reduced after the elution of the captured EV from the coacervates. Additionally, TEM images of the starting sample displayed a significant presence of contaminants, which were largely removed after elution from the coacervates. Western blot analysis verified the presence of common EV markers, such as ALIX (96 kDa) and TSG101 (50 kDa), inner proteins involved in EVs

biogenesis, the presence of these markers in the release fraction confirm the integrity of EVs along al the process (*Figure 2C*) [4]. The liquid-like nature of coacervates and their stimulus-responsiveness towards changes in the environment represent important advantages over traditional heterogeneous bead-based affinity assays. To demonstrate the efficiency in a isolation strategy, the liquid-like coacervate was compared with commercially available carboxylic beads i.e., magnetic silanized iron oxide- and latex-based beads. HEK-EVs were spiked in artificial urine were isolated in parallel using both the coacervates and the commercial beads. Then, coacervate and bead pellets were suspended in 600 mM NaCl and 500 mM $MgCl_2$ to trigger the release of EVs from the MSP. The amount of isolated EVs was quantified in terms of transmembrane biomarker expression (CD81 and CD63) using a well-established bead-assisted flow cytometry method [5]. This assay involves capturing EVs with anti-CD81 beads, followed by immunostaining with anti-CD63 and anti-CD81 antibodies. The concentration of EVs released from the coacervate was determined using biomarker-specific calibration curves. Results indicated that the coacervate-based method achieved a higher yield, recovering 50% and 28% of CD81- and CD63-positive EVs, respectively, from the initial sample (*Figure 2E*).

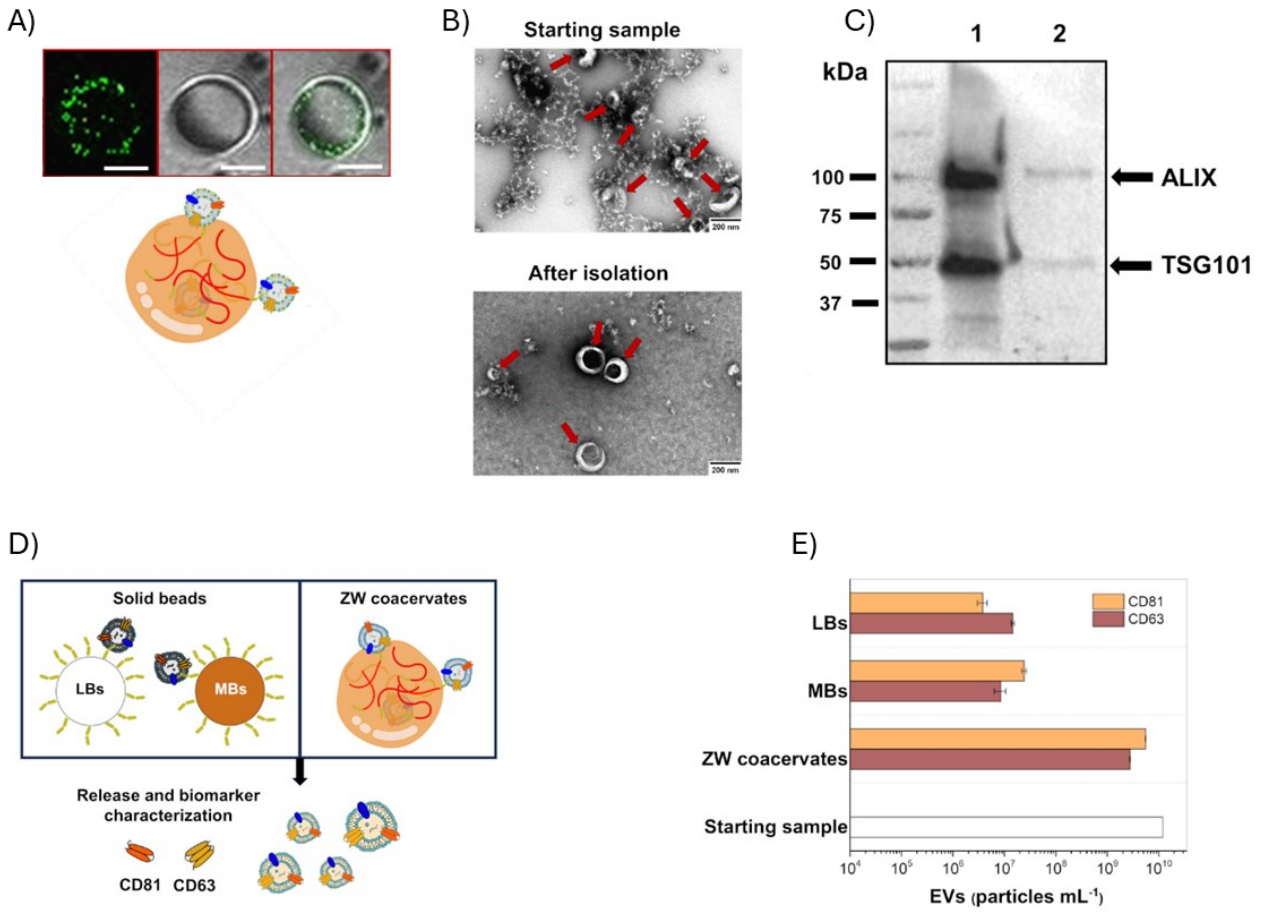

Figure 2: Isolation of EVs from HEK 293 cells spiked in artificial urine: A) Confocal microscopy image of labelled-EVs spiked in artificial urine with functionalized coacervate. From left to right, confocal, brightfield, and merged images (scale bar: 10 µm). B) TEM images of the initial sample and of the isolated EVs. C) Western blot analysis of inner EVs proteins ALIX and TSG101: lane 1, initial sample and lane 2, EVs isolated and released. D) Schematic representation of two different isolation methods. The CD63 and CD81 biomarkers were evaluated in isolated EVs by flow-cytometry. Bars represent the amount of EVs (particles/mL) recovered from the coacervates and the beads, compared to the initial sample.

A similar experimental approach was applied to isolate EVs from human urine. TEM analysis confirmed the successful capture and release of EVs, demonstrating their integrity post-isolation and a reduction in impurities compared to the starting sample (*Figure 3A*). Specifically, fewer protein aggregates and LPs were observed, which are commonly co-isolated using conventional methods based on physical-chemical proprieties [6] [7]. The post-isolation LP content was measured using a commercial Apo-A ELISA kit, revealing that functionalized coacervates effectively excluded LPs, as evidenced by their low abundance in the dense phase (*Figure 3B*). In contrast to the previous experiment performed with HEK-EVs, the presence of nanosized contaminants in human urine can affect the evaluation of the particle concentration. Therefore, in this case, the amount of EVs is estimated from the fluorescence signal associated with the anti-CD9 and anti-CD63 (*Figure 3C*). For the coacervates, we obtained a signal corresponding to 84% of the starting "unprocessed" samples [4] [8], confirming the higher yield achieved by our coacervate-based approach compared to the solid bead strategy, which failed to isolate EVs in this experiment. These results can be partially explained by the larger surface area offered by the polymer coacervate population compared to the solid beads. The increased surface area enhances the interaction and binding capacity of the coacervates, allowing for more efficient EV capture and detection. In contrast, the low signal observed with the solid beads can be attributed to their lower density of carboxylic group functionalization. This limited functionalization results in a reduced amount of MSP immobilized on the bead surfaces, thereby decreasing their capacity to capture EVs effectively. The disparity in performance highlights the importance of surface area and functionalization density in optimizing capture efficiency, particularly for assays that rely on immobilized molecules like MSP.

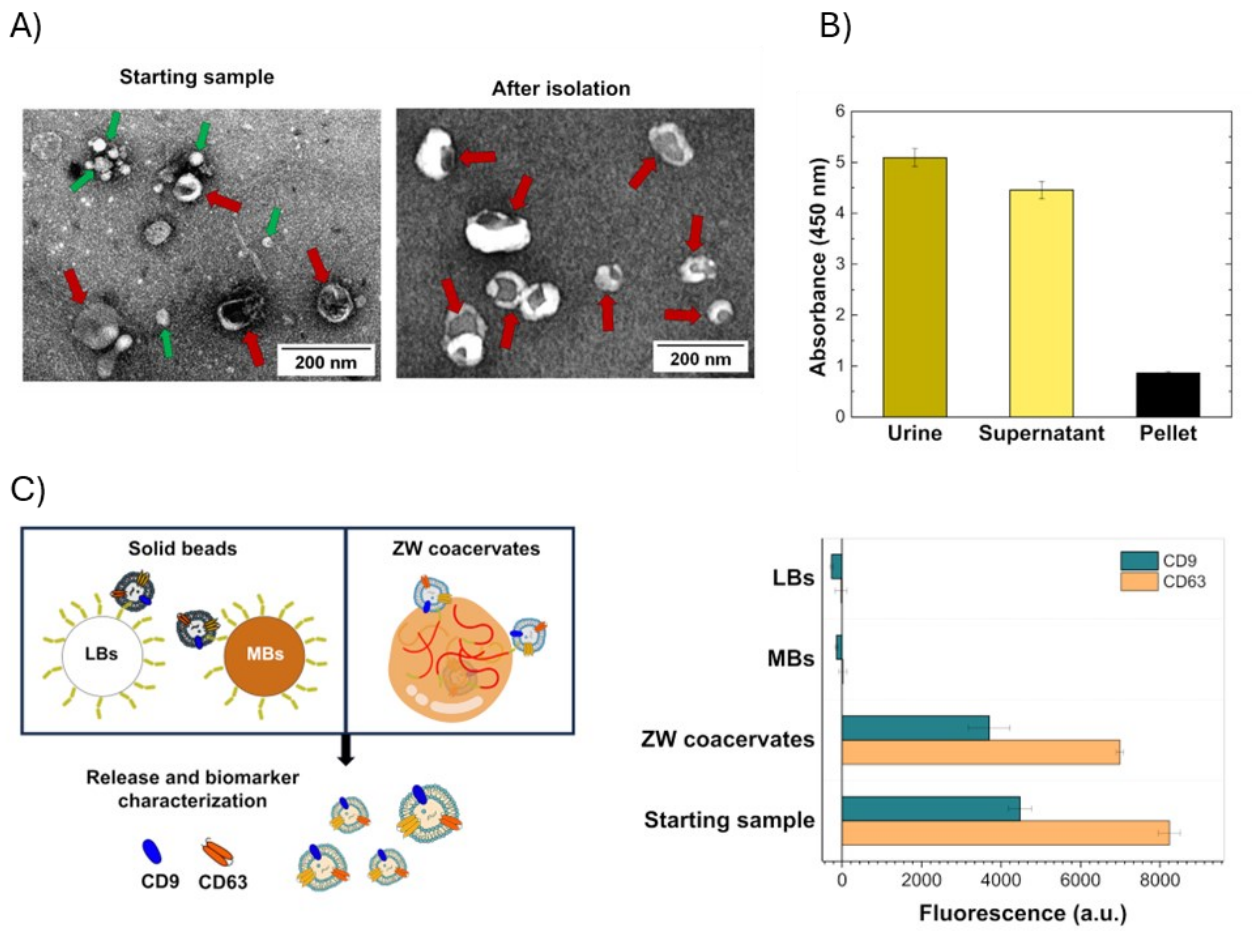

Figure 3: Isolation of EVs from human urine. A) TEM imagines comparing the un-pretreated urine sample and the isolated urinary EVs (indicated by red arrows). Green arrows in the starting sample indicate the presence of contaminants. B) ELISA analysis of the amount of Apo-A in the original urine sample, in the dilute phase (supernatant) after separation from the dense phase, and in the dissolved dense phase (pellet) containing isolated EVs. The bar graph shows the mean absorbance at 450 nm value from triplicate samples. C) Schematic representation of two different isolation methods (left panel). Bar graph indicates the signal fluorescence mean associated to the tetraspanins (CD63 and CD9) present on EVs after isolation by the polymer coacervates and beads, compared to the EV amount in the initial sample.

4.2.2 EVs- Coacervates: "One-pot" analysis

In addition to the preparative step for downstream analysis, the ability of coacervates to selectively localize and concentrate EVs can also be used to perform EV phenotyping through fluorescence immunostaining. This "one-pot" analysis, performed by analyzing stained coacervates with a conventional flow cytometer, a common tool in clinical settings, offers a streamlined alternative to standard bead-based assays. Unlike solid-phase assays, the liquid coacervate-based "one-pot" method reduces preparation time, cost, and specimen handling requirements. Furthermore, the antifouling

properties of the zwitterionic coacervates minimize non-specific adsorption, eliminating additional steps typically required for solid surfaces.

The "one-pot" zwitterionic coacervate-MSP assay was employed to detect HEK-derived EVs spiked into artificial urine, using an anti-CD81 antibody as a fluorescent marker. This innovative approach leverages the zwitterionic coacervate system's ability to concentrate and isolate EVs in a single step, streamlining the assay process. Artificial urine, free of endogenous EVs, serves as a controlled medium that closely mimics the physiological conditions of human urine. This setup enables the introduction of a known quantity of EVs into the system, providing a standardized baseline for detection and quantification. The baseline signal was subtracted from each data point prior to plotting, ensuring accurate analysis of the assay's performance. Furthermore, the use of artificial urine facilitates the evaluation of how sample complexity—similar to that found in real biological fluids—affects the assay's analytical capabilities. This controlled approach allows for a precise assessment of the assay's sensitivity, specificity, and robustness in conditions that resemble those encountered in clinical or research applications.

A calibration curve was established over a concentration range of 8.1×10^7 to 5.2×10^{10} EVs/mL, achieving a limit of detection (LOD) of 5.0×10^8 EVs/mL and a limit of quantification (LOQ) of 2.3×10^9 EVs/mL (*Figure 4A*).

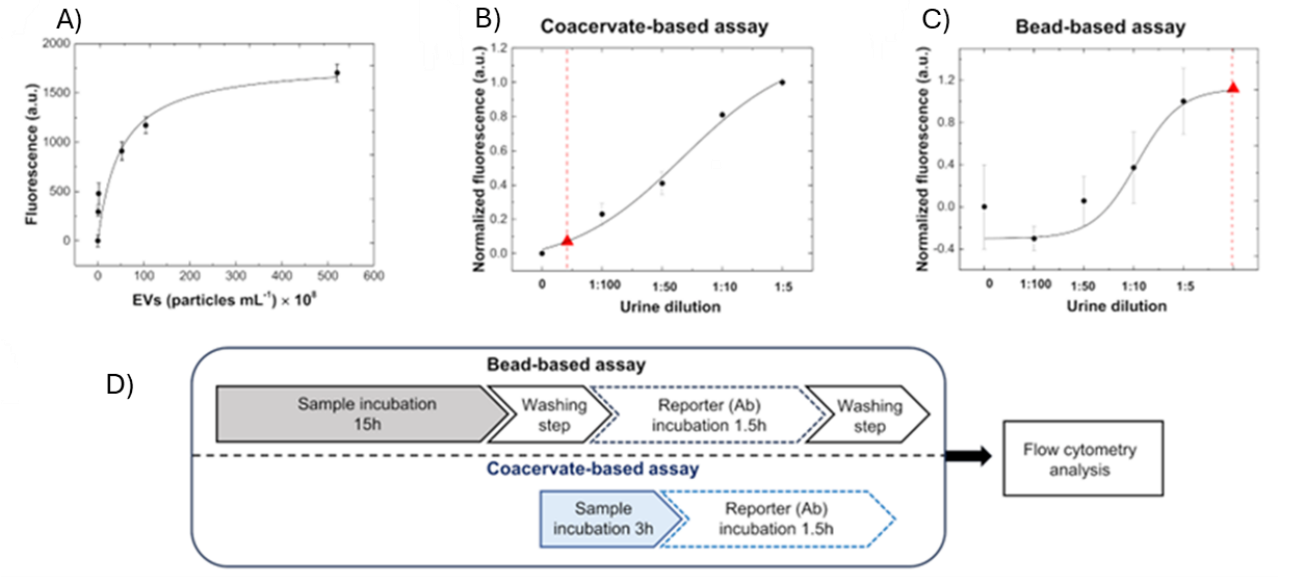

Figure 4: A) Calibration curve for HEK293 EVs spiked in artificial urine, measured with the "one-pot" analysis using fluorescence-labeled anti-CD81 antibody over a concentration range of 8.1×10^7 to 5.2×10^{10} particles/mL. Dilution curve for the "one-pot" analysis of human urine with EV detection via anti-CD9 antibody. (B) and with the magnetic beads-based assay (C). The blank mean was subtracted to all samples. D) Schematic of pre-analytical workflows for conventional flow cytometry with bead-based assay (top) and coacervate-based assay (bottom).

The coacervate-based approach was then applied to real matrices by analyzing a human urine sample from a healthy donor. A dilution-response curve was observed using serial dilutions of human urine (ranging from 1:5 to 1:100), profiling CD9, a classic urinary EV marker *(Figure 4B)*. Noise levels were evaluated using non-functionalized coacervates at the highest dilution (1:5). In contrast, the bead-based assay exhibited high standard deviations across the same tested range, complicating the determination of an optimal dilution factor *(Figure 4C).*

The coacervate-based assay streamlined the pre-analytical workflow, reducing the overall analysis time from 17 hours to just 4.5 hours compared to conventional bead-based methods *(Figure 4D)*. In clinical settings, the high dilution factors achievable with the coacervate method are particularly advantageous when working with limited sample volumes or samples containing high levels of contaminants, which often require dilution to minimize matrix effects.

4.3 Conclusion

This chapter highlights the integration of MSP with zwitterionic polymer coacervates, demonstrating its versatility in both analytical and preparative workflows for EVs. The functionalized coacervates enable selective and gentle isolation of intact EVs from diverse biofluids across varying pH levels and salt concentrations, making the method compatible with various biofluids. Additionally, these coacervates exhibit antifouling properties, allowing for the gentle isolation of intact EVs.

We showcased two key applications of this technology: as a preparative step for downstream analysis and as a "one-pot" assay for EV biomarker profiling. The method effectively captured and released EVs from urine samples, successfully separating EVs from lipoproteins, a common challenge for conventional methods. It achieved high yields of intact recovered EVs, a signal corresponding to 84% of the starting “unprocessed” samples was observed for CD9 at the flow cytometer. This approach concentrates EVs within the coacervates during isolation, enabling direct biomarker profiling using standard flow cytometry with specific staining. The polymer droplets serve as a substrate for analysis, replacing the solid beads typically used in flow cytometry for EV studies. Unlike other techniques, such as SiMoA, this method offers greater flexibility, allowing the substitution of conventional beads with these innovative analytical tools.

The "one-pot assay" simplifies the workflow and enhances the signal-to-noise ratio by minimizing non-specific binding, allowing for the analysis of diluted samples. Compared to traditional bead-based assays, this method streamlines the process and improves overall assay performance. Overall, the phase-separated zwitterionic coacervate platform offers a promising solution for affinity-based

EV isolation from complex mixtures, with potential applications in large-scale manufacturing and liquid biopsy analysis.

4.4 Experimental section

4.4.1 HEK-EVs Cell Culture

HEK 293 cells were cultured following the large-scale process as previously described [5]. 50 mL of medium was clarified by centrifugation at 3000 rcf for 15 min and by filtration through a 0.22 µm membrane. Subsequently, 25 U of Pierce Universal Nuclease was added to the medium and incubated for 2 hours at room temperature. The medium was concentrated 100 times, to achieve approximately 500 µL through Amicon filters with 50 kDa cutoff; before collecting the EV-enriched fractions via SEC as previously described [9].

4.4.2 Zwitterionic polymer-MSP functionalization

The multiblock polymer was synthesized according to a previous well-established procedure [1]. Polymer (DP_{ZB} =140 ZB; DP_{SB} = 60, HEMA-Succ., MW= 58000 g/mol) was dissolved in MES buffer pH = 6, under stirred at RT until complete dissolution. The functionalization of the polymeric chains was achieved using click chemistry. In the first step, a DBCO-NH_2 linker was covalently coupled to the polymer by activating the carboxylic groups. The amine-coupling reaction was allowed to proceed for 1 hour at room temperature under magnetic stirring. Afterward, the modified polymer was washed with 15 mL of Milli-Q water to induce phase separation and was then centrifuged at 7,000 rpm for 30 minutes. The recovered pellet was resuspended in 10 mM PBS pH 7.4 with 1.2 M NaCl, and MSP with an azide group was added. The reaction was allowed to proceed overnight at 25°C under orbital shaking. Final washing steps were performed using Milli-Q water, and the MSP-conjugated polymer was resuspended in 10 mM PBS pH 7.4 with 1.2 M NaCl.

4.4.3 EVs isolation with Zwitterionic polymer-MSP

A final concentration of 3.3 g /L of functionalized polymer in 10 mM phosphate solution at pH ~ 10, were incubated with 9×10^8 EVs/mL of HEK-EVs spiked in artificial urine, for 3 hours under constant stirring. Following the phase separation was induced, with 15 mL of Milli-Q water, and polymer pellet was washed two times. The release of EVs was achieved suspending the polymer pellet in 600 mM NaCl and 500 mM MgCl2 for 15 minutes, at RT under stirring.

4.4.3 EVs isolation with Magnetic Beads-MSP

Commercial carboxylate beads, specifically MagnaBind™ Carboxyl Derivatized Beads (ThermoFisher, 21353) and CML Latex Beads (4% w/v, 5 μm) from Invitrogen (C37255), were functionalized with MSP, following the procedure described above. 400 μL of each bead type was washed three times with PBS and then, carboxylic groups were activated by EDC and following incubated with DBCO-NH2 in MES buffer. The amine-coupling reaction was allowed to proceed for 1 hour at 25°C under orbital shaking at 800 rpm. After incubation, the beads were precipitated, and the supernatant was removed. The beads were then washed, and MSP functionalized with azide group was added to both bead preparations. The click chemistry reaction was performed, allowing the mixture to react overnight at 25°C under orbital shaking at 800 rpm. The following day, the beads were pulled down, the supernatant was removed, and the beads were washed three times. Finally, the peptide-conjugated beads were resuspended in 400 μL of PBS and stored at 4°C.

For the EV uptake, magnetic beads were incubated (4 hours at 10°C) in an orbital shaker (800 rpm with 9×10^8 EVs/mL of HEK-EVs spiked in artificial urine. Then, the beads were washed 3 times with PBS pH 7.4 and were resuspended in 500 mM MgCl2 (200 μL) to trigger the EVs release from the peptide. After 1 hour at 25°C and 800 rpm, the beads were pulled down and the supernatants were collected and characterized for EVs tetraspanin fingerprints using a flow cytometer (Cytoflex S) with commercial anti-CD81-beads.

4.4.4 Flow Cytometer: Bead-based assay

HEK-EVs, human urine and isolated EV preparations were analyzed to obtain an overview of the tetraspanin profile using a commercial bead-based assay. The assay was performed following the manufacturer's instructions and a previously published protocol [5]. Three different fluorescent monoclonal antibodies were used: anti-CD63 PE (bandpass filter: 585/42 nm, gain = 3000), anti-CD81 APC (bandpass filter: 660/10 nm, gain = 3000), IgG1 isotype control APC, and anti-CD9 FITC (bandpass filter: 525/40 nm, gain = 3000). All the samples were analyzed at a medium flow rate of 30 μL min-1 for 60 s after mixing for 3 s.

4.4.5 Flow cytometry analysis of EVs: bead- vs. coacervate-based strategy

Coacervate-based assay: The recruitment of EVs was conducted in two steps. In the first step, 3.3 g/L of functionalized polymer in 10 mM phosphate solution at pH ~ 10 (with 90.4 mM NaCl and 0.1% BSA) was incubated with different concentration of HEK-EVs (range: 8.1×10^7 to 5.2×10^{10} particles/mL) spiked in artificial urine and incubated with the polymeric solution at 10°C for 3 hours under constant stirring (500 rpm). In the second step, anti-CD81-APC Ab diluted 1:500 (3 nM) was

added to each sample. The solutions were further incubated for 1 hour at 25°C (magnetic stirring: 750 rpm) and measured using FACSymphony A5 flow cytometer. A similar procedure was followed to analyze several dilution of human urine, and the detection was performed using anti-CD9-FITC.

*Magnetic beads-based assay :*Peptide-functionalized magnetic beads (MagnaBindTM Carboxyl Derivatized Beads), as well as functionalized-coacervates, were incubated with serial of human urine sample. Specifically, the interaction time of the functionalized-coacervates was set to 3 hours, while the functionalized-beads are left to react overnight, both at 10°C (800 rpm). Follow, the incubation of Ab anti-CD9 (1:500 diluted) and several washing steps for the bead-based strategy. All the controls were conducted in the same experimental conditions.

4.5 References

[1] U. Capasso Palmiero, C. Paganini, M. R. G. Kopp, M. Linsenmeier, A. M. Küffner, and P. Arosio, "Programmable Zwitterionic Droplets as Biomolecular Sorters and Model of Membraneless Organelles," *Advanced Materials*, vol. 34, no. 4, Jan. 2022, doi: 10.1002/adma.202104837.

[2] C. Paganini *et al.*, "High-Yield Separation of Extracellular Vesicles Using Programmable Zwitterionic Coacervates," *Small*, vol. 19, no. 1, Jan. 2023, doi: 10.1002/smll.202204736.

[3] L. Pascucci and G. Scattini, "Imaging extracelluar vesicles by transmission electron microscopy: Coping with technical hurdles and morphological interpretation," *Biochim Biophys Acta Gen Subj*, vol. 1865, no. 4, Apr. 2021, doi: 10.1016/j.bbagen.2020.129648.

[4] C. J. Blijdorp *et al.*, "Comparing approaches to normalize, quantify, and characterize urinary extracellular vesicles," *Journal of the American Society of Nephrology*, vol. 32, no. 5, pp. 1210–1226, May 2021, doi: 10.1681/ASN.2020081142.

[5] C. Paganini, H. Boyce, G. Libort, and P. Arosio, "High-Yield Production of Extracellular Vesicle Subpopulations with Constant Quality Using Batch-Refeed Cultures," *Adv Healthc Mater*, vol. 12, no. 8, Mar. 2023, doi: 10.1002/adhm.202202232.

[6] S. Busatto *et al.*, "The nanostructured secretome," Jan. 01, 2020, *Royal Society of Chemistry*. doi: 10.1039/c9bm01007f.

[7] J. B. Simonsen, "What are we looking at? Extracellular vesicles, lipoproteins, or both?," Sep. 01, 2017, *Lippincott Williams and Wilkins*. doi: 10.1161/CIRCRESAHA.117.311767.

[8] C. Campos-Silva *et al.*, "High sensitivity detection of extracellular vesicles immune-captured from urine by conventional flow cytometry," *Sci Rep*, vol. 9, no. 1, Dec. 2019, doi: 10.1038/s41598-019-38516-8.

[9] K. Normak *et al.*, "Multiparametric Orthogonal Characterization of Extracellular Vesicles by Liquid Chromatography Combined with In-Line Light Scattering and Fluorescence Detection," *Anal Chem*, vol. 95, no. 33, pp. 12443–12451, Aug. 2023, doi: 10.1021/acs.analchem.3c02108.

Chapter 5

Investigate EV-LP interactions

5.1 Introduction

In biological fluids, various eNPs, such as EVs and LPs, coexist in the same environment. These two classes of eNPs arise from different biogenesis pathways, leading to distinct structures and functions. Structurally, EVs are membranous particles that encapsulate a variety of biomolecules, whereas LPs are micellar particles composed of a phospholipid monolayer that encloses a hydrophobic core of cholesteryl esters and triglycerides, with cholesterol and apolipoproteins embedded in the monolayer. Like EVs, the surface properties of LPs make them susceptible to biomolecular corona formation, which can alter their lipid transport function and impact their interactions with other biological entities. EVs, with their high surface area, are particularly prone to interactions with the surrounding environment. These interactions with soluble components, such as proteins and nucleic acids, or with nanostructures like LPs, can significantly change their physic-chemical properties [1]. Traditionally, the EV field has regarded LPs as noninteracting contaminants; however, emerging research indicates that these biological nanoparticles can dynamically interact with EVs to form complexes, highlighting an important area of study due to their potential biological significance [2].

In blood secretome landscape, LPs are approximately six orders of magnitude more abundant than EVs, which may have significant implications [3]. While studying individual eNP classes remains important, it is now crucial to explore their interactions with each other and their environment, particularly under crowded conditions that reflect physiological states. Recent studies suggest that EV-LP complexes may play roles in both physiological and pathological processes. For instance, these associations can preserve the integrity of EVs during cellular internalization and release, potentially facilitating their transport or enhancing cellular uptake of EVs, triggering a cellular response. Additionally, another study indicated that brain cancer-derived EVs tend to interact with LDLs, leading to LDL aggregation and enabling their passage across the blood-brain barrier [4] [5].

Investigating these complexes in actual biological samples is challenging, so we applied a "bottom-up approach" to enable detailed study of particle interactions using multiple techniques. In this chapter, a model system was established to study EV-LP interactions under conditions that mimic the physiological environment. Standard materials, including commercially available lipoproteins (LDL and VLDL) and RBC-derived EVs (REVs), were used as references. High-sensitivity techniques such as Super-Resolution Microscopy (SRM), Flow Cytometry (FACS), and Single Molecule Array

(SiMoA) were employed for analysis. Labeled standard materials enabled the observation of EV-LP interactions through colocalization events detected by SRM and demonstrated the stability of EV-LP complexes on platforms like FACS, where LP dose-response curves were generated using different stoichiometric ratios of EV-LP particles. Additionally, an immunophenotyping assay was developed on the SiMoA platform, utilizing distinct probes to capture EVs and detect LPs, enabling the analysis of multiparticle complexes. This innovative system allows the investigation of EV-LP interactions across a range of stoichiometric ratios, providing a precise method to assess the stability of these complexes in conditions closely resembling physiological states.

5.2 Results and discussion

5.2.1 Biophysical and biochemical characterization of REVs and LPs

Biophysical and biochemical analyses, including BCA assay, Western blotting, and dynamic light scattering (DLS), were used to characterize REVs and LPs. REVs were isolated using calcium ionophore induction of red blood cells following Usman et al.'s protocol. The BCA assay revealed protein concentrations of 2.08 ± 0.12 μg/μL for REVs, 12.81 ± 2.14 μg/μL for LDL, and 4.17 ± 0.52 μg/μL for VLDL. While, DLS was used to assess size distribution, ζ-potential, and particle concentration, showed monomodal size distributions: 120 nm for REVs, 30 nm for VLDL, and 15 nm for LDL. Particle concentrations were 7.66×10^{11} particles/mL for REVs, 5.38×10^{13} particles/mL for LDL, and 2.92×10^{11} particles/mL for VLDL (*Figure 1*). Results were based on particle count rather than intensity to ensure accurate representation. Western blotting confirmed the presence of Band 3 in REVs and ApoB-100 in LDL and VLDL, verifying the purity of each sample and ruling out cross-contamination (*Figure 1*). For fluorescence labeling, REVs and LPs were labeled with Atto NHS 633 and Atto DPPE 488, respectively, with no significant changes in size distribution or hydrodynamic diameter after labeling. In summary, REVs and LPs were thoroughly characterized through biochemical assays and DLS, confirming their identity, purity, and stability post-labeling.

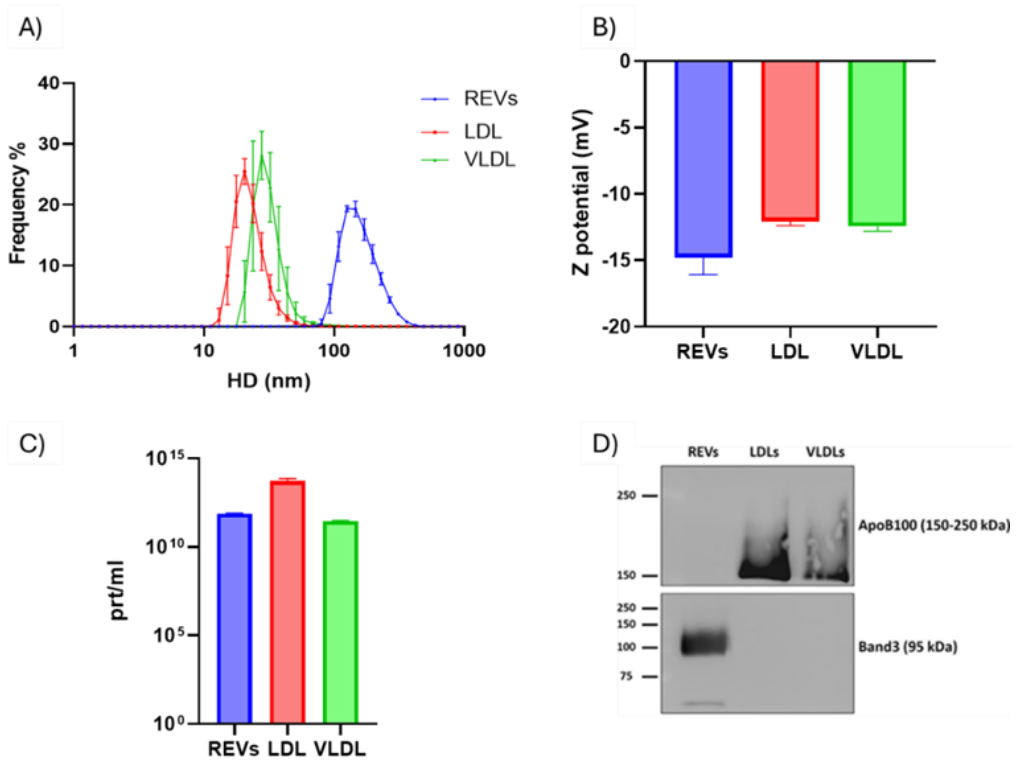

Figure 1: The graphs report: the particles size distribution, based on DLS measurements (A); the particles negative ζ-potential in DLS measurements (B); particles concentrations determined by DLS (C); and the Western Blot analysis that confirm the present of specific biomarkers for REVs (BAND-3) and LPs (Apo-B 100).

5.2.2 Super Resolution Microscopy

A single-particle technique, SRM, was employed to assess the presence of EV-LP complexes using labelled REVs (Atto-647) and labelled LPs (Atto-488). EVs, at final concentrations of 10^{11} EVs/mL, were mixed with a single class of LP at concentrations of 5×10^{12} LPs/mL for LDL, and 5×10^{11} LPs/mL for VLDL. The EV-LP complexes were tested under two conditions: *(1)* diluted in PBS and *(2)* diluted in LP-depleted human plasma. These conditions were chosen to evaluate whether the plasma environment enhances particle interactions.

In both conditions, colocalized events, where particles were positive for both fluorophores, were observed, indicating potential interactions between EVs and LPs. The percentage of EVs also positive for LPs was calculated to estimate the formation of EV-LP complexes. However, no significant difference in the percentage of colocalized events was observed between the PBS and LP-depleted plasma samples. As shown in *Figure 2*, approximately 30% of the total REVs colocalized with both LDL and VLDL under both conditions, with a slight but statistically insignificant increase seen in the LDL-PBS sample.

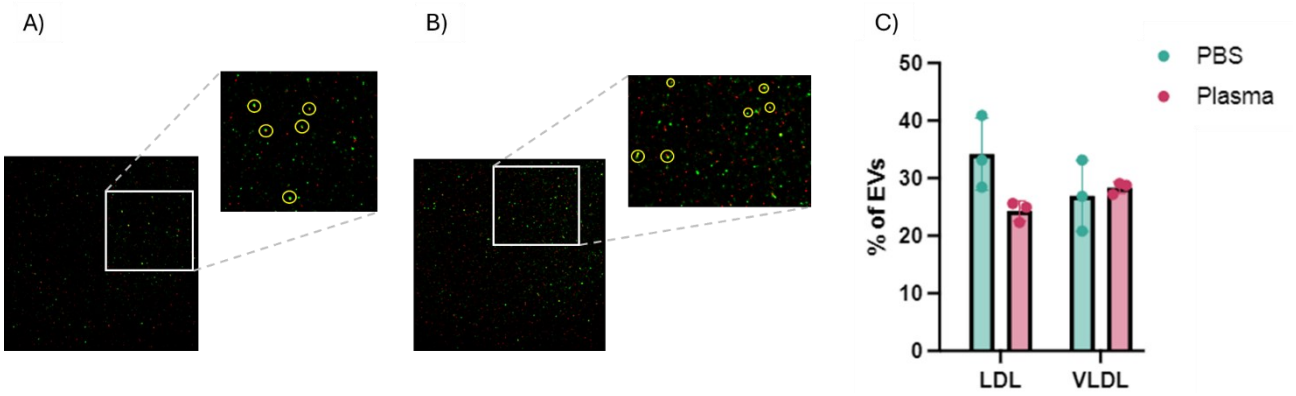

Figure 2: Representative SRM images showing colocalized complexes. (A) REVs/LDL sample in human plasma and (B) REVs/LDL sample in PBS. Complexes are indicated with yellow circles. (C) Graph showing the percentage of colocalized events across samples.

5.2.3 Flow Cytometer analysis

Bead-based FACS analysis is a commonly used method for evaluating EVs and their marker expression. In this chapter, MSP-functionalized beads were employed to investigate EV-LP interactions using the same labeled particles as in the SRM experiments. MSP beads allow to capture EVs involved in the complexes, enabling detection of fluorescence signals from both REVs and LPs. This platform also facilitates the analysis of EV-LP interactions across a wide range of stoichiometric ratios.

To assess these interactions, a fixed amount of REVs (10^{11} EVs/mL) was incubated with varying LP concentrations. The concentration range for LDL was from 5×10^{12} to 3×10^{9}, while for VLDL, it ranged from 5×10^{11} to 3×10^{8} , with seven dilution points tested for each. To evaluate non-specific signals from free LPs, the highest LP concentrations were incubated with MSP beads. Importantly, when either EVs or LPs were incubated alone with MSP beads, no significant signal was detected in the LP channels *(Figure 3)*. A detectable signal was only observed when EV-LP interactions occurred, confirming the specificity of MSP beads for EVs and their minimal affinity for free LPs. Furthermore, this approach thus proves effective for studying EV-LP complexes, as a positive signal is generated exclusively when EV-LP interactions are present.

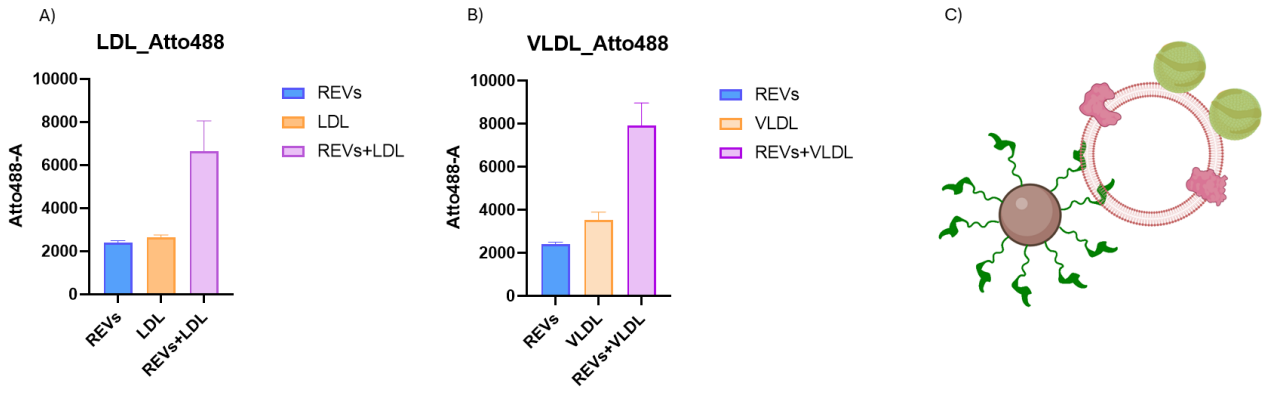

Figure 3: Negative controls for both LPs are shown. MSP-beads captured REVs with no signal detected in the LP channels (blue bars). Minimal non-specific interaction was observed between MSP and the highest concentrations of either LDL (A) or VLDL (B). Signal intensity notably increased when EVs and LPs were incubated together (purple bars); in both cases, REVs-LDL and REVs-VLDL complexes displayed higher signals compared to their controls. Schema (C) illustrates the assay used, with MSP-beads capturing EV-LP complexes via EV binding.

The MSP-bead strategy allows for the investigation of dilution curves across different stoichiometric ratios of particles. A fixed concentration of EVs was incubated with varying concentrations of LPs in PBS and analyzed using a CytoFLEX (Beckman Coulter). Tracking the LP signal revealed dose-response curves for both LDL and VLDL, enabling us to compare their stability under these analytical conditions *(Figure 4C)*. The data indicated that REVs/VLDL interactions exhibited greater stability in this context..

When examining the EV channel (red signal), which was expected to remain constant, we observed a decrease in signal at higher LP concentrations. As the LP concentration decreased, the EV signal progressively increased until it plateaued at the baseline REV signal intensity seen in the absence of LPs (Figure 4). This trend suggests that at higher LP/EV ratios, more interactions occur between LPs and the EV surface, reducing the available surface area of EVs. Consequently, fewer binding sites are accessible for MSP to attach to the EV lipid bilayer, resulting in a lower EV signal.

These findings support the hypothesis that LPs interact with the EV surface, which in turn affects MSP’s capacity to capture EVs. This observation aligns with MSP's known binding mechanism and is consistent with the data obtained in this analysis.

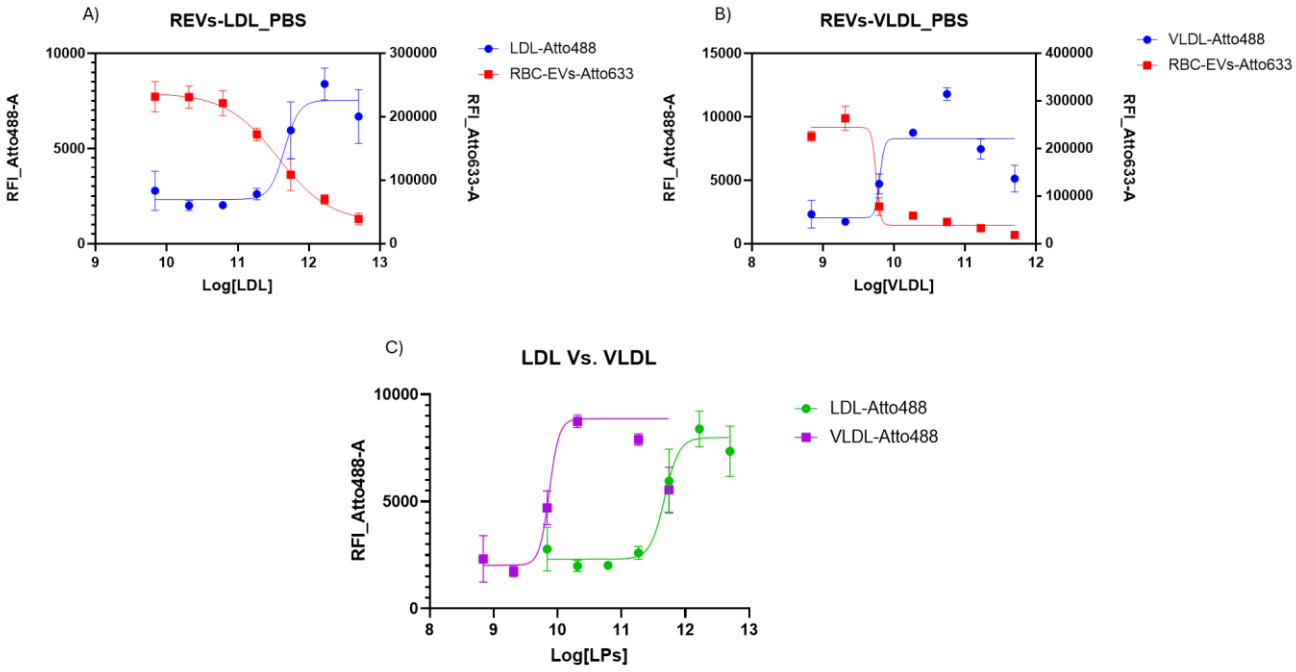

Figure 4: The graphs display dilution curves with various stoichiometric particle ratios. The blue curves represent LPs, LDL (A) and VLDL (B), while the red curves indicate REVs. In graph (C), LDL and VLDL curves are compared.

5.2.4 SiMoA analysis

SiMoA technology, introduced earlier in this thesis, is a single-molecule/particle digital platform based on immunoaffinity. This chapter presents a novel assay utilizing SiMoA to deeply investigate EV-LP complexes. The assay uses two distinct immune-affinity probes: anti-Band 3 antibodies immobilized on beads to capture EVs, and antibodies against Apo-B 100 to detect LPs. This immuno-hetero-sandwich format enables the analysis of multi-particle complexes across a wide range of EV-LP stoichiometric ratios. Unlike FACS analysis, which relies on labelled samples, this platform accommodates unlabeled samples, this approach allows for tracking a specific marker and analyzing its correlation with LPs interactions. Additionally, this method provides a precise assessment of the stability of LP interactions with EVs under near-physiological conditions.

As in the FACS analysis, control experiments were conducted to evaluate non-specific signals. To do this, two control samples were assessed: REVs diluted in PBS and REVs spiked into LP-depleted human plasma. In the PBS sample, the ApoB 100 signal was negligible, while in the depleted plasma sample, a higher signal was observed (*Figure 5*). This elevated signal was expected, indicating that residual LPs in the depleted plasma interact with REVs. To further validate these findings, LDL and VLDL standards were incubated with REVs in both conditions. The unbalanced LP-to-EV ratio, which favored LPs, enhanced particle interactions. Both samples showed higher signals compared to

EVs alone in the same conditions without LPs, confirming the presence of interactions and validating the use of this novel assay for studying EV-LP complexes.

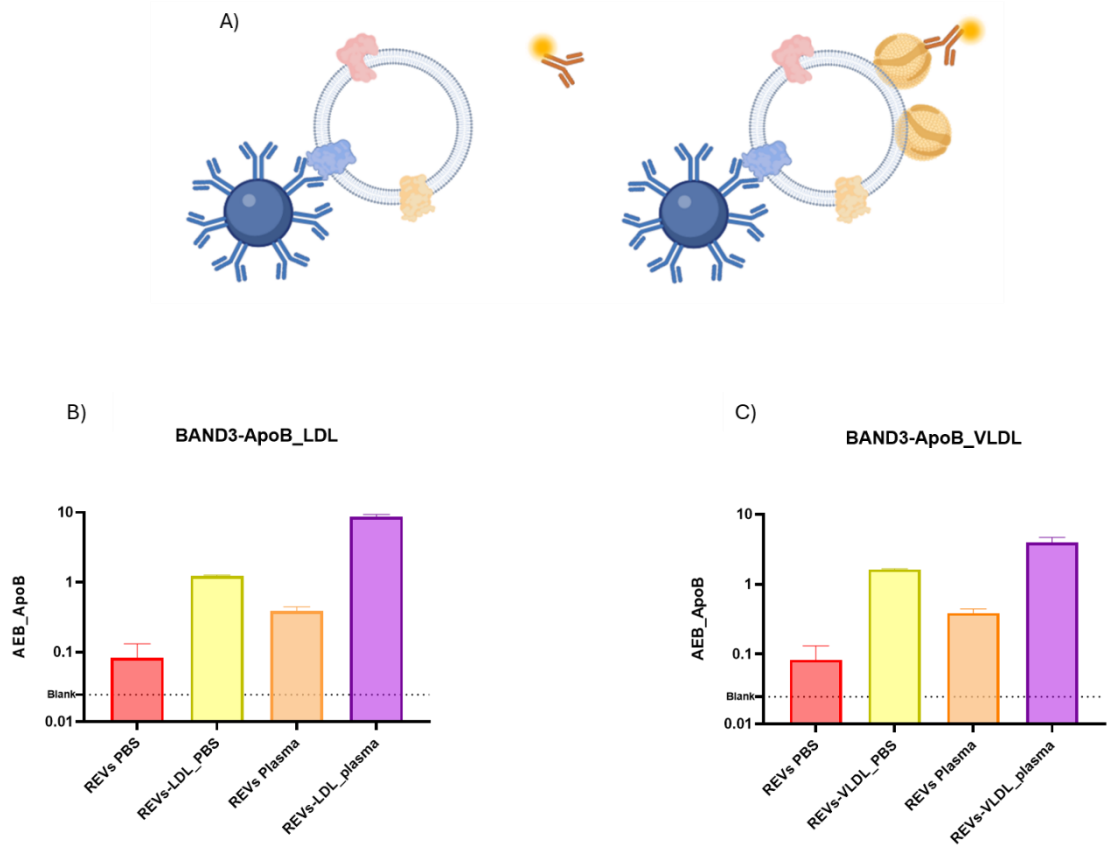

Figure 5: A) A schematic of the control assays, showing both REVs alone and RBC-EV-LP complexes, each detected with anti-Apo-B 100. (B) Bar graphs display control tests to assess non-specific signals; LDL controls and complexes are shown, while (C) presents the VLDL data.

The same concentration range and stoichiometric ratios of EVs and LPs analyzed by FACS were also examined using the SiMoA assay described above. In all conditions, a clear dose-response curve was observed. In LP-depleted plasma preparations, a slight increase in signal was detected at higher LP concentrations for both LDL and VLDL samples. Notably, when comparing equivalent stoichiometric ratios for both LDL and VLDL, insights into the stability of each LP class in relation to REVs could be drawn.

Our results indicate that REVs/VLDL complexes exhibit greater stability than REVs/LDL complexes, both in PBS and LP-depleted plasma preparations. In both conditions, VLDL interactions showed slightly higher stability. Interaction stability was evaluated using the dissociation constant (Kd) derived from the interpolated dose-response curve. Additionally, Bmax values suggest that LDL may access a higher number of binding sites compared to VLDL.

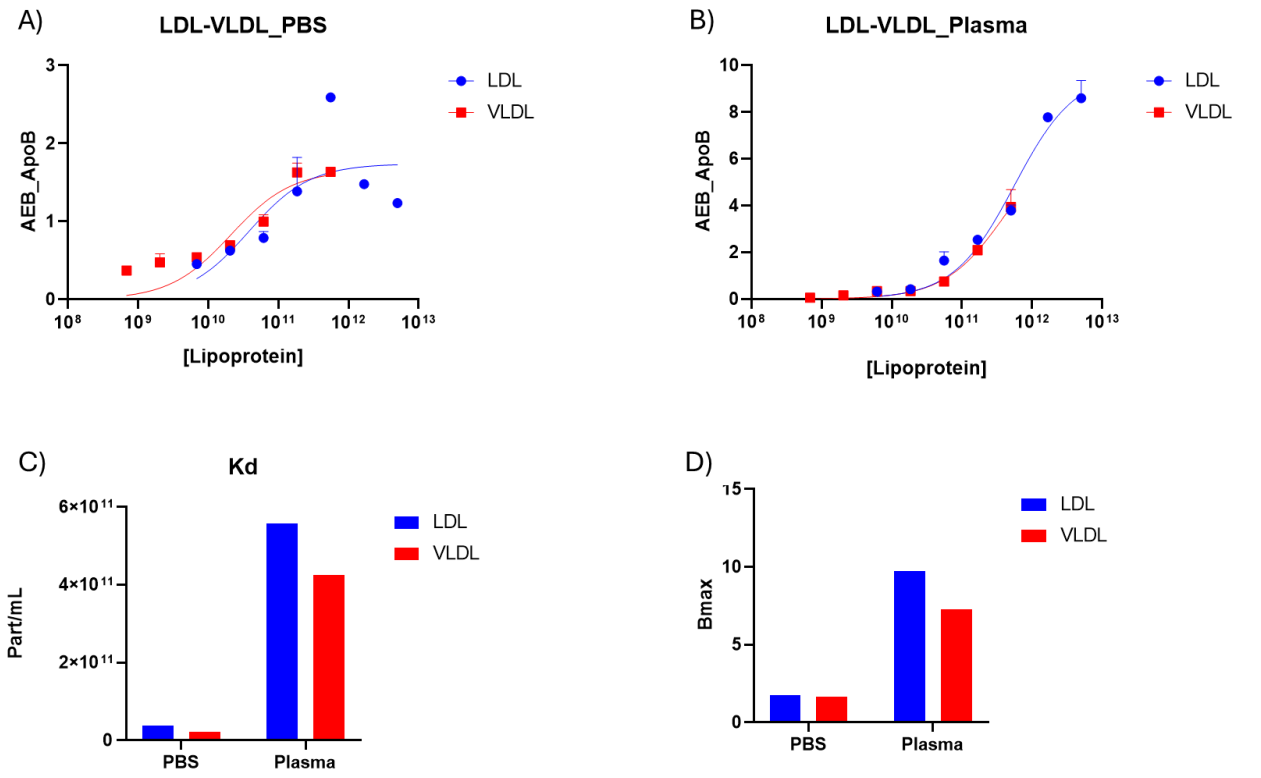

Figure 6: Dose-response graphs showing REV-LDL (blue line) and REV-VLDL (red line) curves in PBS (A) and depleted plasma (B). The bar graphs present the Kd values obtained from the fitted curves (C) and Bmax data (D).

5.3 Conclusion

EV-LP interactions have gained significant interest due to their potential role in physiological and pathological pathways, where they may alter the physical properties of EVs in real samples. To investigate these interactions in depth, a "bottom-up approach" was used, leveraging standard materials to mimic and induce complex formation. In summary, data indicate that interactions between REVs and LPs (LDL and VLDL) occur, with SRM co-localization confirming these complexes when the EV-LP ratio is skewed toward LPs.

Further, two analytical techniques, FACS and SiMoA, were applied to examine these complexes. FACS analysis revealed a higher stability for REVs/VLDL interactions under specific analytical conditions, while also highlighting the behavior of MSP in capturing these complexes. When the EV-LP ratio favors LPs, increased interactions between LPs and the EV surface reduce available surface area on EVs, likely limiting MSP binding sites on the EV lipid bilayer and resulting in a decreased EV signal. Additionally, SiMoA technology, an immunophenotyping assay, confirmed the greater stability of REVs/VLDL complexes compared to REVs/LDL complexes in both dilution conditions.

The interaction stability was assessed using the Kd value derived from interpolated curves, while the Bmax value suggested that LDL can access a larger number of binding sites than VLDL. This assay can also be extended to evaluate EV-LP complexes in real biofluids, providing a valuable approach for studying nanoparticle interactions under physiological and pathological conditions in real biofluids.

5.4 Experimental section

5.4.1 Super resolution Microscopy

Labelled REVs (Atto-647) and LPs (Atto-488) were used for this analysis, with final concentrations of 10^{11} EVs/mL for EVs, 5×10^{12} LPs/mL for LDL, and 5×10^{11} LPs/mL for VLDL. These were mixed overnight in PBS or in lipoprotein-depleted human plasma to facilitate EV-LP interactions. Next, 100 µL of the EV-LP sample was added to a freshly plasma-treated 18-well µ-Slide (Ibidi, Germany) and incubated for 1 hour. After incubation, the supernatant was aspirated and replaced with a blocking buffer (1% BSA in PBS). Prior to imaging, the blocking solution was removed and replaced with 250 µL of freshly prepared standard STORM blinking buffer. Samples were imaged using a Nikon Ti2 Eclipse inverted microscope system equipped with an ANDOR iXon DU897 EM-CCD camera (16x16 µm² pixel size) and an SR Apochromat TIRF 100x 1.49 N.A oil immersion objective. The sample was illuminated in total internal reflection mode, with the laser angle of incidence monitored by a Photometrics Dyno CCD camera at the back focal plane of the objective. Imaging was performed sequentially using 647 nm (125 mW) and 488 nm (80 mW) laser lines, with the laser power set to 40% at 2x magnification. A total of 10,000 images were recorded at an exposure time of 30 msec.

5.4.2 Flow Cytometer MSP-beads

MagnaBind™ Carboxyl Derivatized Beads (Cat. No. 21353) were functionalized as described in the *Experimental section, Chapter 4*. Briefly, conjugation was performed in two steps. First, DBCO-NH_2 was covalently coupled to the beads by activating carboxylic groups with EDC. The beads were then incubated with MSP-N_3. After each step, the magnetic beads were washed with PBS (pH 7.4) using a magnet support.

For analysis, MSP-beads were incubated with 0.1 mL of the sample overnight at 10°C and 800 rpm. Following incubation, three washing steps were performed on the magnetic support using Assay Buffer (PBS, 0.05% BSA). The beads were then resuspended in 0.5 mL of Assay Buffer and analyzed with a flow cytometer (CytoFLEX S). Two different fluorescent channels were used, for REVs (Atto647) bandpass filter: 660/10 nm, gain = 3000, and for LPs (Atto488) bandpass filter: 525/40 nm, gain = 3000. All the samples were analyzed at a medium flow rate of 30 µL min-1 for 60 s after mixing for 3 s.

5.4.3 SiMoA

The assay was run as described in the previous chapters, Band 3-conjugated beads and biotinylated anti-ApoB (0.6 μg/mL) (Santa Cruz, CA, USA) were used. 25 μl of beads were transferred into a 96 microwell plate and mixed with 100 μl EV-LP complexes sample and incubated for 30 min at 25 °C at800 rpm. After incubation, beads were washed with an automatic plate-washer using optimized Tween concentration and then incubated for 10min with 100 μl of detector antibody. After that, beads were washed with an automatic plate-washer and incubated for 10 min with a 150 pm SBG solution (in SBG Diluent, Quanterix). After the SBG incubation step the plate was washed and then inserted into the Quanterix SR-X instrument for analysis where RGP is automatically added. Data were analyzed and processed by Reader Software SiMoA 1.1.0.

5.5 References

[1] E. I. Buzás, E. Tóth, B. W. Sódar, and K. Szabó-Taylor, “Molecular interactions at the surface of extracellular vesicles,” Sep. 01, 2018, *Springer Verlag*. doi: 10.1007/s00281-018-0682-0.

[2] R. E. Ghebosu, J. Pendiuk Goncalves, and J. Wolfram, “Extracellular Vesicle and Lipoprotein Interactions,” Jan. 10, 2024, *American Chemical Society*. doi: 10.1021/acs.nanolett.3c03579.

[3] J. B. Simonsen, “What are we looking at? Extracellular vesicles, lipoproteins, or both?,” Sep. 01, 2017, *Lippincott Williams and Wilkins*. doi: 10.1161/CIRCRESAHA.117.311767.

[4] S. Busatto, Y. Yang, D. Iannotta, I. Davidovich, Y. Talmon, and J. Wolfram, “Considerations for extracellular vesicle and lipoprotein interactions in cell culture assays,” Apr. 01, 2022, *John Wiley and Sons Inc*. doi: 10.1002/jev2.12202.

[5] D. Iannotta, A. A, A. W. Kijas, A. E. Rowan, and J. Wolfram, “Entry and exit of extracellular vesicles to and from the blood circulation,” *Nat Nanotechnol*, vol. 19, no. 1, pp. 13–20, Jan. 2024, doi: 10.1038/s41565-023-01522-z.

Chapter 6

Conclusion and Future perspectives

The role of eNPs has gained increasing relevance in mediating communication in both physiological and pathological processes. Due to these functions, eNPs show great potential as biomarkers in liquid biopsies and as tools for disease monitoring and cellular health assessment, offering minimal discomfort to patients. However, several challenges have been highlighted in this work, including the difficulty of separating and analyzing different classes of eNPs. This is due to the complexity of biofluids where eNPs coexist, the overlap in their physical and chemical properties, and, specifically for EVs, the significant heterogeneity within their populations. This thesis addressed these challenges by developing methods to accurately sort and analyze individual classes of eNPs. Given the complexity of real biofluids, the use of highly sensitive digital platforms for single EV detection is essential.

In *Chapter 2*, two commercially available digital platforms, SiMoA and SP-IRIS, were compared in terms of performance. SiMoA demonstrated superior capabilities, including a lower limit of detection (LOD), a broader operational range, and higher throughput, making it better suited for applications in real biofluids.To address the heterogeneity within EV populations, a pan-specific EV probe was introduced. This new EV ligand, a peptide sequence known as MSP, exhibits strong affinity for high membrane curvature. By targeting the lipid bilayer, this approach represents a potential paradigm shift in EV research, enabling the capture of the entire EV population without restricting the selection to specific subclasses based on surface marker expression.

In *Chapter 3*, the MSP was integrated into SiMoA beads to perform direct single EV analysis in real biofluids. This new MSP-based SiMoA assay was compared with the standard EV SiMoA assay (pan-tetraspanin), and showed comparable results. The MSP-SiMoA assay offers key advantages, including high affinity for EVs, minimal binding to other eNPs, like LPs, and the ability to detect EVs lacking specific surface markers. Indeed, its binding mechanism enable to capture EVs o capture EVs independently of express markers on the surface. This approach may be directly used in real samples without prior EV enrichment; this makes it suitable for clinical applications. In this work, the assay was tested in a real scenario, successfully distinguishing between STEMI and stable angina patients.

In light at these data, in *Chapter 4*, MSP was implemented on a zwitterionic polymer for preparative steps in downstream analysis, and analytical workflow as a "one-pot" assay. On this substrate, MSP effectively captured and released intact EVs, achieving high isolation yields with minimal

contamination. Additionally, this method can be integrated into analytical workflows. The system enables EV biomarker profiling within the coacervates using immune-staining, with a streamlined "one-pot" assay readout via conventional flow cytometry, which is readily accessible in clinical laboratories. The method offers several advantages, in both applications: it is easy to handle, uses cost-effective compounds, and reduces processing time while providing performance comparable or superior to commercially available systems. This makes it well-suited for scale-up and industrial applications.

In *Chapter 5*, the interactions between EVs and lipoproteins (EV-LP) were investigated due to their potential biological roles in both pathological and physiological processes. However, analyzing EV-LP complexes in real fluids is challenging. To address this, a 'bottom-up approach' was employed using standard materials to reconstruct these complexes. A combination of analytical techniques, including SRM, FACS, and SiMoA, was used to study these interactions. A novel SiMoA assay feature distinct probes: one for capturing EVs and another for detecting LPs, enabling the analysis of multi-particle complexes. This system allowed for the investigation of a wide range of EV-LP stoichiometric ratios and provided a precise method to evaluate interaction stability under near-physiological conditions. Additionally, this approach has the potential for application in real fluids to monitor EV-LP complexes.

In conclusion, this thesis addressed various challenges related to the isolation and analysis of eNPs. The issue of EV heterogeneity was tackled using a pan-specific EV probe, MSP. Its integration into different surfaces produced excellent results for both isolation and analytical applications, making it an attractive option for companies interested in developing commercial assays for precise EV detection and isolation.

Appendix

This appendix lists publications from additional "side" activities undertaken to support colleagues on allied topics, utilizing skills and methodologies developed throughout the Ph.D. projects.

Publications

1) Elucidating the 3D Structure of a Surface Membrane Antigen from Trypanosoma cruzi as a Serodiagnostic Biomarker of Chagas Disease. Di Pisa, F., De Benedetti, S., Fassi, E. M. A., Bombaci, M., Grifantini, R., Musicò, A., **Frigerio, R.,** Pontillo, A., Rigo, C., Abelli, S., Grande, R., Zanchetta, N., Mileto, D., Mancon, A., Rizzo, A., Gori, A., Cretich, M., Colombo, G., Bolognesi, M., Grande, R., Zanchetta, N., Gismondo, M. R., Mileto, D., Marcon, A., Gourlay, L. J. *Vaccienes* 2022. 10 (1), 71; Doi: https://doi.org/10.3390/vaccines10010071

2) Peptide–Agarose Hydrogels for Robust and High-Sensitivity 3D Immunoassays. Bergamaschi, G., Musicò, A., **Frigerio, R**., Strada, A., Pizzi, A., Talone, B., Ghezzi, J., Gautieri, A., Chiari, M., Metrangolo, P., Vanna, R., Baldelli Bombelli, F., Cretich, M., and Gori, A. Composite *ACS Appl. Mater. Interfaces*. 2022. 14, 4, 4811–4822. Doi: https://doi.org/10.1021/acsami.1c18466

3) Risk stratification of patients with SARS-CoV-2 by tissue factor expression in circulating extracellular vesicles. Jacopo Burrello, Elena Caporali, Lorenzo Grazioli Gauthier, Enea Pianezzi, Carolina Balbi, Elia Rigamonti, Sara Bolis, Edoardo Lazzarini, Vanessa Biemmi, Alessio Burrello, **Roberto Frigerio**, Gladys Martinetti, Tanja Fusi-Schmidhauser, Giuseppe Vassalli, Enrico Ferrari, Tiziano Moccetti, Alessandro Gori, Marina Cretich, Giorgia Melli, Silvia Monticone and Lucio Barile. *Vascular Pharmacology,* 145, 2022. Doi: https://doi.org/10.1016/j.vph.2022.106999

4) Variations of follicular fluid extracellular vesicles miRNAs content in relation to development stage and season in buffalo. Capra, Emanuele; Kosior, Michal Andrzej; Cocchia, Natascia; Lazzari, Barbara; Del Prete, Chiara; Longobardi, Valentina; Pizzi, Flavia; Stella, Alessandra; **Frigerio, Roberto**; Cretich, Marina; Consiglio, Anna Lange; Gasparrini, Bianca. *Scientific Report,* 12, issue 1, pages 14886, 2022. Doi: https://doi.org/10.1038/s41598-022-18438-8

5) Multifunctional membranes for lipidic nanovesicle capture. Simona Salerno, Sabrina Morelli, Antonella Piscioneri, Mariangela Frangipane, Alessandro Mussida, Laura Sola, **Roberto Frigerio**, Alessandro Strada, Greta Bergamaschi, Alessandro Gori, Marina Cretich, Marcella Chiari, Loredana

De Bartolo *Separation and Purification Technology*, 298 (2022), 121561. Doi: https://doi.org/10.1016/j.seppur.2022.121561

6) Epitope Mapping on Microarrays Highlights a Sequence on the N Protein with Strong Immune Response in SARS-CoV-2 Patients. Roberto Frigerio, Angelo Musicò, Alessandro Strada, Alessandro Mussida, Paola Gagni, Greta Bergamaschi, Marcella Chiari, Luisa Barzon, Alessandro Gori & Marina Cretich. *Peptide Microarrays. Methods in Molecular Biology,* 2022, *vol 2578.* Doi: https://doi.org/10.1007/978-1-0716-2732-7_15

7) Hybrid Peptide–Agarose Hydrogels for 3D Immunoassays. Angelo Musicò, Greta Bergamaschi, Alessandro Strada, **Roberto Frigerio**, Paola Gagni, Marina Cretich & Alessandro Gori. *Peptide Microarrays. Methods in Molecular Biology,* 2022, *vol 2578.* Doi: https://doi.org/10.1007/978-1-0716-2732-7_5

8) Membrane-Sensing Peptides for Extracellular Vesicle Analysis. Alessandro Strada, **Roberto Frigerio**, Greta Bergamaschi, Paola Gagni, Marina Cretich & Alessandro Gori. *Peptide Microarrays. Methods in Molecular Biology,* 2022, *vol 2578.* Doi: https://doi.org/10.1007/978-1-0716-2732-7_18

9) On the interaction and nanoplasmonics of gold nanoparticles and lipoproteins. Andrea Zendrini, Jacopo Cardellini, **Roberto Frigerio**, Marianna Bertoni, Debora Berti, Paolo Bergese. *JCIS Open,* Volume 11, 2023. https://doi.org/10.1016/j.jciso.2023.100088

10) Head-to-Head Comparison of Tissue Factor-Dependent Procoagulant Potential of Small and Large Extracellular Vesicles in Healthy Subjects and in Patients with SARS-CoV-2 Infection. Brambilla, Marta, **Frigerio, Roberto**, Becchetti, Alessia, Gori, Alessandro, Cretich, Marina, Conti, Maria, Mazza, Antonella, Pengo, Martino, Camera, Marina. *Biology* 2023, 12(9), 1233. Doi: https://doi.org/10.3390/biology12091233.

11) Extracellular vesicles from seminal plasma to improve fertilizing capacity of bulls. Anna Lange-Consiglio, Emanuele Capra, Noemi Monferini, Simone Canesi, Giampaolo Bosi, Marina Cretich, **Roberto Frigerio**, Valentina Galbiati, Federica Bertuzzo, Francesco Cobalchini, Fausto Cremonesi, Bianca Gasparrini. *Reproduction and Fertility*, Volume3; issue 4, 313-327, 2022. Doi: https://doi.org/10.1530/RAF-22-0037

12) Endometrial and oviduct extra-cellular vescicles for in vitro equine sperm hyperactivation and oocyte fertilization. Anna Lange-Consiglio, Emanuele Capra, Deborah Giuliani, Simone Canesi, Federico Funghi, Giampaolo Bosi, Marina Cretich, **Roberto Frigerio**, Valentina Galbiati,

Fausto Cremonesi. *Theriogenology.* 194, 35-45, 2022. Doi: https://doi.org/10.1016/j.theriogenology.2022.09.023

13) Amniotic Mesenchymal-Derived Extracellular Vesicles and Their Role in the Prevention of Persistent Post-Breeding Induced Endometritis. Anna Lange-Consiglio, Giulia Gaspari, Federico Funghi, Emanuele Capra, Marina Cretich, **Roberto Frigerio,** Giampaolo Bosi, Fausto Cremonesi. *International Journal of Molecular Sciences*, volume 24, 6, 5166; 2023. Doi: https://doi.org/10.3390/ijms24065166n

The following publication is a direct outcome of the research conducted in this thesis

14) Proof of concept of using a membrane-sensing peptide for sEVs affinity-based isolation. Beatriz Benayas, Joaquín Morales, Alessandro Gori, Alessandro Strada, Paola Gagni, **Roberto Frigerio,** Carolina Egea, Pilar Armisén, Marina Cretich, María Yáñez-Mó. *Frontiers Bioeng. Biotechnol.* Volume 11, 2023. Doi: https://doi.org/10.3389/fbioe.2023.1238898

15) Circulating large extracellular vesicles from STEMI patients contribute to cardiovascular damage. Carolina Balbi, Giorgia Senesi, Stefano Ministrini, Marco Brucale, Francesco Valle, **Roberto Frigerio**, Paolo Bergese, Alexander Akhmedov, Jürg H Beer, Giovanni Camici, Giuseppe Vassalli. *Atherosclerosis.* 2024.

16) Effect of cryopreservation and semen extender on extracellular vesicles isolated from bull semen. Emanuele Capra*, **Roberto Frigerio*,** Barbara Lazzari, Federica Turri, Giulia Gaspari, Luisa Pascucci, Alessandra Stella, Anna Lange Consiglio, Flavia Pizzi, Marina Cretich. *Frontiers in Veterinary Science*. Volume 395, Supplement 1, 118254, Doi: 10.1016/j.atherosclerosis.2024.118254

The following publication is a direct outcome of the research conducted in this thesis

17) Changes in glial cell activation and extracellular vesicles production precede the onset of disease symptoms in transgenic hSOD1G93A pigs. Maria Teresa Golia, **Roberto Frigerio**, Susanna Pucci, Francesca Sironi, Cassandra Margotta, Laura Pasetto, Camilla Testori, Elena Berrone, Francesco Ingravalle, Marcella Chiari, Alessandro Gori, Roberto Duchi, Andrea Perota, Luca Bergamaschi, Antonio D'Angelo, Giulia Cagnotti, Cesare Galli, Cristiano Corona, Valentina Bonetto, Caterina Bendotti, Marina Cretich, Sara Francesca Colombo, Claudia Verderio. *Experimental Neurology*. Volume 374, 2024, 114716. Doi: https://doi.org/10.1016/j.expneurol.2024.114716

18) Extracellular vesicle analysis in supramolecular 3D hydrogels: a proof-of-concept. Greta Bergamaschi*, **Roberto Frigerio*,** Angelo Musicò, Giulia Lodigiani, Paola Gagni, Riccardo Vago,

Marina Cretich, Alessandro Gori. *Sensors & Diagnostics*. 2024, 3, 395-399. Doi: 10.1039/D3SD00313B

19) International Society for Extracellular Vesicles workshop. QuantitatEVs: Multiscale analyses, from bulk to single extracellular vesicle. Manuela Basso, Alessandro Gori, Caterina Nardella, Mari Palviainen, Marija Holcar, Ioannis Sotiropoulos, Sylwia Bobis-Wozowicz, Vito G D'Agostino, Elena Casarotto, Yari Ciani, Shiro Suetsugu, Alice Gualerzi, Lorena Martin-Jaular, Daniela Boselli, Anna Kashkanova, Pietro Parisse, Lien Lippens, Martina Pagliuca, Martin Blessing, **Roberto Frigerio**, Thibaut Fourniols, Ana Meliciano, Anna Fietta, Paolo Vincenzo Fioretti, Karolina Soroczyńska, Silvia Picciolini, Amanda Salviano-Silva, Paolo Bergese, Davide Zocco, Marcella Chiari, Guido Jenster, Levi Waldron, Aleksandar Milosavljevic, John Nolan, Marco P Monopoli, Kenneth W Witwer, Benedetta Bussolati, Dolores Di Vizio, Juan Falcon Perez, Metka Lenassi, Marina Cretich, Francesca Demichelis. *Journal of Extracellular Biology*. 2024. Volume 3, Issue 1 e137. Doi: https://doi.org/10.1002/jex2.137

Acknowledgments

I sincerely thank all the people who helped and supported me during these three years. The work I presented here was possible thanks to:

- Prof. Paolo Bergese, Section of Biotechnology, Department of Molecular and Translational Medicine, University of Brescia, mentor, supervisor, and tutor.
- Dr.ssa Marina Cretich, SCITEC-CNR, Milan, mentor, supervisor, and tutor.
- Prf. Paolo Arosio, supervisor and tutor during my visiting period at ETH Zurich, Switzerland.
- All colleagues at the CTBio Laboratory, SCITEC-CNR, Dr. Alessandro Gori, Dr. Greta Bergamaschi, and Dr. Paola Gagni, Alessandro Mussida, Giulia Lodigiani, Alessandro Strada.
- All colleagues at the University of Brescia, Prof.ssa Annalisa Radeghieri, Dr. Andrea Zendrini, Dr. Lucia Paolini, Dr. Miriam Romano.
- All colleagues and collaborators, with whom I had the pleasure of collaborating during these three years.
- Prof. Marco Presta and Stefania Mitola, Coordinators of the Ph.D. Course in Precision Medicine, Department of Molecular and Translational Medicine, University of Brescia.